

NOTE TO USERS

This reproduction is the best copy available.

UMI[®]

A Soft Sensor System for Cycle-to-Cycle Control of Parison Length in Intermittent Extrusion Blow Molding

By

Himanshu Sikka

Department of Mechanical Engineering

McGill University, Montreal

February 2005

Supervised by Professor Vince Thomson

Department of Mechanical Engineering, McGill University

Co-Supervised by Dr. Azizeh Mitra Yousefi

Industrial Materials Institute, National Research Council

A Thesis Submitted to the Faculty of Graduate Studies and Research in Partial
Fulfillment of the Requirement for the Degree of
Master of Engineering

© Himanshu Sikka, 2005



Library and
Archives Canada

Bibliothèque et
Archives Canada

Published Heritage
Branch

Direction du
Patrimoine de l'édition

395 Wellington Street
Ottawa ON K1A 0N4
Canada

395, rue Wellington
Ottawa ON K1A 0N4
Canada

Your file *Votre référence*
ISBN: 0-494-12647-7
Our file *Notre référence*
ISBN: 0-494-12647-7

NOTICE:

The author has granted a non-exclusive license allowing Library and Archives Canada to reproduce, publish, archive, preserve, conserve, communicate to the public by telecommunication or on the Internet, loan, distribute and sell theses worldwide, for commercial or non-commercial purposes, in microform, paper, electronic and/or any other formats.

The author retains copyright ownership and moral rights in this thesis. Neither the thesis nor substantial extracts from it may be printed or otherwise reproduced without the author's permission.

AVIS:

L'auteur a accordé une licence non exclusive permettant à la Bibliothèque et Archives Canada de reproduire, publier, archiver, sauvegarder, conserver, transmettre au public par télécommunication ou par l'Internet, prêter, distribuer et vendre des thèses partout dans le monde, à des fins commerciales ou autres, sur support microforme, papier, électronique et/ou autres formats.

L'auteur conserve la propriété du droit d'auteur et des droits moraux qui protègent cette thèse. Ni la thèse ni des extraits substantiels de celle-ci ne doivent être imprimés ou autrement reproduits sans son autorisation.

In compliance with the Canadian Privacy Act some supporting forms may have been removed from this thesis.

Conformément à la loi canadienne sur la protection de la vie privée, quelques formulaires secondaires ont été enlevés de cette thèse.

While these forms may be included in the document page count, their removal does not represent any loss of content from the thesis.

Bien que ces formulaires aient inclus dans la pagination, il n'y aura aucun contenu manquant.


Canada

Abstract

Extrusion blow molding is the process of choice for the production of many hollow products. Parison formation is the most critical stage in the process, as the dimensions of the blow-molded part are directly related to the dimensions of the parison. In the intermittent extrusion blow molding process, the length of the parison varies from cycle to cycle since the resin in the accumulator relaxes at different levels depending on the cycle time (extrusion, clamping, blowing, cooling). This variation in length causes a considerable amount of time and cost to the company as a number of trial and error runs have to be performed to get the desired parison length. Swell and sag are the most important phenomena affecting parison dimensions (diameter, thickness and length), and are directly related to the relaxation time of the polymer.

In this work, a ‘soft sensor’ for cycle-to-cycle control of parison length is developed. A model for parison swell is proposed where the parameters of the model can be tuned from cycle to cycle to match the experimental parison dimensions. The technique was tested on a real intermittent extrusion blow molding machine where a target parison length was achieved by either adjusting the flow rate of the polymer or the die gap opening. Good agreement was observed between the flow rate (or die gap) determined by the model and the real values obtained on the machine. The technique has the potential of being extended to optimize the cycle time for a desired parison length using moving mandrels (programming points).

In this work, we have also proposed a technique for estimation of the average relaxation time using a combination of Carreau and Maxwell models. This technique is based on the observed time for parison swell outside the die, and it finds a relaxation time that closely represents the polydisperse nature of blow molding grade resins. The technique could be extended to estimate multiple relaxation times using a generalized Maxwell model.

Résumé

Le moulage par extrusion et soufflage est le procédé industriel le plus utilisé pour la formation de produits creux. La formation de la paraison est l'étape critique du procédé, puisque les dimensions du produit final sont étroitement corrélées à celles de la paraison. Lors du processus de moulage par extrusion-soufflage intermittent, la longueur de la paraison varie de cycle en cycle, étant donné que le matériel accumulé subit des temps de relaxation différents en fonction du temps de cycle (extrusion, moulage, et refroidissement). Plusieurs tests par essai et erreur doivent être effectués afin d'obtenir la longueur désirée. Ces essais augmentent évidemment le coût de fabrication du produit. Le gonflement (swell) et l'affaissement (sag) sont les phénomènes rhéologiques qui affectent les dimensions de la paraison (épaisseur, longueur, et diamètre) ainsi que les temps de relaxation du matériel.

Dans ce travail, un capteur informatique est développé pour la commande automatisée de la longueur de la paraison. Un modèle de gonflement de la paraison est proposé. Les paramètres de ce modèle sont ajustés de cycle en cycle à partir des longueurs de paraisons expérimentales. Cette méthode a été vérifiée sur une machine d'extrusion soufflage intermittent existante. La longueur désirée a été atteinte en faisant varier le débit du polymère et l'ouverture de la filière. Nous avons constaté une bonne corrélation entre les valeurs expérimentales de débit et celles déterminées par le modèle. Cette technique peut aussi être utilisée pour optimiser le temps de cycle pour une longueur de paraison donnée en ajustant les points de programmation.

Nous avons aussi proposé une nouvelle méthode pour estimer le temps de relaxation d'un polymère qui combine les modèles de Carreau et de Maxwell. Ce procédé est basé sur le gonflement de la paraison observé à la sortie de la filière. Le temps de relaxation résultant représente bien la nature polydisperse des résines d'extrusion soufflage. Cette technique pourrait être étendue à la mesure de plusieurs temps de relaxation en utilisant un modèle de Maxwell généralisé.

Acknowledgements

I would like to express my sincerest thanks to my supervisors, Professor Vince Thomson and Dr. Azizeh Mitra Yousefi, first for giving me an opportunity to work on this project and second for the ongoing support, guidance and encouragement throughout all facets of it.

I am grateful to Mr. Patrick Girard for his technical advice, help and discussions.

I am grateful to Dr. Robert DiRaddo for many helpful suggestions.

Special thanks are due to Mr. Marc-André Rainville and Mr. Philippe Courtois for their invaluable assistance with the experimental portion of the work.

I wish to acknowledge the cooperation offered by Industrial Materials Institute (IMI), National Research Council Canada (NRC). This thesis would not have been possible without the use of the resources of IMI. I would like to express my gratitude to my fellow colleagues for their aid in this work.

Finally, I would like to thank my family for their support and encouragement

Table of Contents

Abstract	ii
Résumé	iii
Table of Contents	v
List of Figures	vii
List of Tables	ix
List of Nomenclature	xi
1 Introduction	1
1.1 General	1
1.2 Thesis objectives	3
1.3 Thesis organization	4
2 Blow Molding Process	5
2.1 Introduction	5
2.2 Process description	7
2.2.1 Injection blow molding	7
2.2.2 Stretch blow molding	8
2.2.3 Extrusion blow molding	9
2.2.3.1 Continuous extrusion	10
2.2.3.2 Intermittent extrusion	13
2.3 Parison thickness control	16
3 Previous Studies on Swell	17
3.1 Parison formation	17
3.2 Parameters affecting swell	17
3.3 Methods of measuring swell	22
3.4 Numerical prediction of parison formation	26
3.5 Summary	28
4 Online Approximation of Average Relaxation Time	30
4.1 Methodology	30
4.2 Newtonian and Non-Newtonian fluids	31
4.3 Carreau model	33
4.3.1 Estimation of viscosity using Carreau model	33
4.4 Maxwell model	40
4.4.1 Stress retardation/stress relaxation inside the die	42
4.4.2 Stress relaxation outside die	45
4.5 Summary	53

5 Cycle-to-Cycle Control of Parison Length In Intermittent extrusion	54
blow molding.....	54
5.1 Introduction.....	54
5.2 Material	54
5.3 Machine details	55
5.4 Factors affecting parison length.....	57
5.5 Methodology	57
5.5.1 Flow rate scenario	60
5.5.1.1 Experimentation.....	60
5.5.1.2 Simulation results.....	62
5.5.1.3 Weissenberg and Deborah number calculation.....	67
5.5.1.4 Sigmoid fitting and parison length calculation	69
5.5.1.5 Simulation (sigmoid) tuning	75
5.5.2 Die gap scenario.....	82
5.5.2.1 Experimentation.....	82
5.5.2.2 Simulation Results	83
5.5.2.3 Weissenberg number calculation	85
5.5.2.4 Data plotting and sigmoid fitting	86
5.5.2.5 Operator input estimation	87
5.5.2.6 Simulation tuning.....	90
5.6 Further details on the shape of the sigmoid fitting curves.....	94
5.7 Summary	96
6 Review of the Thesis and its Contributions.....	97
6.1 Recommendations for extensions of this work.....	98
References	100

List of Figures

Figure 2-1 Stages of blow molding.....	5
Figure 2-2 Stretch blow molded product	9
Figure 2-3 Extrusion blow molding process	10
Figure 2-4 Continuous extrusion blow molding - Rising mold assembly	12
Figure 2-5 Continuous extrusion blow molding - Shuttle type arrangement.....	12
Figure 2-6 Continuous extrusion blow molding - Rotary horizontal table machine	13
Figure 2-7 Intermittent extrusion blow molding – Reciprocating screw	14
Figure 2-8 Intermittent extrusion blow molding - Ram accumulator	15
Figure 2-9 Intermittent extrusion blow molding - Accumulator head.....	15
Figure 3-1 Change in the velocity profile in the die exit region	18
Figure 3-2 Swell parameters	19
Figure 3-3 Die profiles	21
Figure 4-1 Relation between viscosity and shear rate for a Newtonian fluid.....	32
Figure 4-2 Relation between viscosity and shear rate for a shear thinning fluid.....	32
Figure 4-3 Cut section view of the flow channel.....	34
Figure 4-4 Pinch-off mold.....	35
Figure 4-5 Flow channel and accumulator arrangement for Placo machine.....	37
Figure 4-6 Path followed by melt from extruder to die exit	38
Figure 4-7 Maxwell model element.....	41
Figure 4-8 Stress relaxation and retardation inside and outside die	50
Figure 4-9 Normalized stress values (outside the die) using Eqs. (4.25) and (4.26)	52
Figure 5-1 Placo intermittent extrusion blow molding machine	55

Figure 5-2 Pinch-off mold used in the study.....	56
Figure 5-3 Pinched parison	57
Figure 5-4 Methodology for parison length control.....	59
Figure 5-5 Extruded parison with programming points.....	64
Figure 5-6 Diverging die.....	65
Figure 5-7 Accumulated flow rate at different extrusion times for $Q = 40\text{g/sec}$	65
Figure 5-8 Instantaneous flow rate curve ($Q = 40\text{g/sec}$).....	66
Figure 5-9 Instantaneous flow rate curve ($Q = 80\text{g/sec}$).....	67
Figure 5-10 Relaxation time as a function of temperature for HDPE DMDF-6200.....	68
Figure 5-11 Diameter swell (B1) versus Deborah number (De).....	69
Figure 5-12 Thickness swell (B2) versus Weissenberg number (We).....	70
Figure 5-13 Fitted Sigmoids (B1 versus De)	71
Figure 5-14 Fitted Sigmoids (B2 versus We)	71
Figure 5-15 Tuned sigmoids for diameter swell (see the end of this chapter regarding the shape of these curves)	80
Figure 5-16 Tuned sigmoids for thickness swell	81
Figure 5-17 Diameter swell (B1) versus aspect ratio at different programming points ..	86
Figure 5-18 Thickness swell (B2) versus Weissenberg numbers at different programming points.....	87
Figure 5-19 Sigmoid tuned to parison pinch-off results	93
Figure 5-20 Sigmoid tuned to experimental observations	93
Figure 5-21 Diameter swell versus Deborah number for the flow rate case (Eq. 5.18) ..	95
Figure 5-22 Diameter and thickness swell for the flow rate case (Eq. 5.18)	96

List of Tables

Table 2-1 Average parison diameter swell for some commonly used plastics	6
Table 4-1 Volumetric flow rate calculation for the extruded parison	36
Table 4-2 Carreau model parameters (Source: IMI material database)	36
Table 4-3 Volumetric flow rate calculation for the extruded parison	40
Table 4-4 Relaxation spectrum data (Source: IMI materials database)	44
Table 4-5 Stress relaxation from die entry to die exit	45
Table 4-6 Parison dimensions as a function of time	48
Table 4-7 Principle strains and overall deformation	48
Table 4-8 Stress relaxation outside die (Eq.4.27)	49
Table 4-9 Normalized stress values for flow outside the die (polydisperse: Eq. 4.27)....	51
Table 4-10 Normalized stress values outside the die (monodisperse: Eq. 4.26).....	51
Table 5-1 Resin properties (Source: IMI material database)	55
Table 5-2 Accumulated flow rate obtained on the machine.....	61
Table 5-3 Simulation results for die gap = 2mm and flow rate = 40g/sec	62
Table 5-4 Simulation results for die gap = 2mm and flow rate = 80g/sec	63
Table 5-5 Weissenberg number calculations for $Q = 40$ and 80 g/sec.....	67
Table 5-6 Values of variables of sigmoids, which gave best fit for the data	72
Table 5-7 Parison length calculation ($Q = 69.58$ g/sec, Iteration-1)	73
Table 5-8 Parison length calculation ($Q = 56.347$ g/sec, Iteration-2)	74
Table 5-9 Parison length calculation ($Q = 54.015$ g/sec, Iteration-3)	75
Table 5-10 Diameter swell measurements from Pinch-off mold	76
Table 5-11 Revised B1 and B2 and parison length calculation	77

Table 5-12 Tuned sigmoid results for diameter swell (B1)	78
Table 5-13 Tuned sigmoid results for thickness swell (B2).....	79
Table 5-14 Simulation data for $Q = 80$ g/sec, $h = 2$ and 6 mm	84
Table 5-15 Weissenberg number calculations for $h = 2$ and 6 mm.....	85
Table 5-16 Calculation results for the first iteration	88
Table 5-17 Summary of parison length obtained for different iterations.....	89
Table 5-18 Diameter swell measurements from pinch-off mold	89
Table 5-19 Revised B1 and B2 and parison length calculation	90
Table 5-20 Tuned sigmoid results for diameter swell (B1)	91
Table 5-21 Tuned sigmoid results for thickness swell (B2).....	92

List of Nomenclature

Symbol	Description
B1	Diameter swell
B2	Thickness swell
D_{die}	Die outer diameter
D_p	Parison outer diameter
h_p	Parison thickness
h	Die gap
E	Exit geometry
t	Time after fluid element leaves the die
t_p	Time required for the melt to pass through the die
L/D	Aspect ratio
MW	Molecular weight
MWD	Molecular weight distribution
De	Deborah number
We	Weissenberg number
t	Characteristic time of the material
Q	Accumulated flow rate
Q_{inst}	Instantaneous flow rate
A	Cross sectional area
n	Power law index
m_g	Mass flow rate of the polymer melt
w_{sec}	Weight of the extruded parison
t_{ext}	Extrusion time
T_{ref}	WLF reference temperature
R	Outer radius
r	Inner radius
T	Circumference of the annular section ($2\pi R$)

h_i	Thickness ($R - r$)
t'	Time at any instant
$t'_{initial}$	Initial time
Δp	Pressure drop
K	Consistency index
ΔT	Temperature increase
G	Elastic modulus
J_s	Shear compliance
I_2	Second invariant of the stress tensor
l_1, l_2, l_3	Principle strains
L_{target}	Target parison length (550 mm)
L_{exp}	Experimental parison length
t_{ext}	Extrusion time
t	Flow time in the die
a,b,c,d	Sigmoid parameters
L_{Total}	Calculated total parison length
Q_{guess}	Accumulated flow rate (guess)
$Q_{inst,i}$	Instantaneous flow rate at programming point, i

Greek symbols	Description
λ	Relaxation time
λ	Time constant (Carreau model)
η	Non-Newtonian Viscosity
μ	Newtonian viscosity
η_0	Zero shear viscosity
η_∞	Limiting Newtonian viscosity
$\dot{\gamma}$	Shear rate
τ	Shear stress

1.1 General

Plastics are an integral part of everyone's lifestyle with applications varying from commonplace domestic articles to sophisticated scientific and medical instruments (Crawford, 1998).

Extrusion blow molding is the most widely used blow molding technique. Typical products of extrusion blow molding are bottles, drums and toys. Recently it has been used in the manufacture of complex automobile parts such as gas tanks, bumpers, seats, oil tanks, business machine panels, etc.

As the name suggests the process is made up of three main stages, namely, extrusion, blowing and molding. In the extrusion stage, a hollow tube of molten polymer melt called a parison is extruded through an annular die. In the blowing stage, the parison is enclosed by two mold halves and inflated against the walls of the mold in order to take the shape of the product, and finally in the molding stage, the parison is cooled in contact with the mold and the finished article is ejected. A detailed description of the process is given in chapter 2.

Advancement in machinery and control, and an enhanced confidence about the potential of the process, has given a big boost to blow molding practitioners for cost-effective production of large industrial parts.

Blow molding has advanced significantly from the relatively crude process it was in years past to one that has incorporated many of the benefits in part complexity and precision that derive from today's computerized controls.

Current growth in blow molding is driven by an increased awareness of the advantages of the process, including rigid double wall construction, design flexibility, relatively low

tooling cost and comparatively short lead times for starting production (Plastics Engineering, 1998).

In the parison formation stage prior to mold closure, parison dimensions are influenced by two phenomena, swell and sag. Die swell is a flow phenomenon, which commonly occurs when a polymer melt emerges out from a confined boundary (Wong, 1997). Parison sag on the other hand occurs as a result of the parison stretching under its own weight. Thinning of the parison results and the effect is greater closer to the die (Midgley, 2002).

Parison swelling takes place in two directions: increasing diameter and increasing thickness, and is widely accepted to be caused by the elastic nature of the polymers that recover from the deformations (shear and extensional) imposed on them during the flow through the die. The degree of swell and sag are controlled by die design, extrusion conditions and rheological properties of the resin (Orbey, 1984).

Predicting parison dimensions just prior to inflation is useful for minimizing resin usage while providing the necessary strength and rigidity to the blow molded part.

This thesis is divided into two parts namely online estimation of average relaxation time and cycle-to-cycle control of parison length in intermittent extrusion blow molding. In part one, we have proposed a method for online estimation of average relaxation time of a resin. Relaxation time is an important rheological property of the resin as many occurring phenomena such as swell and sag are directly dependent on it. In general up to six relaxation times are required to adequately represent the resin behavior. In the approach developed in this thesis, we have simplified the approach to one relaxation time.

In part two, we propose a new technique for cycle-to-cycle control of parison length in intermittent extrusion blow molding. Parison length is an important parameter in the extrusion blow molding industry, as correct parison length can save a significant amount of cost and material. On any intermittent extrusion blow-molding machine, the parison length can be altered by changing the flow rate, the die gap or allowing for a longer period of flow. Presently, an operator relies on experience, and a trial and error approach

to obtain the parison of the correct length. In the technique developed in this thesis, both the flow rate and die gap scenarios were studied and good accuracy was obtained. This approach can be extended to optimize the cycle time (extrusion, clamping and blowing) for a given operating range (flow rate) and die geometry (minimum and maximum die gaps).

For both parts of the thesis, we have used a simulation tool (BlowView), developed by the National Research Council's Industrial Materials Institute (NRC-IMI). BlowView is a finite element software package designed to simulate the extrusion blow molding, injection stretch blow molding and thermoforming processes. BlowView uses finite element analysis to simulate the successive steps of the process. It is used to simulate the parison formation process and to estimate the dimensions at one point (Part-1) or various points (Part-II) along the length of the parison. In extrusion blow molding, the following steps can be simulated:

- Flow in extrusion dies
- Parison sag
- Mould clamping
- Parison inflation
- Part cooling
- Part shrinkage and warpage

1.2 Thesis Objectives

The objectives of the present research are:

- 1) to develop a technique for online estimation of average relaxation time,
- 2) to identify the changes in the rheological properties of the melt from temperature increase in the die, and
- 3) to develop a model to predict the total length of the parison at any given time taking in to consideration the combined effect of swell and sag.

1.3 Thesis Organization

In chapter 2, the general blow molding process is described with emphasis on extrusion blow molding. Advantages and disadvantages of each process are also outlined.

In chapter 3, previous works on parison formation, swell and sag are reviewed. This chapter also covers in detail the work done up until now regarding the measurement of parison profiles.

Chapter 4 presents the details of the machine used for the study. Rheological properties of the resin used are also given. It also details the methodology used for online estimation of average relaxation time.

Chapter 5 describes the new technique for cycle-to-cycle estimation of parison length in intermittent extrusion blow molding. Both die gap and flow rate scenarios are included.

Chapter 6 summarizes the thesis and also makes recommendations for future research.

2.1 Introduction

Blow molding is a commercially important method for the production of hollow articles such as bottles and drums. It is probably the second most common method to Injection molding for the manufacture of plastic parts. The main stages of extrusion blow molding are listed below:

- A hollow tube of semi-molten polymer melt called a “*parison*” is formed by forcing material between a die and a mandrel.
- While the tube is still hot, the plastic is trapped in the mold, and a hot knife cuts it off at the top. The parison is pinched at the bottom.
- In case of continuous extrusion blow molding, the mold is moved to the blowing station where, the blow pins are inserted.
- Blow pins are inserted into the top of the tube, forming the neck. Compressed air expands the parison to conform against the cold mold cavity walls.
- When the part is sufficiently cooled, the two halves of the mold separate and the finished part is ejected and trimmed of extra plastic or flash.

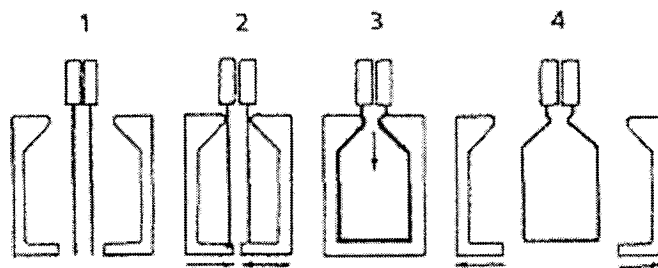


Figure 2-1 Stages of blow molding

Parison formation is the most important stage in the blow molding process because of the fact that dimensions of the final part are dependent on the dimensions of the forming

parison. When the melt leaves the die, it is subjected to stress relaxation on account of high shear stresses that it experienced in the die. As a result, parison swelling takes place.

Parison swelling is composed of diameter swell and thickness swell. Excessive diameter swell could cause curtaining (The tendency for a parison to lose its tubular shape because of conditions in the extrusion process) and stripping problems. Lower diameter swell on the other hand could increase the number of rejections on account of defective handles, or other asymmetrical features. Table 2.1 lists diameter swell experienced by commonly used plastics.

Table 2-1 Average parison diameter swell for some commonly used plastics

(Source: Rosato, 1997)

Plastics	Diameter Swell (percent)
HDPE (Phillips)	15-40
HDPE (Ziegler)	25-65
LDPE	30-65
PVC (rigid)	30-35
PS	10-20
PC	5-10

Low thickness swell will result in a product having insufficient wall thickness and strength, whereas high thickness swell will result in excessive wastage of the resin.

As the parison is extruded, it also sags under its own weight. This is mainly caused by gravity acting on the freely hanging parison. Hence, parison dimensions at a particular location and time are dependent on the simultaneous phenomena of swell and sag.

This chapter discusses different types of blow molding along with the advantages and disadvantages associated with each of them.

2.2 Process description

Blow molding is a process used to produce hollow objects from thermoplastic (Lee, 1990). Its application is not limited to simple products like bottles and drums, but also includes more complex parts, which require detailed knowledge about design, and engineering such as gas tanks, bumpers, cabinet panels, etc.

Many materials such as cellulose nitrate, cellulose acetate, low-density polyethylene (LDPE), etc. have been used in the early stages of blow molding for the production of various articles. However, as time progressed and until the invention of high-density polyethylene (HDPE) in 1953, the use of these materials was restricted in the blow molding industry. The availability of high-density polyethylene at an attractive price was mostly responsible for the development of blow molding.

The three major variations of the process are:

- injection-blow molding
- stretch-blow molding
- extrusion-blow molding

They have in common the formation of the precursor, a simple hollow tube known as a preform or parison. One end of the parison is closed so that it can be inflated in the heated, softened state. It inflates until it touches the walls of the cooled mold. The parison at once takes the shape of the mold and cools. The mold is then opened and the bottle removed. Extrusion blow molding is the most widely used blow molding method.

2.2.1 Injection blow molding

This is a two-step process in which, a preform is molded and kept in a near-molten condition. It is then indexed into another machine and blown into a finished part. In the injection phase of the process a tube shaped article called a preform is formed by injection molding the thermoplastic resin in a hollow cavity. In this process, the threaded neck is formed. With the help of the core rod, the preform is transferred to the blowing mold where it is blown into the shape of the mold by the air coming out of the opened

core rod. The completed bottles are then transferred to the stripping station for ejection. The detailed description of the process can be found elsewhere (Lee, 1990). The main advantages of injection blow molding are:

- scrap-free, close-tolerance products
- perfect neck finish
- good surface finish

The main disadvantages of the process are:

- blown handleware is not possible
- size limitations
- containers with offset necks are difficult to make
- longer cycle times

2.2.2 Stretch Blow Molding

The soft drink industry's adoption of oriented polyethylene terephthalate (PET) bottles for its two-liter package catapulted injection stretch blow molding into the spotlight (Lee, 1990). In 2002, nine million tons of PET resin worldwide were converted into containers and PET still enjoys the highest growth rate of any major plastic.

In this process, the preformed parison is reheated to its orientation temperature and stretched in two directions (hoop and axial) before the blowing stage. Stretching causes an increase in the materials tensile strength, drop impact, clarity, toughness, and barrier properties, as well as reduced creep.

Injection stretch blow molded bottles can be made by two methods, one stage/inline and two stage processes. The in-line method involves continuous forming, heating and blowing of preforms on a single machine.

In a two-stage process, preforms are injected on one machine and blown on the other. In both single stage and two stage processes, the preform has to pass through a thermal conditioning stage before reaching the blowing station. The preform has to travel inside

convective-radiative ovens that will impart to the rotating preform a preset temperature distribution along its length (Garcia-Rejon, 1995b). Fig 2.2 shows various products manufactured by stretch blow molding.



Figure 2-2 Stretch blow molded products

The main advantages offered by stretch blow molding process are:

- accurate control of wall thickness
- improved physical and barrier properties of the resin
- lower material cost due to weight reduction

Disadvantages are:

- The top and bottom of the containers are not biaxially oriented, so they have different properties from the rest of the container.

2.2.3 Extrusion blow molding

As mentioned earlier, the extrusion blow molding process consists of three main stages, namely, extrusion, blowing and molding. In the extrusion stage, the plastic is compressed in the barrel and is melted as it moves through the barrel because of the shearing action of the screw and heated barrel. The screw finally pumps the melt through a tubing die to form the hollow cylindrical tube called a ‘parison’. The mold halves are then closed around the parison to pinch it at one end, and if a bottle is to be made, to form

a threaded neck at the other. The parison is then blown against the walls of the mold to take the shape of the mold cavity and the formed article is cooled and ejected (Fig 2.3).

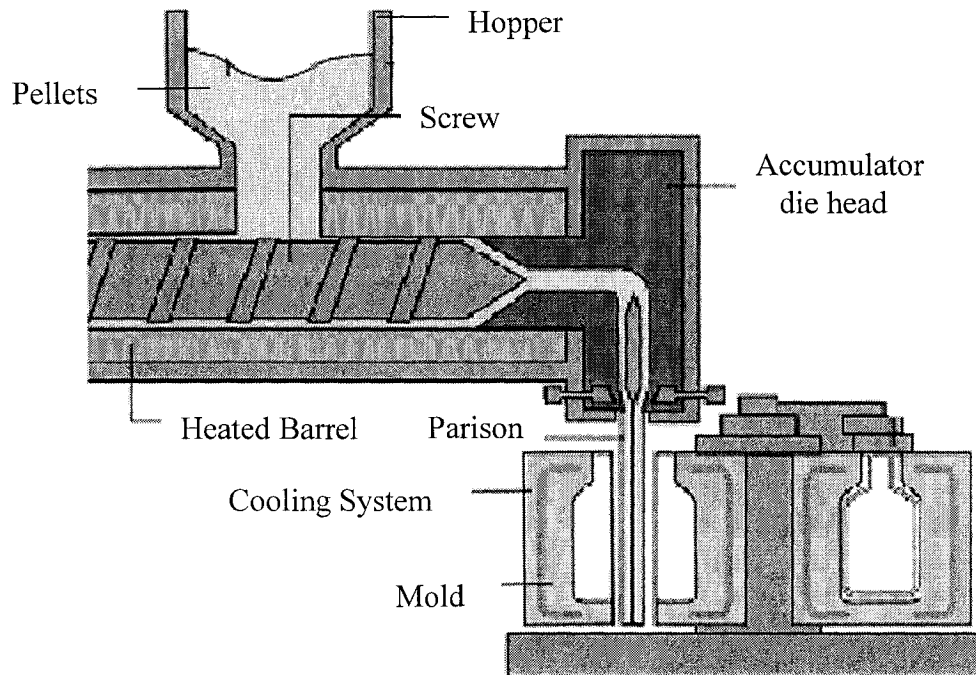


Figure 2-3 Extrusion blow molding process

Various techniques are used to introduce air into the parison. It may be accomplished through the extrusion die mandrel, through a blow pin over which the end of the parison has dropped, through blow heads applied to the mold, or through a blowing needle, which pierces the parison (Rosato, 1989).

There are two methods by which the parison is extruded through the annular die:

- continuous extrusion
- intermittent extrusion

2.2.3.1 Continuous Extrusion

The continuous extrusion blow molding process is the most common method used for the production of an extensive array of hollow blow molded articles. Over 750 U.S companies use the process to produce such items as wide mouth jars, handle ware

containers, medical items, technical parts and toys. Compatible thermoplastic resin materials that can be used include: high density polyethylene (HDPE), polyvinyl chloride (PVC), low density polyethylene (LDPE) and polycrystalline (PC) (Modern plastics-world encyclopedia, 2002).

In the continuous extrusion blow molding process, the parison is extruded as a long endless tube from the die. The process employs a rotating screw, which continuously pumps the resin at a constant rate. Since parison production is a non-stop process, molds are moved in and out of the die area to capture the required amount of the hollow tube as per the product specification. There are different types of continuous extrusion blow molding processes, the choice of which depends on the type, size and number of parts to be produced.

Different types of mold used for this process are:

- vertical movement mold
- horizontal movement mold
- molds on rotary wheels.

In the vertical movement type (Fig 2.4), the mold rises under the die head and pinches the parison at the desired length. The mold then moves to the station where the parisons are blown with the help of an injection pin inserted from the top or bottom of the parison. Blowing is followed by cooling and ejection. Once the part is ejected the mold again rises and captures the extruded parison, and the process sequence is repeated.

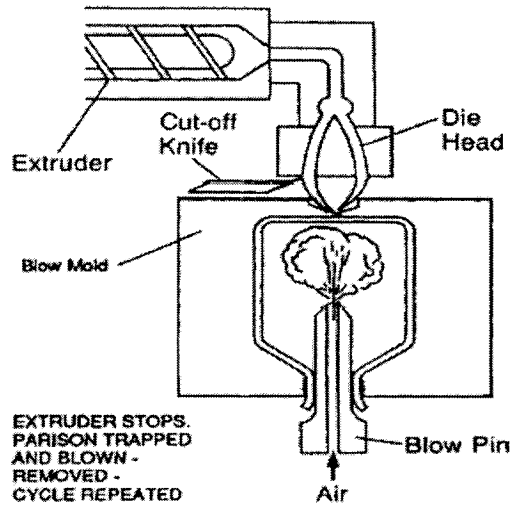


Figure 2-4 Continuous Extrusion Blow Molding - Rising mold assembly

(Source: Berins, 1991)

In the sliding mold or shuttle type operation (Fig 2.5), there are two mold assemblies located on the left and right of the parison. When the parison is extruded, one of the two molds moves to the parison and clamps it while the other mold is blowing/cooling the previously extruded parison. Once the part is ejected, this mold again moves to the extruded parison and clamps it and the process is repeated. In this process, the blow pin enters from the top of the parison.

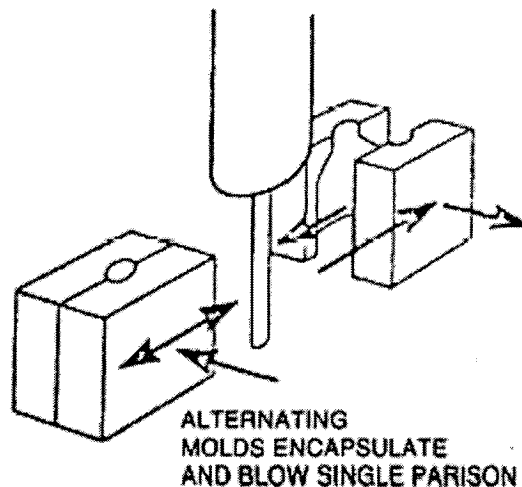


Figure 2-5 Continuous Extrusion Blow Molding - Shuttle type arrangement

(Source: Berins, 1991)

In a rotary mold type, continuous blow molding machine (Fig 2.6), a wheel (either horizontal or vertical) is mounted close to the extrusion die. The wheel consists of a series of hydraulically or pneumatically controlled split molds. As the wheel rotates, one mold at a time passes under the die to receive and close around the parison; this motion is continuous. Blow air is introduced through a hollow needle inserted into the parison from the side. The air is fed through the wheel axle as is the water used to cool the molds. Rotary cams, located in the wheel axle, govern the mold opening, closing, blowing air start, and blowing needle insertion. Upright rotary wheels may carry up to 20 molds (Lee, 2000). Rotary equipment provides very high output. High tooling cost for the equipment limits its usage to high volume parts.

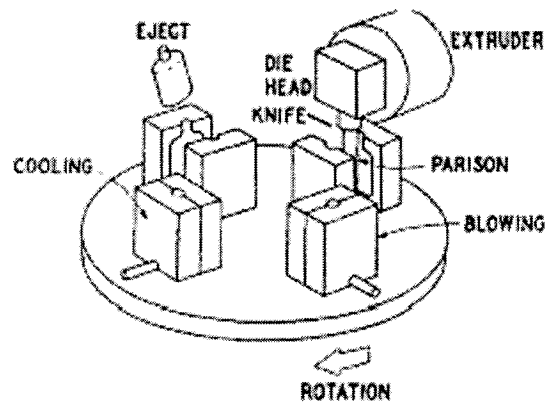


Figure 2-6 Continuous Extrusion Blow Molding - Rotary horizontal table machine
(Source: Berins, 1991)

Advantages:

- Processing of variety of materials.
- Quick changeovers.
- In-mold labeling.
- Multilayer capability.

2.2.3.2 Intermittent Extrusion

In the intermittent process, the melt is accumulated in the barrel and forced out in one shot through the die to make a parison, once the mold opens. The main advantage

associated with this process is that here, unlike a continuous process, molds are not moved around the die head to pinch the parison.

As mentioned before different types of intermittent blow molding are:

- reciprocating screw
- ram extrusion
- accumulator head

A reciprocating screw machine is shown in Fig 2.7. These are extruders which work in precisely the same way as injection molding units, releasing the volume of melt stored in the barrel by retracting the screw during plasticization and then ejecting the melt by moving the screw forward again. In this process as the screw rotates, the melted resin is collected at the end of the barrel. The accumulated molten polymer then exerts pressure on the screw and moves it backward. When required, an amount of resin is collected, a hydraulic mechanism moves the screw forward, forcing the melt through one or multiple die heads to form a parison. These machines are used for a shot weight of not greater than 2.5 kg's.

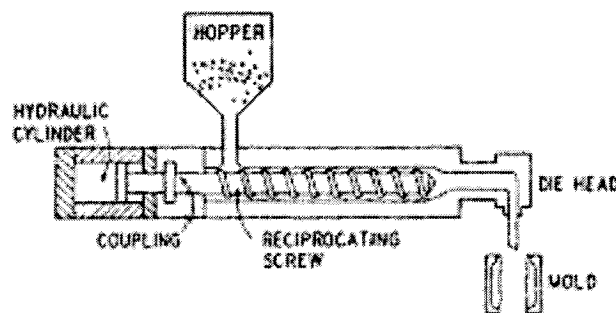


Figure 2-7 Intermittent Extrusion Blow Molding – Reciprocating screw
(Source: Berins, 1991)

In ram accumulator machines (Fig 2.8) the extruder supplies the melted resin that collects in a separate channel called an accumulator cylinder. It works on a first in, last out principle, i.e., the material, which first enters the accumulator, is the last to leave. An hydraulic cylinder operates the ram movement. This system has been used for parts weighing between 2.5 kg to 25 kg.

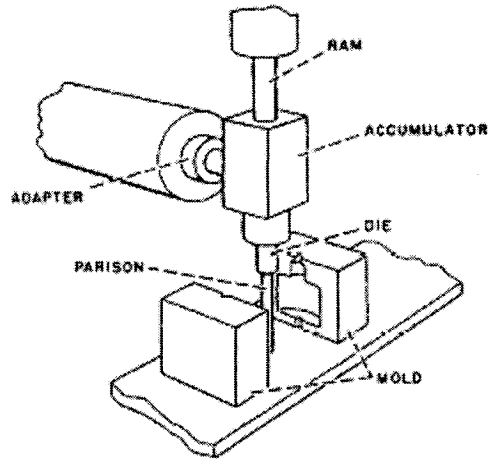


Figure 2-8 Intermittent Extrusion Blow Molding - Ram Accumulator
 (Source: Berins, 1991)

In accumulator head systems (Fig 2.9), the melt that first enters the accumulator is the one to leave first; hence, this process is suitable for heat sensitive materials. The accumulator cylinder is of annular shape with a mandrel in the center. The melt from the extruder enters the accumulator head from the side and flows around a mandrel. The annular ram is forced downward for producing the parison.

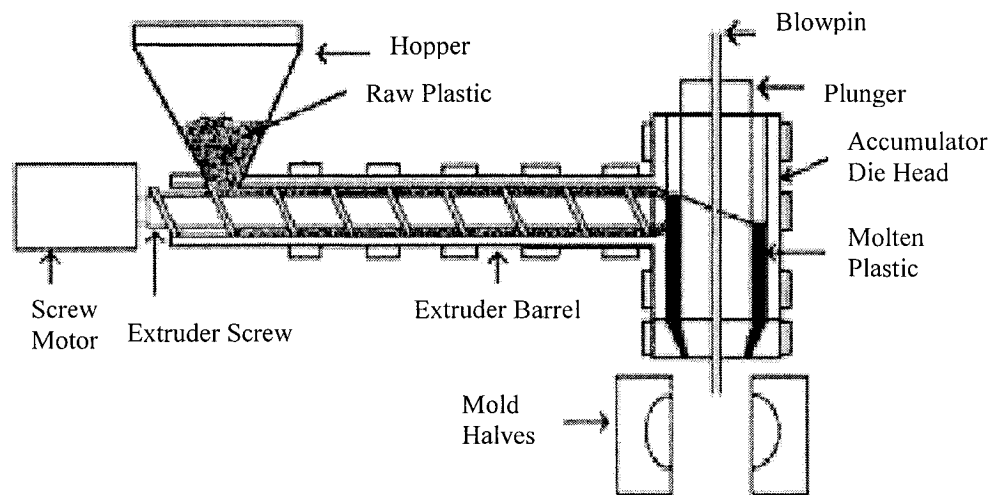


Figure 2-9 Intermittent Extrusion Blow Molding - Accumulator head
 (Source: www.crockerltd.com- html document)

The main advantages of extrusion blow molding are highlighted as,

- low tooling cost
- high rates of production. (for continuous extrusion blow molding)
- blown handle articles can be manufactured
- large parts can be blown

2.3 Parison thickness control

Parts produced by extrusion blow molding have different thickness along their lengths, and therefore, require parisons of variable thicknesses. Had a parison of uniform thickness been used for every part, there would have been considerable wastage of material. To avoid this, the thickness of parison is varied as it is extruded using a process known as "*parison programming*". This is done by moving the mandrel up or down as required along the mandrel axis during the extrusion of the parison. This process helps to control the wall thickness distribution along the parison and consequently its weight. The X and Y coordinates of the desired parison profile are keyed in. When all the points along the parison length are inputted, a complete parison program is displayed on the screen. Parison programming can be accomplished in two different ways. In one method, the die gap is changed as required, as the parison is extruded. In the second method, the flow rate is varied.

3.1 Parison formation

Parison formation in extrusion blow molding consists of the extrusion of a polymer melt through a complex annular die (Rosato, 1989). The die gap is determined from the distance between the moveable mandrel and the fixed bushing. Movement of the mandrel during extrusion results in a parison with variable thickness along its length. Mandrel movement is controlled by a process known as parison programming. Material characteristics like swell and sag also influence the geometry of the extruded parison. Parison swell, occurring both in diameter and thickness, is due to the elastic recovery of the polymer melt from the imposed nonlinear viscoelastic deformations in the extrusion die. Sag is caused by the gravitational forces that act on the freely suspended parison.

3.2 Parameters affecting swell

As the polymer emerges from the die exit, its cross-sectional area is larger than that of the die exit. This is caused by the swelling of the polymer melt as it exits the die. The extent of swelling is quantified by the ratio of the diameter of the parison to the outer diameter of the die. As the polymer melt exits the die, significant rearrangement of the velocity profile of the molecules takes place causing the extrudate to swell (Fig 3.1). In fact, the swelling of viscoelastic fluids upon exiting a die can be thought of as a three-step process consisting of a small Newtonian swelling, a sudden elastic recovery and a further swelling due to stress relaxation. For a parison (extrusion from annular die), two swell values are required to describe its dimensions, a diameter swell and thickness swell (Swan et al, 1991). Mathematically they are given by (Fig 3.2):

$$B1 = \frac{D_p}{D} \text{ and } B2 = \frac{h_p}{h} \quad (3.1)$$

where,

D_p, h_p = outer diameter and thickness of the parison.

and D , h = outer diameter of the die and die gap respectively.

For round dies (or capillary), die swell is simply the ratio of extrudate diameter to the die diameter. It is given by, $B = \frac{D_e}{D}$

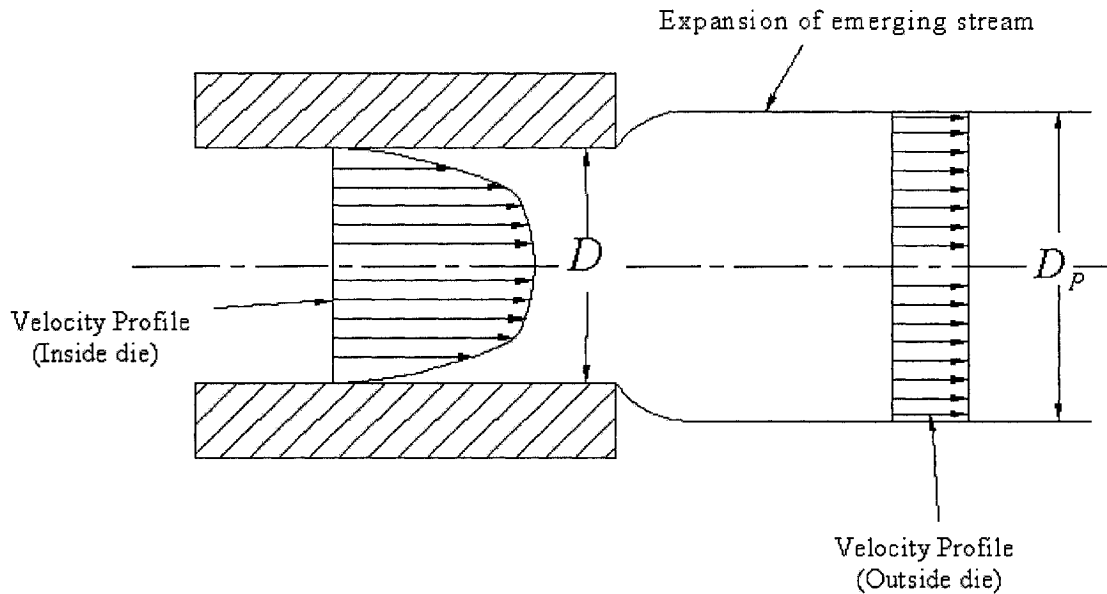


Figure 3-1 Change in the velocity profile in the die exit region

Nearly 60 to 80 percent of both the diameter and thickness swell occurs in the first few seconds after extrusion, but the equilibrium swell value is reached only after 5 to 8 minutes have elapsed. The exact relation between swell and time depends on the resin and the die geometry (Orbey and Dealy, 1984).

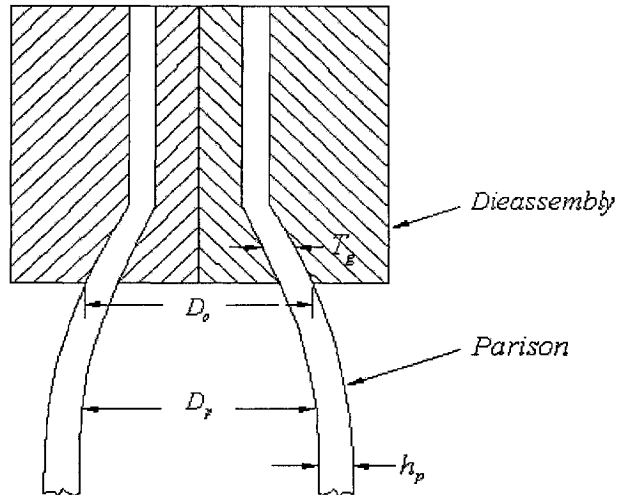


Figure 3-2 Swell parameters

Swell is affected by process variables as well as by the rheological parameters of the resin. In summary, capillary die swell, is a function of the following variables:

$$B = f(L/D, h, E, t, t_p / \lambda, \tau_R)$$

where,

L/D : die aspect ratio

h : die gap (mm)

E : exit geometry

t : time after fluid element leaves the die (sec)

t_p : time required for the melt to pass through the die (sec)

λ : relaxation time (sec)

τ_R : wall shear stress (Pa)

In addition, die swell also depends on the method used to measure it; for example, the highest swell values are obtained for the polymers that are extruded under isothermal conditions into an oil bath and lowest for the ones extruded in ambient conditions.

Shear rate:

For capillary dies, as shear rate is increased, die swell is increased. This is due to the fact that the material is exposed to high stresses under high shear rate, and as soon as it exits the die, it swells more as it tries to return to the original configuration as soon as possible (Santelices, 1994).

For annular dies, DiRaddo and Garcia-Rejon (1997) determined that thickness swell is unaffected by increasing shear rate whereas Yousefi et al. (2002) found that it is more sensitive to shear rate than the diameter swell.

Aspect ratio:

The degree of swell decreases as the L/D ratio is increased approaching a constant value at large L/D ratios. This is due to the fact that as the length of the cross section increases, the polymer has more time to relax and eventually when the polymer melt exits the die it would have already relaxed in the passage thereby resulting in less swell.

Effect of die geometry:

Die geometry has a significant effect on parison swelling (annular die). It is observed that the effect of extrudate swelling due to die geometry is in the following order:

$$B_{Diverging} < B_{Straight} < B_{Converging}$$

Fig 3.3 gives a description of the die geometries. In a diverging die, circumferential stresses acting on the melt produce recoil action when the extrudate exits the die thereby reducing the swell. In a straight annular die, there is partial axial orientation in the axial direction due to the shearing deformation of a fluid element (Orbey, 1984). In a converging die, stretching along streamlines occurs due to decreasing cross-sectional area, which considerably enhances the swell.

Koopmans (1992, III) provided a demonstration of the major effect of die-mandrel geometry on parison swell. He showed that small variations in the die geometry have a much stronger effect than variations in flow rate or stress. Yousefi et al. (2002) observed that as the die length is decreased, parison diameter swell is increased. Thickness swell seemed to be unaffected by the length of the die.

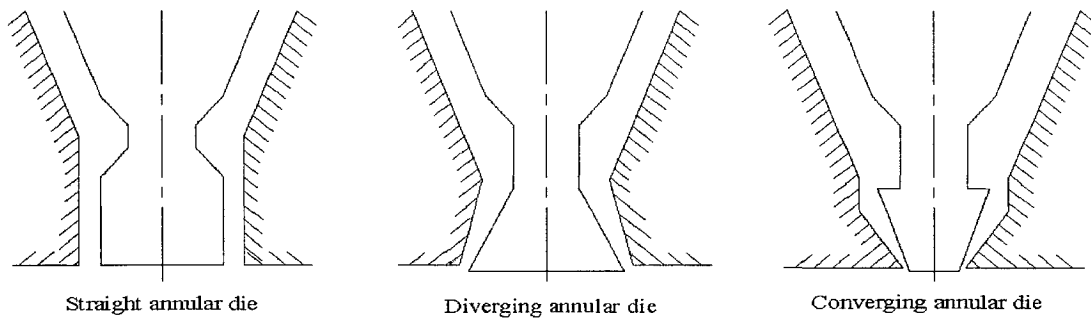


Figure 3-3 Die profiles

Effect of molecular weight:

Molecular structure, long chain branching in particular, has significant effect on the swelling behavior of the extrudate (annular and round dies). Koopmans (1992a) studied the swell characteristics of two high-density polyethylene (HDPE) resins taken from successive batches of the same commercial grade. He observed that the maximum swell and the time to reach this value are very sensitive to the molecular weight distribution (MWD) of the resin. Polymers with the broadest MWD showed less maximum swell.

The largest diameter swell potential is seen for the resin with the lowest molecular weight (MW) and narrowest MWD. However, owing to lower melt strength, this polymer sags more, and thus, obtains the smallest diameter and thickness in the upper parts of the parison once the parison reaches critical length (Eggen and Sommerfeldt, 1996).

Orbey and Dealy showed that the polymer with highest MWD shows the lowest swell for all dies. DiRaddo and Garcia-Rejon (1992) observed that swelling increases with MWD. This can be attributed to the increased chain disentanglement that occurs in broad MWD materials.

Effect of flow rate:

For a given die configuration and material, the effect of flow rate on extrudate swell is nearly negligible (Koopmans, 1992c). Yousefi et al. (2002) and Yang (1987); however, it has been observed that as the flow rate increases, parison diameter and thickness swell also increase.

For capillary dies, Wong (1998) obtained a relation of the type $MFR = A \exp(ESR)$, where MFR is the melt flow rate, A is a constant (0.839), and ESR represents the corresponding extrudate swell ratio.

Effect of Temperature:

There exists a discrepancy concerning the effect of temperature on die swell. Huneault et al. (1990) found a positive influence of temperature on extrudate swell for PVC. For polypropylene however, Millar et al. (2003) found that increasing melt temperature resulted in only a slight decrease in die swell. Wong (1998) observed that for HDPE, for a fixed L/D ratio, swell increases as temperature increases until it reaches a maximum value and decreases thereafter. For HDPE, Santelices (1994) observed that as temperature increases die swell increases. Yang and Lee (1987) found that melt temperature has much less influence on the extrudate swell than the die wall temperature does.

It is concluded that the effect of temperature is specific to the resin, process and equipment.

Effect of die gap:

Increasing the die gap reduces both diameter swell and thickness swell (Yousefi et al., 2002). This is due to the fact that as the gap increases, shear rate decreases, which subsequently decreases the parison swell.

3.3 Methods of measuring swell

An efficient blow molding process requires optimization of wall thickness distribution and parison diameter. Knowledge of parison thickness and diameter before inflation can help to achieve this. Many attempts to measure annular extrudate dimensions have been made in the recent past. Measurements of these parameters boost an understanding of resin behavior and thus help in the development of new blow molding resins.

The magnitude of swelling also depends on the method used for measuring it. Over the years different researchers have proposed different methods. One method involves extruding the parison in ambient conditions and measuring swell using a micrometer while others involve extruding the parison in a bath of oil which has the same density as

that of the melt and air, and measuring swell using a photographic technique or laser optometry. In the cases mentioned, the swelling of a polymer melt extruded into oil will have a higher amount of swelling than that of the one extruded in ambient conditions because extruding the parison in air will result in freezing of stresses in the parison.

The earliest study to obtain experimental data for parison weight distribution was carried out by Sheptak and Beyer (1965). They employed a “pinch-off” mold, consisting of a series of thirteen blades, which pinched the parison into twelve 2.54cm segments. Cutting and weighing the segments obtained the weight distribution of the material in the parison. They obtained pure swell data from the bottom of the parison by considering that the end portion of the parison represents a sag free zone (because there is no weight acting below that portion). The drawdown contribution is then obtained by subtracting the pure swell contribution to the incremental weight from the experimental incremental weight. This study was restricted to one temperature and one shear rate and this prevented it from giving a wider view of the problem. Moreover, the data obtained by the pinch-off mold was not continuous in time.

Kalyon and co-workers (1980) improved the technique proposed by Sheptak and Beyer by utilizing cinematography in conjunction with a pinch off mold. The thickness distribution was calculated using the weight distribution obtained from the pinch-off technique and diameter swell obtained from cinematography. Excellent agreement between the area swell values was obtained on the basis of capillary and parison swell measurements. Thus, it was concluded that the use of cinematography along with pinch-off measurements is essential to obtain reliable results.

The main drawbacks associated with the isothermal extrusion method are:

- it is difficult to mount the hot oil bath on the rheometer,
- parison diameter measured by the above method tends to scatter a lot owing to the change of oil refractive index by natural convection,
- it is hard to find oils that maintain density and solubility requirements with variable temperature.

Dealy and Orbey (1985) developed a simple model to predict the shape of a parison at the moment of inflation. In this approach, the parison was considered to be made up of individual elements. The model requires extrudate swell and storage modulus data. Two types of experiments were carried out in this study. First, the parison swell was studied in the absence of gravitational force by extruding the parison into an oil bath having the same density as that of the melt and the same temperature as that of the extrudate. Secondly, sets of experiments were carried out to study the combined effects of sag and swell. Here, the parison was extruded into an isothermal air oven and the length of parison was monitored as a function of time.

Since this is a contact technique it cannot be employed online with a blow-molding machine. Moreover, prior knowledge of rheological data is desirable.

DiRaddo, Patterson and Kamal (1988) developed a technique to estimate the on-line thickness profile of annular extrudate. The length and diameter of the parison were measured using a video camera in conjunction with an image analysis system. However, the technique did not take into account the effects of sag and cooling of the parison due to small extrusion times employed in the study.

Swan, Dealy, Garcia-Rejon and Derdouri (1991) developed a new technique to measure time dependent parison diameter and thickness swell without the use of an oil bath. In addition, they also studied the effect of molecular weight on parison swell of high-density polyethylene. This scheme used an oven maintained at the extrudate temperature. Two cameras mounted on a slide carriage view the parison. The upper camera provides a signal to control the position of the carriage and the lower one is focused on the parison end to determine the values of thickness and diameter swell. An accuracy of 15% and 2% for thickness swell and diameter swell respectively was obtained.

This method cannot be used online as the presence of an isothermal oven and carriage slide arrangement interferes with normal operation.

Eggen and Sommerfeldt (1996) utilized an image analysis system for online measurement of parison dimensions (diameter and thickness). This is the modification of a technique used by Kaiser (1991).

They assumed that the amount of material between two ink marks on an extruded parison remains constant and is equal to the output rate times the time between each ink mark. A program was developed to convert the relative position of ink marks into distance. Parison thickness was then calculated with a set of equations along with the data of diameter and distance measurement. They obtained a reproducibility of greater than 98.5% for parison diameter and 96-97% for parison thickness. They also demonstrated the effect of molecular weight (MW) and molecular weight distribution (MWD) on the parison swell and sag. Multivariate analysis technique was used to develop a model incorporating the effect of MW, MWD and rate of output on diameter and thickness.

Swan et al. (1996) developed an optical sensor for online measurement of parison thickness distribution. The measurement technique was based on the principle of beam reflection. The distance between two partially reflected beams produced by striking the parison with a laser beam represents the thickness of the parison. The reflected beams were focused through a lens on a CCD array, which measured the separation between the beams. This separation is a function of thickness, refractive index and geometry of the parison. The value of refractive index was assumed to be constant. Thickness was determined with an accuracy of 20%.

Langkamp and Michaeli (1996) also developed a sensor that measured the on-line thickness profile of the parison. Their technique was also based on the principle of laser beam reflection as developed by Swan et al. (1996). The accuracy of the measurement system was based on the performance of the CCD camera and image-processing system.

DiRaddo and Garcia-Rejon (1997) modified the technique developed by DiRaddo, Patterson and Kamal (1988) by taking into account the effects of in-cycle sag and thermal effects. This approach is applicable to continuous extrusion blow molding. This approach

was based on the measurement of parison diameter, length profile during extrusion as well as parison temperature profile for the estimation of parison thickness profile. The effects of process parameters like flow rate, die gap and die temperature on parison thickness profile are also discussed. This technique could be employed online with some minor modifications as it is a non-contact measurement technique. Also prior knowledge of rheological data was not desirable.

3.4 Numerical prediction of parison formation

The use of numerical techniques for simulation of parison formation stage has increased significantly in the last decade. This has been possible on account of the following advantages associated with numerical modeling:

- reduced machine setup times
- reduced tooling cost
- optimization of process parameters.

Earlier use of numerical techniques for parison formation was based on conservation principles. These principles are not feasible for simulation of the intermittent blow molding process. The effect of sag and parison programming cannot be coupled; moreover, accurate prediction of swell at high shear rates is not possible.

Some researchers predicted annular swell using differential viscoelastic material behavior models. However, this technique over predicted the swell values. Attention was then focused on using a semi-empirical approach for simulation purposes.

Ajroldi (1978) used the above-mentioned approach for the prediction of effects of relaxation and sag on parison formation. Total strain on the particular section of the parison was assumed to be the sum of time dependent creep and recoverable strain.

Basu and Fernandez (1983) utilized a numerical technique to predict parison length with time. A generalized Jeffery's¹ model was used to describe the material behavior.

¹ Jeffery's model is used for small deformations. It is applied to the movement of rigid crystals embedded in a melt.

Deformation of a parison due to gravity was taken into account. They were able to predict the parison cross sectional area and temperature as a function of distance from the die.

This was the first attempt in which unsteady state heat transfer was combined with dynamics of parison sag and swell. This method also requires prior knowledge of rheological data.

Tanoue et al. (1996) used a numerical technique for parison profile estimation. A Giesekus² model was used as a constitutive equation in simulation and examined outer diameter, thickness and area swells obtained from extrudate swell. Tanoue et al. also developed a method for predicting parison thickness and outer diameter using the relation between swells. Their approach was based on dividing the parison formation process into two regions namely the extrudate swell region and parison formation region. The effect of drawdown was also taken into consideration. The relationship between the three swell values at low Weissenberg number (see section 5.5.1.2) was obtained by examining simulation results. By using these relationships, the swell values were predicted at high Weissenberg number (in the range of 50-300). This prediction procedure was then applied to the parison formation stage. The effect of the Weissenberg number on the three swell values is also discussed. The simulation results for thickness swell did not match the experimental results obtained by other researchers, such as Tan et al. (1979) and Kamal et al. (1981). Moreover, they did not take into account the effect of converging and diverging annular die on swell values at high shear rates which is not the case proved by Orbey and Dealy (1984). An error of 20% was observed in the parison formation process. This study was limited to one resin and die geometry.

Laroche et al. (1999) attempted the integrated modeling of the entire blow molding process. Earlier integration studies have been performed by Laroche et al. (1996, 1997) and DiRaddo et al. (1997). The parison formation process was modeled with an integral type constitutive equation for the sag behavior and a semi-empirical equation for the swell behavior. Good agreement was obtained between the numerical predictions and the experimental results. An optimization analysis was performed for minimizing part weight for a given uniform part thickness.

² Giesekus model is used to numerically describe the nonlinear behavior of polymer flows.

Modeling the parison formation with numerical methods, however, has the following limitations:

- limited accuracy due to simplifying assumptions,
- non-availability of a reliable constitutive equation,
- inability to handle the effects of parison programming,
- greater computational effort for online usage.

Recently, Huang and Liao (2002) used a back propagation neural network model for prediction of parison diameter and thickness swell. Unlike the numerical prediction techniques, the neural network technique requires a minimal number of assumptions. It needs no constitutive equation, can be used online and has a faster response. The effects of die temperature and flow rate on swell were also studied. Earlier DiRaddo and Garcia-Rejon (1993) used the same approach for predicting final part dimensions from initial parison dimensions and vice versa. For initial training of a neural network, the parison dimensions were predicted using the technique utilized by Eggen and Sommerfeldt (1996). Four different die temperatures and seven different flow rates were employed to obtain twenty-eight sets of swell data. Out of twenty-eight sets of data, twenty sets were used to train the model and the remaining eight were used for model testing and verification. Very good agreement between the predicted and experimental results was obtained. The effect of sag was accounted for in the whole process.

3.5 Summary

In this chapter, literature review on the parison formation process in extrusion blow molding (EBM) and various parameters affecting parison behavior was presented. Different techniques for offline and online estimation of parison dimensions as developed by various researchers over the years have also been highlighted.

The approach detailed in this thesis (Chapter 5) for parison length control (swell estimation) is different from the ones previously developed. This research is focused on the intermittent extrusion blow molding process, which, as compared to continuous extrusion, is difficult to control. In our work we study the effect of flow rate and die gap

on the parison length. Our technique for cycle-to-cycle control of parison length is not based on any of the approaches discussed above. Instead it relies on an initial set of experiments and simulation results. The technique developed was tested in real time on an actual intermittent extrusion blow molding machine.

A viscoelastic material is, as the name suggests, one that shows a combination of viscous and elastic effects. Under the action of an external force, a viscoelastic material like solids can partially retain elastic energy and at the same time like liquids can partially dissipate it.

Polymer melts are viscoelastic fluids. When they are subjected to mechanical work, they develop stresses, which unlike elastic solids do not immediately become zero when the load is removed. The time required for the stresses to relax is referred to as “relaxation time”.

Relaxation time is one of the most important parameters of a polymer melt. Various phenomena such as sag and swell are directly coupled to the relaxation time of the polymer. In this chapter, a new technique for online approximation of average relaxation time is discussed.

4.1 Methodology

Koopmans (1992b) studied the high density polyethylene resin (HDPE) to determine the effects of time dependency, cooling and sagging on the extrudate swell. He determined that shorter relaxation time corresponds to lower maximum swell value. In other words, the higher the relaxation time, the higher the swell.

In this thesis, the diameter and thickness swell are related to the relaxation time by means of Deborah and Weissenberg numbers. Mathematically, these dimensionless numbers are given by,

$$De = \frac{\lambda}{t} \text{ and } We = \frac{\lambda Q_{inst}}{Ah} \quad (4.1)$$

where,

De : Deborah number.

We : Weissenberg number.

λ : relaxation time (sec)

t : characteristic time of the material (sec)

Q_{inst} : instantaneous flow rate (mm³/sec)

A : cross sectional area (mm²)

h : die gap (mm)

In the approach developed in this thesis, the relaxation time is estimated by using a combination of Carreau model and Maxwell model to represent the stress retardation and stress relaxation during the flow of the polymer in the die. Stress relaxation outside the die is obtained by using simulation results (BlowView software), combined with Maxwell model.

To obtain the flow kinematics required by Maxwell model, the changes in the Carreau model viscosity caused by temperature and shear rate in the die were obtained by conducting an experiment on the machine. The resulting viscosity and shear rate values were then inputted into the Maxwell model to determine the amount of shear history that the material experienced during its flow in the die as a result of viscoelastic deformations. This shear history is responsible for the stress relaxation outside the die leading to time-dependent parison swell. The combination of inside and outside stresses were used to get an estimation of the average relaxation time.

4.2 Newtonian and Non-Newtonian fluids

Fluids, which exhibit constant viscosities independent of shear rate are called Newtonian fluids. Some examples of Newtonian fluids are water, syrups, oil. Their behavior is represented by a simple constitutive equation of type,

$$\tau = \mu \dot{\gamma} \quad (4.2)$$

where, τ is the shear stress (Pa), μ (Pa-sec) is the viscosity, and $\dot{\gamma}$ (sec⁻¹) is the shear rate. Fig 4.1 gives a viscosity versus shear rate curve for such fluids.

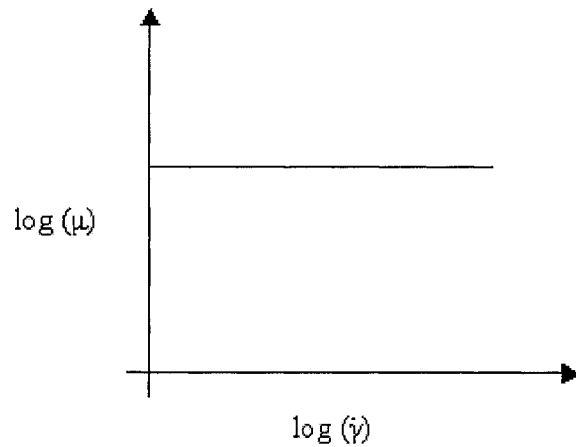


Figure 4-1 Relation between viscosity and shear rate for a Newtonian fluid.

Non-Newtonian fluids on the other hand have viscosities that depend on the shear rate. Cereal corn suspension in water, toothpaste, soap solutions, paint and, ketchup, fall under this category. This shear rate dependence of non-Newtonian fluids characterizes them into several types such as,

- pseudoplastic fluids (or shear-thinning fluids).
- dilatant fluids (or shear-thickening fluids).
- Bingham fluids (linear relationship of shear stress against shear rate).

Certain polymer fluids are shear-thinning fluids. For such fluids, the viscosity decreases with increasing shear rate. Fig 4.2 shows the viscosity curve of shear thinning fluids.

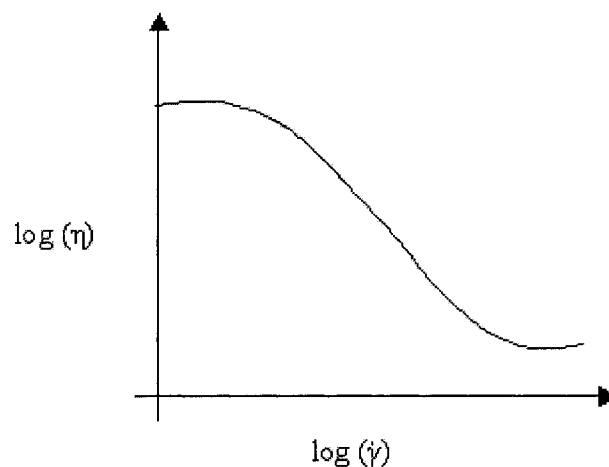


Figure 4-2 Relation between viscosity and shear rate for a shear thinning fluid

4.3 Carreau model

Many models have been proposed to fit the viscosity versus shear rate for non-Newtonian fluids. One such model was proposed by Carreau (1968). This model is a modification of the power-law model³. The main drawback of the power law model is its inability to fit the plateau region of the viscosity versus shear rate curve for non-Newtonian fluids. The Carreau model takes into account the limiting values of viscosities, and thus, fits the viscosity-shear rate data for a non-Newtonian fluid to a reasonable accuracy. Mathematically, it is given by,

$$\frac{\eta - \eta_0}{\eta_0 - \eta_\infty} = \left[1 + \left(\lambda \dot{\gamma} \right)^2 \right]^{\left(\frac{n-1}{2} \right)} \quad (4.3)$$

where η_0 is the zero shear viscosity, η_∞ is the upper limiting Newtonian viscosity, λ ⁴ is the time constant, and n is the power law index. The variation in the viscosity was obtained from an experiment conducted on the Placo machine as explained below.

4.3.1 Estimation of viscosity using Carreau model

Preliminary experiments were conducted on an intermittent extrusion blow-molding machine (Placo). The objective of the experiments was to determine the viscosity of the Carreau model for the polymer of interest (HDPE-DMDF6200) as it flowed through the channel (Fig 4.3).

³ A simple mathematical expression ($\eta = K(\dot{\gamma})^{n-1}$) describing the shear thinning behavior of polymers.

Here K is the consistency index, n is the power law index and $\dot{\gamma}$ is the shear rate. Power law model does a good job in fitting high shear rate viscosity data but does a poor job in fitting low shear rate viscosity data.

⁴ Lambda (λ), here is different from the relaxation time. In the Carreau model, lambda is a time constant dependent on the temperature of the melt, and represents the inverse of the shear rate where transition from Newtonian to shear thinning behavior occurs.

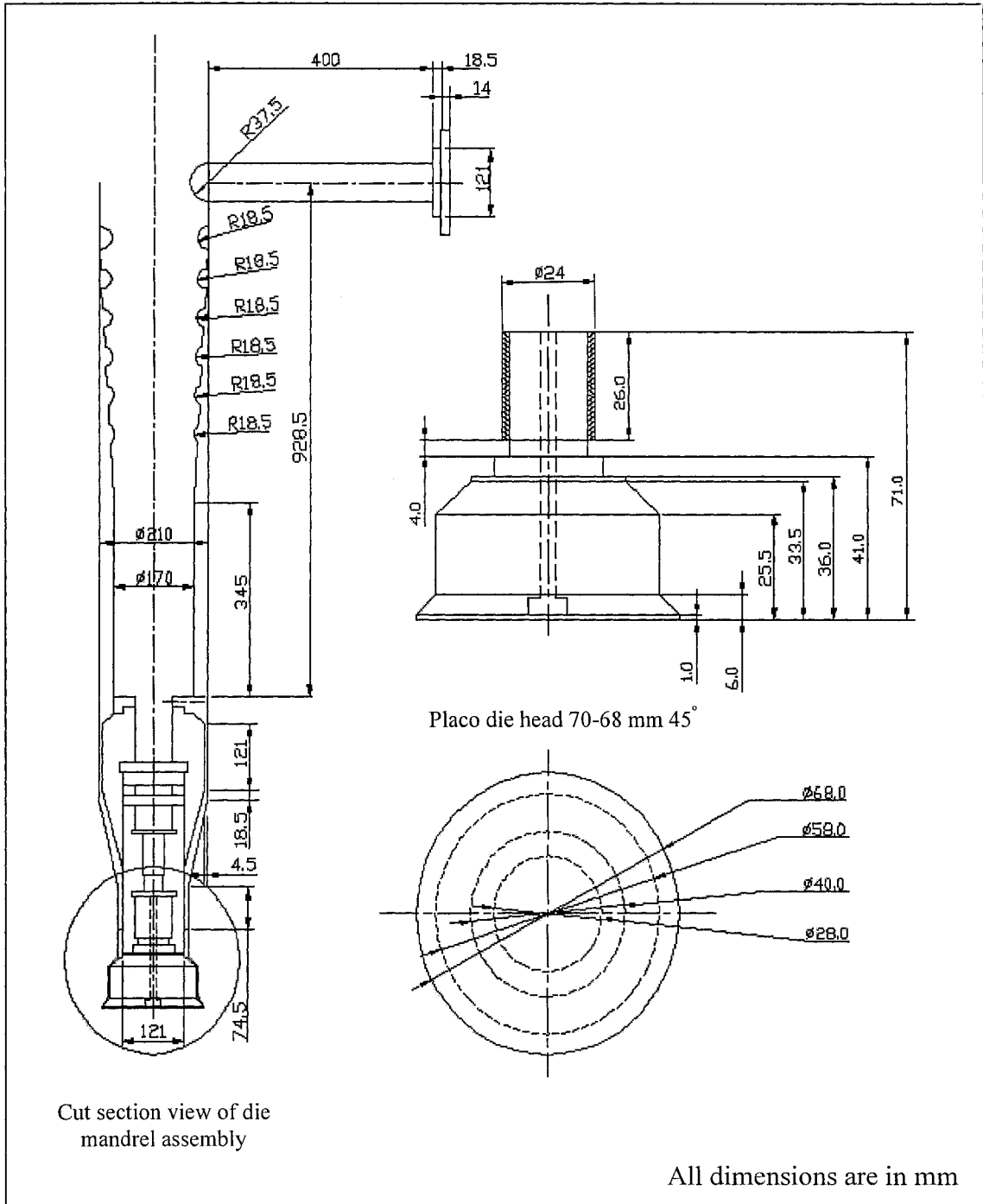


Figure 4-3 Cut section view of the flow channel

The extrusion time on the machine was set to 11.1 seconds. A parison (hollow tube of molten polymer) was extruded from a 68mm internal diameter annular diverging die. The

die gap opening was set to 2 mm. The extruded parison was pinched using a pinch-off mold (Fig 4.4), akin to the one used by Sheptak and Beyer (1965).

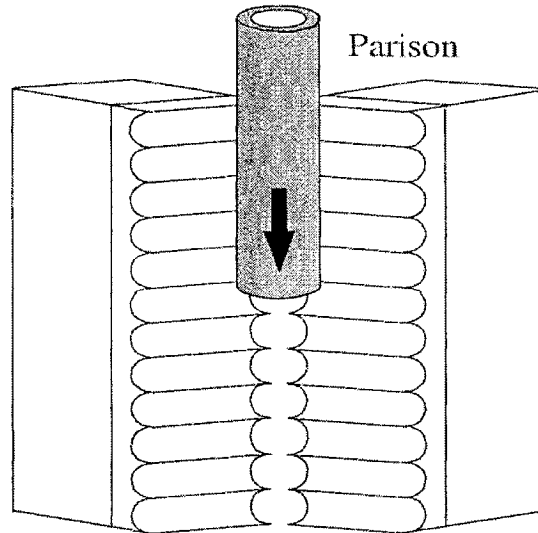


Figure 4-4 Pinch-off mold

The pinched parison once cooled was cut into three sections. Each section of the parison was then weighed and averaged to determine the average volumetric flow rate using formula,

$$m_g = \frac{w_{\text{sec}}}{t_{\text{ext}}} \quad (4.4)$$

where m_g is the mass flow rate of the polymer melt in g/sec, w_{sec} is the weight of the extruded parison in grams and t_{ext} is the extrusion time in seconds. Volumetric flow rate Q was then obtained by dividing m_g with density of the melt (761 Kg/m^3). The calculated parameters are listed in Table 4.1.

Table 4-1 Volumetric flow rate calculation for the extruded parison

Volumetric flow rate						
Parison weight (g) W_{sec}			Average weight (g)	t_{ext} (sec)	m_g (Kg/sec)	Q (mm ³ /sec)
Section-1	Section-2	Section-3				
271	229	349.3	283.1000	11.1	0.025504505	33514.46058
266.6	226.9	354.7	282.7333	11.1	0.025471471	33471.05318
269.3	228.8	350.7	282.9333	11.1	0.025489489	33494.72995
265.6	225	359.7	283.4333	11.1	0.025534535	33553.92186
265.8	225.8	361.6	284.4000	11.1	0.025621622	33668.35956
266.2	225.7	358.5	283.4667	11.1	0.025537538	33557.86799
266.3	225.6	360	283.9667	11.1	0.025582583	33617.0599
264.3	222.8	366.3	284.4667	11.1	0.025627628	33676.25181
265.8	225.4	361.4	284.2000	11.1	0.025603604	33644.68279
					Average Volumetric Flow Rate	33577.59862

The following physical and thermal properties of the resin (HDPE-DMDF6200) were obtained from the IMI materials database:

Resin: HDPE

Grade: DMDF 6200

Manufacturer: Petromont

Extrusion temperature: 170-210 °C

Density (melt) at 200 °C: 761 Kg/m³

Specific heat constant (melt): 2730 J/Kg.°C

Table 4-2 Carreau model parameters (Source: IMI material database)

CARREAU MODEL PARAMETERS	
Zero shear viscosity (η_0)	88401 Pa.sec
Time constant (λ)	27.1 sec
Power law index (n)	0.530
WLF ⁵ Reference temperature (T_{ref})	150 °C

⁵ The Williams-Landel-Ferry (WLF) equation is the function of the temperature that shift the viscosity from a given reference temperature.

For the experiments described, a 68 mm internal diameter and 70mm outer diameter die was used. The polymer material in the form of pellets was then fed into the hopper. As the pellets entered the screw section, they were melted by the shearing action of the rotating screw as well as due to the heat produced by the heaters placed around the barrel. The pellets, which were in the form of a melt, were now forced into the accumulator by the rotating action of the screw.

The accumulator is a cylinder with a piston-rod like attachment. When material flows from the screw to the accumulator, the piston retracts and creates a space to be filled by the material. When there is no more space left, the piston forces the melt through the die head in the form of an endless parison. Though the Placo machine has two accumulators and one direct feed section, but only one accumulator (A) was used in the study (Fig 4.5).

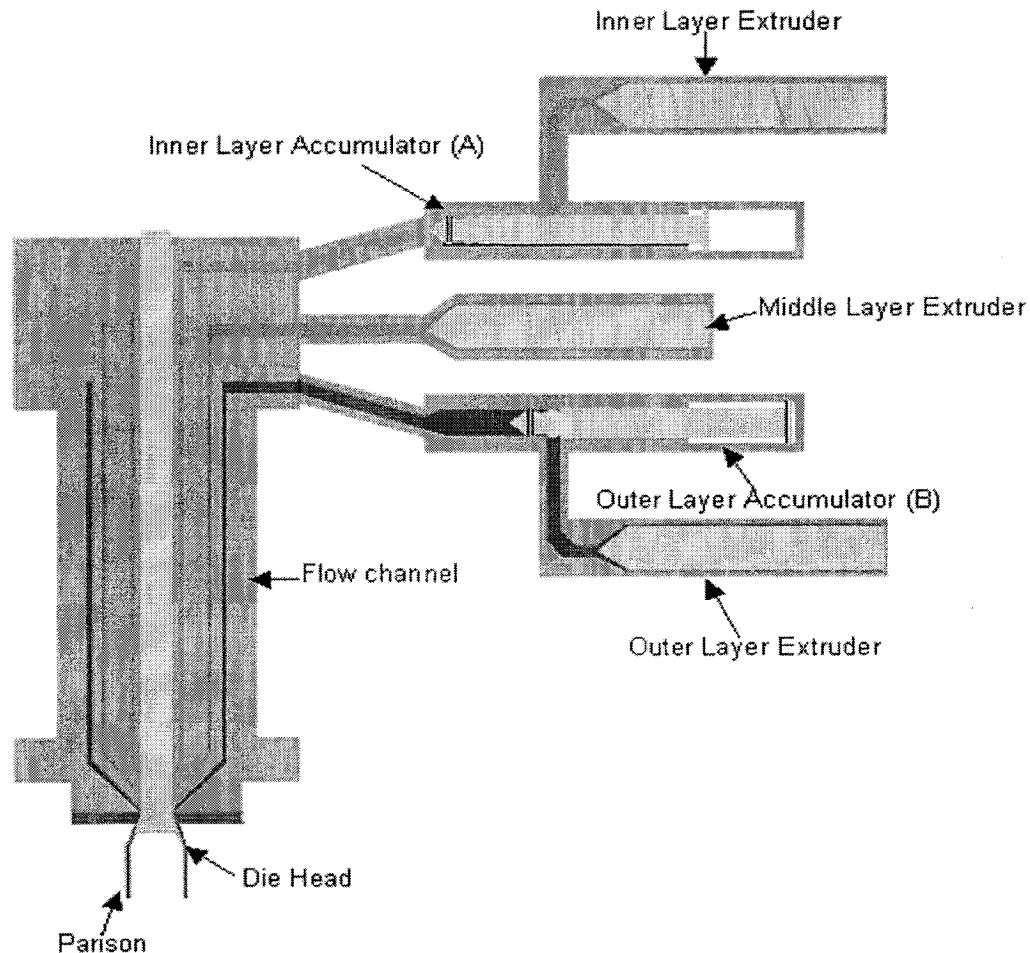


Figure 4-5 Flow channel and accumulator arrangement for the Placo machine

For the calculations described, the inertial effects were ignored. Earlier the region of interest was from the accumulator exit to the die exit (Fig 4.6), but was later limited to die entry to die exit. This is because the Maxwell model (with a single relaxation time) becomes insensitive to the magnitude of λ for long flow times ($t \gg \lambda$), due to the presence of the exponential term in this model (see section 4.4).

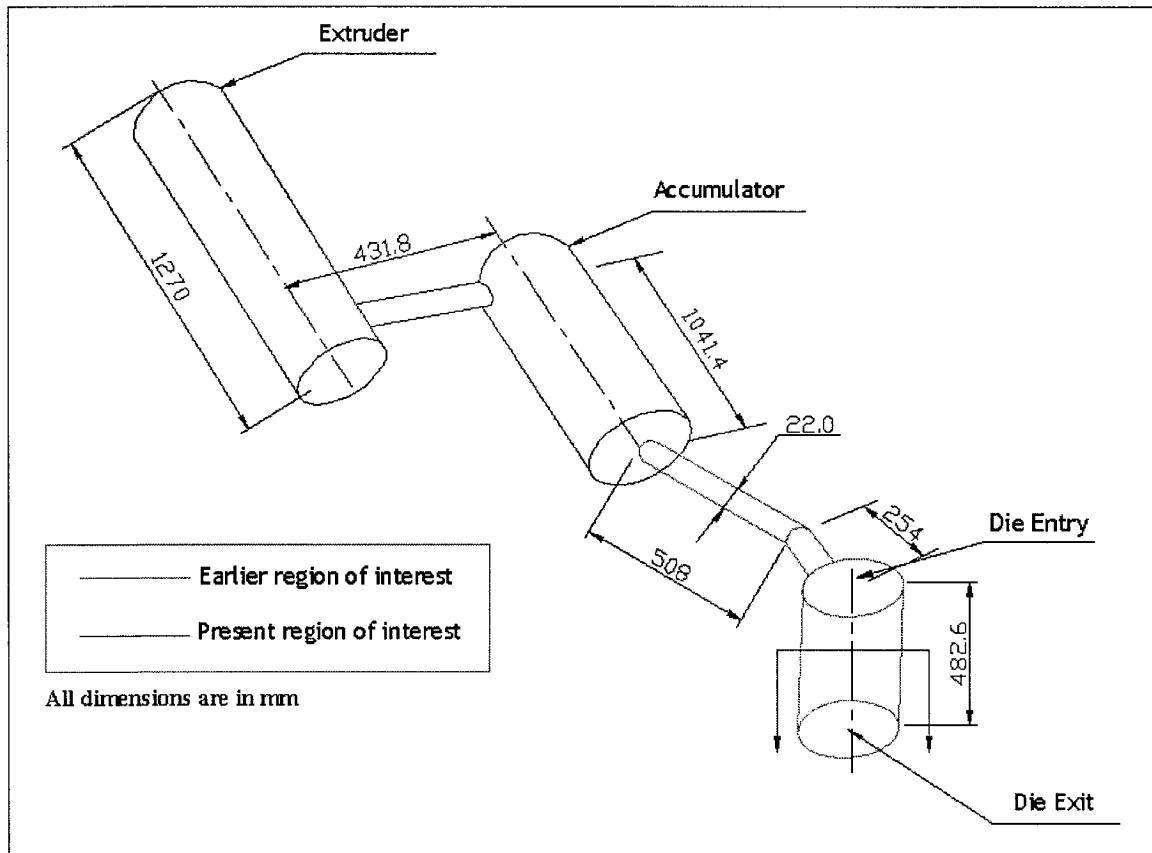


Figure 4-6 Path followed by melt from extruder to die exit

The flow of polymer melt around the die was assumed to be a non-Newtonian flow through an annular cross-section. The following formula was used to calculate the shear rate at all points along the die.

$$\dot{\gamma} = \left(\frac{2n+1}{n} \right) \left(\frac{2Q}{Th_i^2} \right) \quad (4.5)$$

where, $\dot{\gamma}$ is the shear rate at the wall at the region of interest, n is the power law index, Q is the volumetric flow rate, T is the width ($T = 2 * \pi * R$), h_i is the thickness ($R - r$) and, R and r are the outer and inner radii respectively.

Knowing the shear rate in the die, the viscosity was evaluated using the Carreau model (Eq. 4.3). Shear stress was then obtained by multiplying viscosity and the shear rate.

$$\tau = \eta \left(\dot{\gamma} \right)^n \dot{\gamma} \quad (4.6)$$

Two cases, namely, constant viscosity (Newtonian) and variable viscosity (Carreau model) were considered.

Flow time in the die, required by the Maxwell model, was calculated using following formula, by dividing the flow path into several segments:

$$t' = t'_{initial} + \frac{\left(\pi \left(R^2 - r^2 \right) \right) * L}{Q} \quad (4.7)$$

where t' is the time at any particular instant, $t'_{initial}$ is the initial time before entering a specific segment, R is the outer radius along die, r is the inner radius along the die, L is the distance along the die for each segment (taking die exit as reference) and, Q is the average volumetric flow rate.

The pressure drop along the flow was calculated using following formula:

$$\Delta p = \left(\frac{4n + 2}{n} \right)^n * \left(\frac{Q}{Th_i^2} \right)^n * \frac{2LK}{h_i} \quad (4.8)$$

where K , the consistency index (Pa.sec), is the value of viscosity at zero shear rate.

The amount of heat generated along the path due to shearing action was then calculated using,

$$q = Q^* \sum \Delta p \quad (4.9)$$

where, $\sum \Delta p$ is the total pressure drop and Q is the average volumetric flow rate

Now, since $q = mC_p \Delta T$

$$\Delta T = \frac{q}{mC_p} \text{ } ^\circ\text{C}. \quad (4.10)$$

Using the above formulas, the temperature increase due to melt shearing was found to be 0.679°C (Table 4.3). Consequently, the changes in the viscosity through the die caused by the temperature increase were negligible.

Table 4-3 Volumetric flow rate calculation for the extruded parison

Distance Along Die (L) mm	Outer Radius (R) mm	Inner Radius (r) mm	Shear rate ($\dot{\gamma}$) sec^{-1}	Viscosity (η) Pa-sec	Time (t') sec
36	35	20	9.2316	3543.3853	0.0000
33.5	35	20	9.2316	3543.3853	0.1930
25.5	35	29	39.7914	1783.2565	0.4804
6	35	29	39.7914	1783.2565	1.1810
1	35	34	1221.8311	356.6322	1.2133
0	35	34	1221.8311	356.6322	1.2197

$t-t'$	Shear stress (τ) Pa	Pressure Difference (Δp) Pa	Heat Generation (q) J/sec	Temperature Increase (ΔT) $^\circ\text{C}$
1.21972	32711.1614	8078.71539	47.4142	0.6796
1.02675	32711.1614	25851.8892		
0.73932	70958.3361	416095.7971		
0.03873	70958.3361	106691.23		
0.00645	435744.361	855362.6716		
0	435744.361			
	Sum ($\sum \Delta p$)	1412080.303		

4.4 Maxwell model

The Maxwell model is a type of mechanical model, which provides a method of describing viscoelastic behavior. It results from a direct combination of viscous and elastic behavior in one constitutive equation. The Hookean deformation is represented by

a spring and viscous behavior by a dashpot. Both spring and dashpot are connected in series as shown in Fig 4.7.

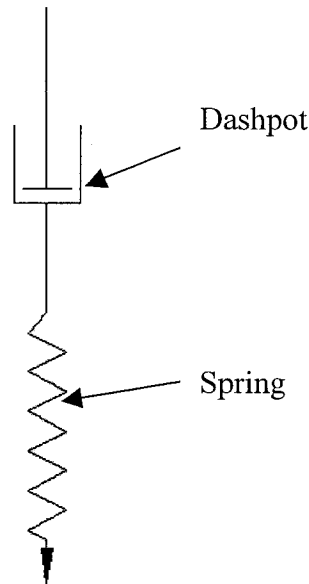


Figure 4-7 Maxwell model element

The Maxwell equation in its simplest form is given by (Bird, 1987):

$$\tau + \frac{\mu}{G} \frac{\partial \tau}{\partial t} = -\mu \dot{\gamma} \quad (4.11)$$

where τ , is the shear stress, μ is the viscosity, G is the elastic modulus, and $\dot{\gamma}$ is the shear rate.

For steady state motions ($\frac{\partial \tau}{\partial t} \rightarrow 0$), the above equation simplifies to the Newton's law of viscosity, and for sudden changes in stress ($t \rightarrow 0$), the time derivative term dominates the left side of the equation, and then, integration with respect to time gives Hooke's law with elastic modulus G .

Replacing $\frac{\mu}{G}$ by λ and μ by η_0 , equation (4.11) becomes an ordinary differential equation for τ .

$$\tau + \lambda \frac{\partial \tau}{\partial t} = -\eta_0 \dot{\gamma} \quad (4.12)$$

We replaced μ by η_0 since we are limited to small rates only.

Assuming a single Maxwell element and solving the ordinary differential equation (4.12) for τ we have,

$$\tau(t) = - \int_{-\infty}^t \left[\frac{\eta_0}{\lambda} e^{-\frac{-(t-t')}{\lambda}} \right] \dot{\gamma}(t') dt' \quad (4.13)$$

When written in this form, the Maxwell model says that the stress at the present time t depends on the rate of strain at time t as well as on the rate of strain at all past times t' , with a weighting factor (the relaxation modulus) that decays exponentially as one goes backwards in time (Bird, 1987).

The function $\left(\frac{\eta_0}{\lambda} \right) e^{-\frac{-(t-t')}{\lambda}}$ in the Maxwell model serves as the weighting function or memory function, and indicates how much of past deformation is remembered by the fluid at time t . In the actual case, the lower limit of the integral is not $-\infty$, but 0 because the flow commenced at $t' = 0$.

4.4.1 Stress retardation/stress relaxation inside the die

Equation (4.13) was further simplified as shown in the following derivation:

$$\tau(t) = - \int_{-\infty}^t \left[\frac{\eta_0}{\lambda} e^{-\frac{-(t-t')}{\lambda}} \right] \dot{\gamma}(t') dt'$$

Taking $v = e^{-\frac{-(t-t')}{\lambda}}$ and $u = \dot{\gamma}(t')$ and using integration by parts $\left(\int u dv = uv - \int v du \right)$ we have,

$$du = \frac{d\dot{\gamma}(t')}{dt'} dt' \quad (4.14)$$

$$dv = e^{-\frac{(t-t')}{\lambda}} dt' \quad (4.15)$$

$$v = \int e^{-\frac{(t-t')}{\lambda}} dt' = \lambda e^{-\frac{(t-t')}{\lambda}} \quad (4.16)$$

Substituting Eqs. (4.14), (4.15) and (4.16) into (4.13), for variable shear rate case we have,

$$\tau = -\frac{\eta_0}{\lambda} \left[\dot{\gamma}(t') * \lambda * e^{-\frac{(t-t')}{\lambda}} \Big|_0^t - \int_0^t \lambda e^{-\frac{(t-t')}{\lambda}} \frac{d\dot{\gamma}(t')}{dt'} dt' \right]$$

$$\tau = -\eta_0 \left[\dot{\gamma}(t')_{t'=t} - \dot{\gamma}(t')_{t'=0} * e^{-\frac{t}{\lambda}} - \int_0^t e^{-\frac{(t-t')}{\lambda}} \frac{d\dot{\gamma}(t')}{dt'} dt' \right] \quad (4.17)$$

Note: $t' = 0$ and $t' = t$ represents conditions at the die entry and exit respectively.

And for constant shear rate case Eq. (4.17) can be simplified to,

$$\tau = -\eta_0 \left[\left(\dot{\gamma}(t) - 1 \right) * e^{-\frac{t}{\lambda}} \right] \quad (4.18)$$

The approach developed in this thesis aimed to find an average relaxation time representing the polydisperse nature of the polymers (featuring multiple relaxation times). In the search for this average value we focused on a range between 0.1 s and the longest relaxation time defined for polydisperse polymers. For the resin used (HDPE DMDF-6200), the longest relaxation time was obtained using the following equation (Dealy and Kurt, 1990).

$$J_0 = \frac{\sum G_K \tau_K^2}{\left(\sum G_K \tau_K \right)^2} \quad (4.19)$$

where G_K , is the relaxation modulus and τ_K is the shear stress. These values were obtained from the IMI materials database.

Table 4-4 Relaxation spectrum data (Source: IMI materials database)

Relaxation Modulus (G_K)	Shear Stress (τ_K)	τ_k^2	$G_k \tau_k^2$	$G_K \tau_K$
0.208593	0.00714	5.09796E-05	1.0634E-05	0.001489354
0.07385	0.049979	0.0024979	0.00018447	0.003690949
0.03031	0.349854	0.122397821	0.003709878	0.010604075
0.01061	2.44898	5.99750304	0.063633507	0.025983678
0.003034	17.14286	293.877649	0.891624787	0.052011437
0.001119	120	14400	16.1136	0.13428

$$\sum G_K \tau_K^2 = 17.07 \quad (4.20)$$

$$\left(\sum G_K \tau_K\right)^2 = 0.052 \quad (4.21)$$

$$\therefore J_0 = \frac{17.07276}{0.052011} = 328.25 \quad (4.22)$$

The longest relaxation time, $\lambda = \frac{\eta_0}{G} = \eta_0 * J = 29.01 \text{ sec}$ (4.23)

Equation (4.17) is the equation for stress retardation (for an imposed shear rate) and simultaneous stress relaxation during the flow in the die. In other words, it represents the stress relaxation that takes place when the melt flows from die entry to die exit for an imposed shear rate. The basic idea is that by using this equation, we can determine the cumulative shear stress at the exit corresponding to different relaxation times.

Different cases were studied for the stress relaxation,

- variable shear rate from die entry to die exit
- constant shear rate from die entry to die exit
- variable shear rate with variable viscosity from die entry to die exit.

Of all the cases mentioned above, the variable shear rate with variable viscosity from die entry to the die exit gave reasonable results in terms of sensitivity with respect to the relaxation time. Table 4.5 lists the shear stress values corresponding to different relaxation times at the die exit for the case mentioned.

Table 4-5 Stress relaxation from die entry to die exit

Relaxation time (sec)	Shear Stress (Pa)
0.1	-188106.18
0.5	-90392.06
1	-61459.22
2	-37289.41
3	-26692.80
4	-20771.58
5	-16996.17
6	-14380.51
7	-12461.85
10	-8898.55
20	-4555.10
29	-3164.65

4.4.2 Stress relaxation outside die

On exiting the die, the parison swells in both the planar and longitudinal directions to recover from the imposed shear and extensional deformations during the flow inside the die. After emerging from the die, there is no shear rate imposed on the parison; so, the Eq.4.12 is reduced to:

$$\tau + \lambda \frac{d\tau}{dt} = 0 \quad (4.24)$$

or:

$$\tau = \tau_0 e^{-t/\lambda} \quad (4.25)$$

This equation shows how the stress is relaxed outside the die in an exponential manner, where τ_0 is the stress accumulated inside the die. This equation is better suited for monodisperse polymers (narrow MWD). For blow molding grade polymers, the relaxation phenomena occurs slower than what is predicted by this model because of polydispersity (broad MWD). So, we decided to use time dependent swell values collected in this thesis in combination with the original definition of the Maxwell model (Fig 4.7) to represent the relaxation phenomena for polydisperse polymers. According to Fig 4.7, the overall stress in a Maxwell element is the sum of individual stresses (for spring and dashpot):

$$\tau = \gamma * G + \mu * \frac{\partial \gamma}{\partial t} \quad (4.26)$$

This equation requires the parison deformation ($\dot{\gamma}$) and the rate of deformation ($\partial \dot{\gamma} / \partial t$) as a function of time outside the die. The overall deformation of the parison can be represented by (Agassant, 1991):

$$\gamma = \sqrt{I_2} \quad (4.27)$$

where I_2 is the second invariant of the strain tensor. For a 3-dimensional case, this tensor can be given by,

$$\begin{bmatrix} l_1 & 0 & 0 \\ 0 & l_2 & 0 \\ 0 & 0 & l_3 \end{bmatrix} \quad (4.28)$$

Here l_1 , l_2 and l_3 are the principle strains and are solutions of the characteristic equation,

$$\lambda^3 - I_1 \lambda^2 + I_2 \lambda - I_3 = 0 \quad (4.29)$$

where I_1 , I_2 , and I_3 are the invariants of the strain tensor defined as:

$$I_1 = l_1 + l_2 + l_3$$

$$I_2 = l_1 l_2 + l_2 l_3 + l_3 l_1$$

$$I_3 = l_1 l_2 l_3$$

In the case of an extruded parison, we simplified the case by assuming a lay-flat geometry. As a consequence, a parison can be represented by a rectangular prism (brick) where the principle strains are defined as,

$$l_1 = \frac{h_p}{h}, \quad l_3 = \frac{D_p}{D} \quad \text{and} \quad l_2 = \frac{1}{l_1 * l_3} \quad (4.30)$$

h_p , D_p are the thickness and diameter of the parison (accounting for swell).

h , D are the die gap and outside die diameter.

Note: the definition of the l_2 comes from the conservation of the volume ($I_3 = 1$).

We relied on simulation results (swell prediction) obtained using BlowView simulation software for the measurement of these values. The various inputs for the simulation were,

- extrusion time, 11.1 seconds
- flow rate, $Q = 25.5$ g/sec
- 68/70 mm diverging die
- constant die gap, 2mm.

Since the bottom of the parison is not affected by gravitational forces, a single point (node #1) at the bottom of the parison was located and the predicted values of diameter and thickness swell as a function of time for this node were collected as the parison was virtually extruded using BlowView software.

It should be mentioned that BlowView accounts for multiple relaxation times and could represent the relaxation phenomena for polydisperse polymers. On validating simulation results, we found that the simulation was overestimating the thickness swell and underestimating the diameter swell, but since the length prediction was accurate, the product of the two swell values, which is the area swell, was found to be accurate enough.

The results obtained from the simulation were,

- parison diameter
- parison thickness

The parison dimensions as a function of time could also be estimated by an experimental technique as outlined below. However, the complexity of these experiments surpasses the time allocated for this thesis.

The technique for experimental estimation of parison dimension is similar to the one used by Kalyon (1980). The parison could be extruded into oil having the same density and temperature as that of the melt. Since there will be no density variations, the swelling of the polymer would be maximum (complete relaxation). The whole process could be recorded by a camera and the film could be analyzed to determine the parison dimensions (diameter swell) at the point of interest. The evolution of the parison length as a function of time could be used to approximate the thickness swell. Table 4.6 gives the simulation results.

Table 4-6 Parison dimensions as a function of time

Time	D_p (mm)	h_p (mm)	L_p (mm)
1	83.72	5.20	28.42
2	85.94	5.40	52.09
3	87.23	5.52	71.65
4	87.98	5.60	92.67
5	88.45	5.66	110.19
6	88.74	5.70	129.53
7	88.94	5.73	146.12
8	89.09	5.75	164.26
9	89.20	5.77	179.91
10	89.30	5.79	197.21
11.1	89.39	5.81	213.34
58.2	90.01	5.95	198.4

Table 4-7 Principle strains and overall deformation

l_1	l_3	l_2	$\dot{\gamma}$
2.606	1.196	0.321	2.0813
2.702	1.227	0.301	2.1218
2.763	1.246	0.2903	2.1467
2.803	1.256	0.2837	2.1625
2.831	1.263	0.2795	2.1730
2.850	1.267	0.2766	2.1802
2.865	1.270	0.2746	2.185
2.877	1.272	0.2730	2.1899
2.887	1.274	0.2717	2.1934
2.896	1.275	0.2705	2.1965
2.90577	1.277	0.2694	2.1995
2.975	1.285	0.2614	2.2224

The Maxwell model (Eq.4.26) is used to estimate the stress relaxation outside the die. The stresses obtained for each time interval (assuming various relaxation times) were

summed and plotted along with the data obtained for stress relaxation inside the die.

Table 4.8 gives the values obtained for the stress relaxation outside the die.

Table 4-8 Stress relaxation outside die (Eq.4.26)

Modulus (G) Pa	884010	88401	44200.5	29467	17680.2	14733.5	12628.71	8840.1	3048.31
Relaxation time (sec)	0.1	1	2	3	5	6	7	10	29
Stress Relaxation (for each time interval (1s increment))	1870860	214880.5	122881.6	92215.3	67682.3	61549.0	57168.1	49282.5	37227.5
	1879325	191151.9	97364.5	66102.0	41092.0	34839.6	30373.5	22334.6	10045.2
	1899920	191969.6	97083.5	65454.8	40151.8	33826.1	29307.7	21174.6	8741.3
	1913113	192570.5	96984.8	65122.9	39633.4	33261.0	28709.3	20516.3	7991.2
	1921880	193019.8	96972.0	64956.1	39343.4	32940.2	28366.5	20133.8	7548.2
	1928042	193384	97014.1	64890.8	39192.2	32767.5	28178.5	19918.2	7290.4
	1932654	193695.4	97086.6	64883.7	39121.3	32680.7	28080.3	19799.5	7140.5
	1936319	193971	97173.8	64908.1	39095.5	32642.4	28033.0	19736.1	7052.4
	1939386	194220.4	97266.7	64948.8	39094.5	32630.9	28014.1	19703.8	6999.5
	1942052	194448.9	97359.8	64996.8	39106.4	32633.8	28010.5	19688.6	6966.6
	1944657	194681.3	97460.5	65053.5	39128.0	32646.6	28017.0	19683.8	6944.5
1964704	196509.1	98276.1	65531.7	39336.2	32787.3	28109.6	19689.6	6817.7	
Sum	23072913	2344502	1192924.1	809064.6	501977.0	425205.2	370368.1	271661.4	120764.9

Fig 4.8 shows the stress values inside and outside the die plotted on the same scale. As can be seen from the graph, the stresses outside the die are higher than those inside. Our assumption was that they would fall on the same scale and would show a crossover point representing the average relaxation time. Since this did not happen due to the numerous assumption made by using Maxwell model inside the die, we had to normalize the stress values and use a different approach to estimate the average relaxation time.

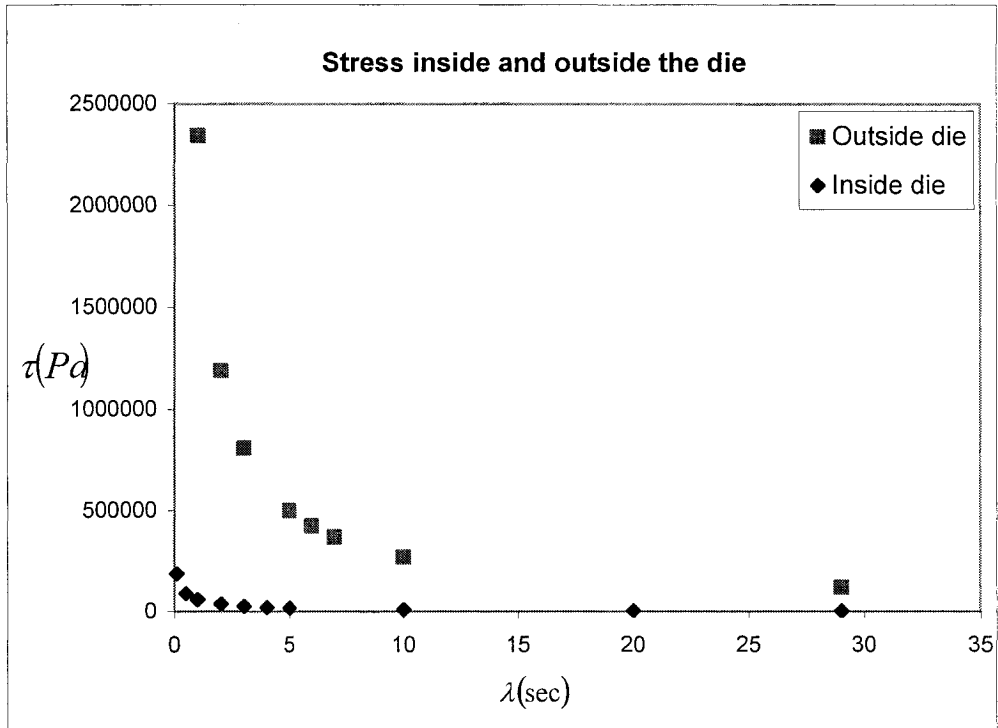


Figure 4-8 Stress relaxation and retardation inside and outside die

For the normalization, the stress values outside the die at different time intervals (0.1 to 11 sec) were subtracted from the sum and then divided by the sum to show how the stress relaxes. This curve is representative of time dependent swell (outside the die) for a polydisperse polymer. Once compared with the stress relaxation curve (outside the die) obtained by Maxwell model for monodisperse polymers, an average relaxation time can be estimated. Table 4.9 and Table 4.10 lists the normalized stress values for polydisperse and monodisperse assumptions (Eqs. 4.26 and 4.25, respectively).

Table 4-9 Normalized stress values for flow outside the die (polydisperse: Eq. 4.26)

		Stress Relaxation (τ/τ_0) – Outside the die (normalized)								
$t \backslash \lambda$		0.1	1	2	3	5	6	7	10	29
0		1	1	1	1	1	1	1	1	1
1		0.918	0.908	0.896	0.886	0.865	0.855	0.845	0.818	0.691
2		0.837	0.826	0.815	0.804	0.783	0.773	0.763	0.736	0.608
3		0.755	0.744	0.733	0.723	0.703	0.693	0.684	0.658	0.536
4		0.672	0.662	0.652	0.642	0.624	0.615	0.606	0.582	0.470
5		0.588	0.580	0.571	0.562	0.545	0.538	0.530	0.508	0.407
6		0.505	0.497	0.490	0.482	0.467	0.461	0.454	0.435	0.347
7		0.421	0.415	0.408	0.402	0.389	0.384	0.375	0.362	0.288
8		0.337	0.332	0.327	0.322	0.312	0.307	0.302	0.289	0.229
9		0.253	0.249	0.245	0.241	0.234	0.230	0.227	0.217	0.171
10		0.169	0.166	0.164	0.161	0.156	0.153	0.151	0.144	0.113
11.1		0.085	0.083	0.082	0.080	0.078	0.077	0.075	0.072	0.056

Table 4-10 Normalized stress values outside the die (monodisperse: Eq. 4.25)

		Stress Relaxation (τ/τ_0) – Outside the die (normalized)								
$t \backslash \lambda$		0.1	1	2	3	5	6	7	10	29
0		1	1	1	1	1	1	1	1	1
1		4.54E-05	0.367	0.6065	0.7165	0.8187	0.8464	0.8668	0.9048	0.9661
2		2.06E-09	0.135	0.3678	0.5134	0.670	0.7165	0.7514	0.8187	0.9333
3		9.36E-14	0.049	0.2231	0.3678	0.5488	0.6065	0.6514	0.7408	0.9017
4		4.25E-18	0.018	0.1353	0.2635	0.4493	0.5134	0.5647	0.670	0.8711
5		1.93E-22	0.0067	0.0820	0.1888	0.3678	0.4345	0.4895	0.6065	0.8416
6		8.76E-27	0.0024	0.0497	0.1353	0.3011	0.3678	0.4243	0.5488	0.8131
7		3.98E-31	0.0009	0.0301	0.0969	0.2465	0.3114	0.3678	0.4965	0.7855
8		1.8E-35	0.00033	0.0183	0.0694	0.2018	0.2635	0.3189	0.4493	0.7589
9		8.19E-40	0.00012	0.0111	0.0497	0.1652	0.223	0.2764	0.4065	0.7331
10		3.72E-44	4.54E-05	0.0067	0.0356	0.1353	0.1888	0.2396	0.3678	0.7083
11.1		6.21E-49	1.51E-05	0.0038	0.0247	0.1086	0.1572	0.2048	0.3295	0.6819
29		1.1E-126	2.54E-13	5.04E-07	6.34E-05	0.0030	0.00796	0.0158	0.0550	0.3678
58.2		1.7E-253	5.3E-26	2.3E-13	3.76E-09	8.81E-06	6.13E-05	0.0002	0.00296	0.1344

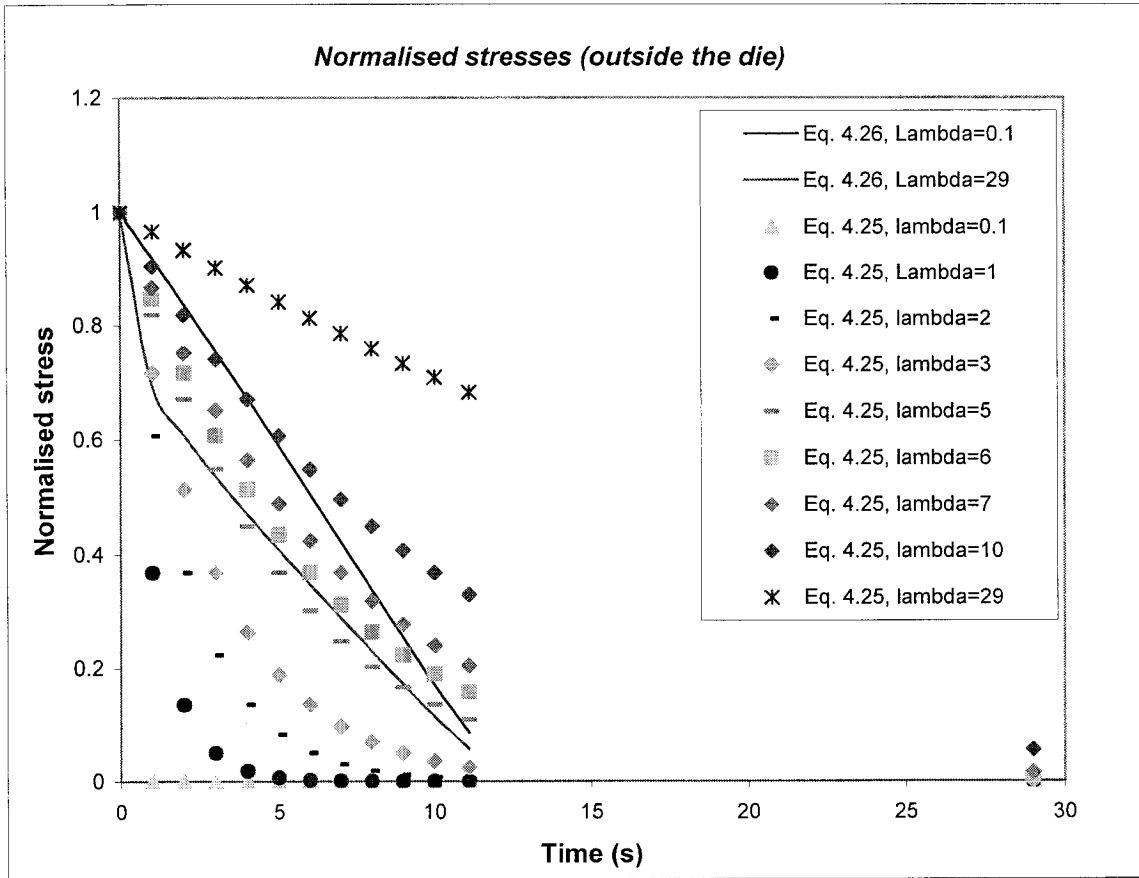


Figure 4-9 Normalized stress values (outside the die) using Eqs. (4.25) and (4.26)

The results for the normalized stresses were then plotted on the same graph as shown in Fig 4.9. As can be seen, the normalized stress relaxation using both equations shows the same trend for some values of relaxation times. The two curves (black and grey, upper and lower) represent the stress relaxation outside the die for relaxation times of 0.1 and 29 seconds (polydispersive). On plotting the stress relaxation for the monodisperse case, we observe that the points corresponding to relaxation times of 6 and 7 seconds fall inside the stress relaxation curves for the polydispersive case. Hence, it is concluded that the average relaxation time for the resin is about 6 seconds.

4.5 Summary

The value of average relaxation time for a polydispersive resin (HDPE) is determined. The stress relaxation and retardation of the polymer molecules inside the die is represented by a combination of Carreau and Maxwell models. For stress relaxation outside the die, a combination of simulation results and Maxwell model is used. We obtained a relaxation time of about 6 seconds for the resin mentioned.

The effect of temperature and shear rate on viscosity was also studied. Flow inside die is an isothermal process. Viscosity at extrusion temperature 210 °C was used in the study. Change in viscosity due to viscous heating was found to be negligible.

5.1 Introduction

This chapter outlines a new approach for online estimation of parison length in intermittent extrusion blow molding. Parison length control in intermittent extrusion blow molding is a complicated process as the extruded parison is subjected to the simultaneous effect of swell and sag, which oppose each other in terms of parison length. Moreover, between each run the rheological properties of the melt are altered as resin gets some time to relax. Therefore, each parison is different from the last extruded one even though the operating conditions remain the same.

On any extrusion blow molding machine, parison length can be adjusted by varying either the resin flow rate or the die gap. Both of these cases are considered in the approach developed in this thesis.

5.2 Material

One high density polyethylene resin (HDPE DMDF-6200) was used for the study. The reason for choosing this resin was based on the fact that HDPE is the material most commonly used for extrusion blow molding. Table 5.1 lists the rheological properties of the resin used. Though only one resin is used for the study, the approach developed is generic, i.e., it can be used for any resin and for any machine.

Table 5-1 Resin properties (Source: IMI material database)

Type	HDPE
Grade	DMDF-6200
Manufacturer	PETROMONT
Extrusion Temperature	170-260 °C
Melting Point	132 °C
Density (Solid)	955 Kg/m ³
Density(melt @ 200° C)	761 Kg/m ³
Melt index	0.35 dg/min

5.3 Machine details

A 3-Dimensional multilayer Placo intermittent extrusion blow molding machine (Fig 5.1) was used in the study. The machine could be run in both manual and automatic modes. The main objective of using the machine was to establish the accuracy of the approach developed.

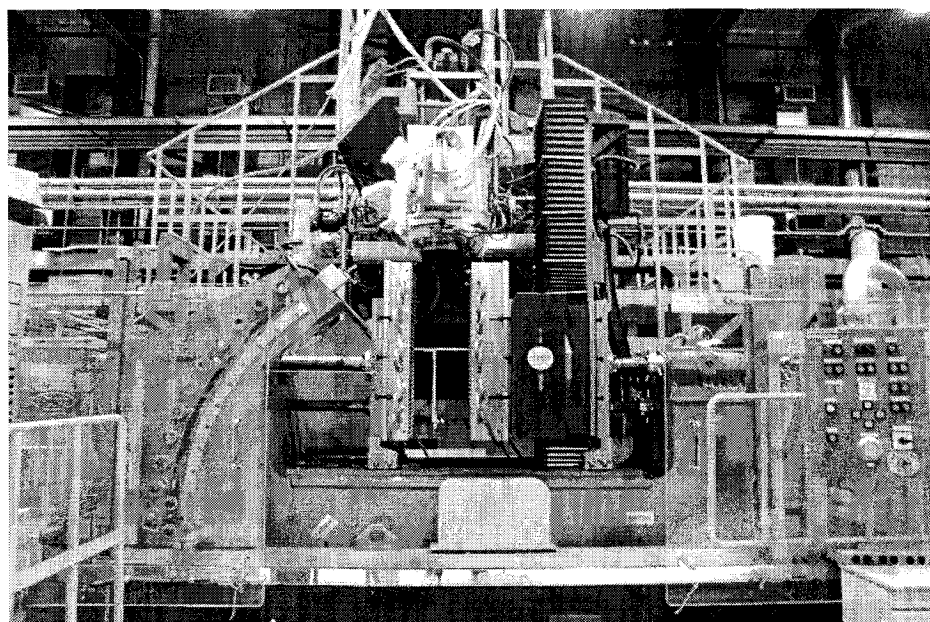


Figure 5-1 Placo intermittent extrusion blow molding machine

Of the three extruders (A, B and C) (Fig 4.5) available on the machine, two are connected to the accumulators. The other extruder (C) is used for directly transporting the less viscous adhesive without the need of an accumulator. Before material is transported to the annular die, it flows through a short cylindrical section. The mold on the machine can be inclined at an angle to produce irregular symmetrical shaped containers.

For our purpose, only one of three available extruders was used (Extruder A). The mold (Fig 5.2) used was analogous to the one used by Sheptak and Bayer (1965) for their studies on parison behavior. The end product of the experiment was a pinched parison (Fig 5.3).

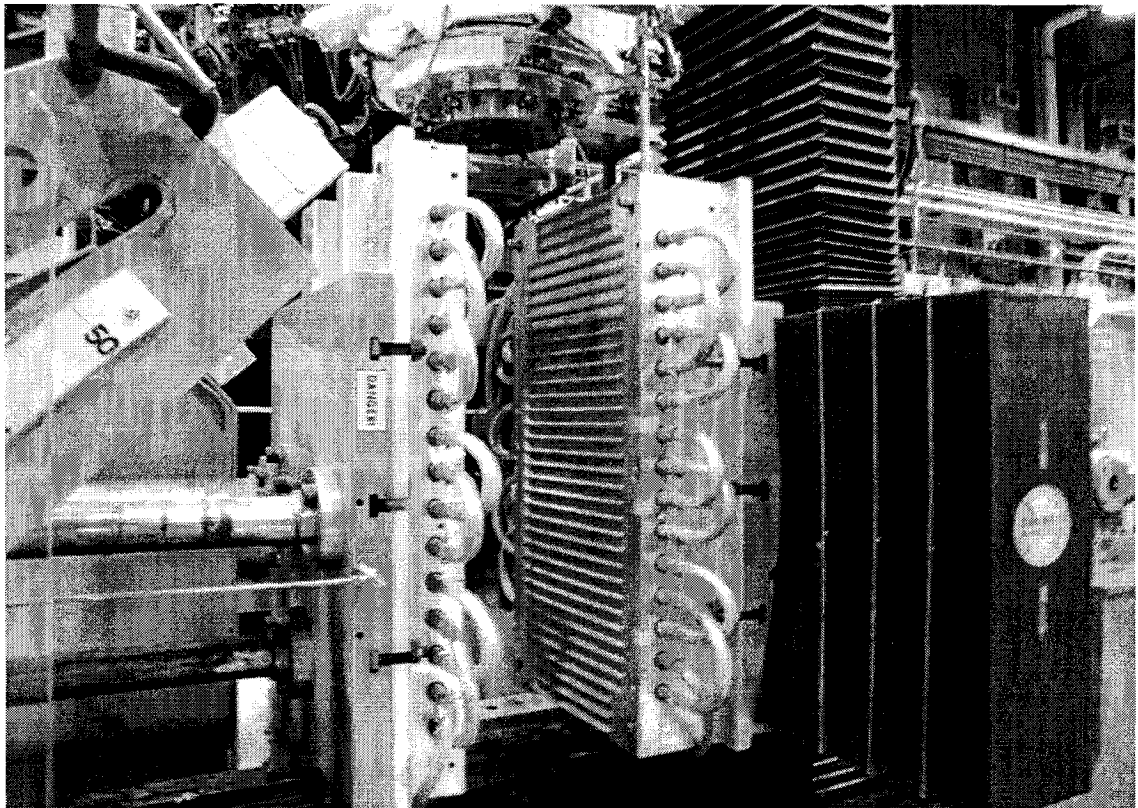


Figure 5-2 Pinch-off mold used in the study

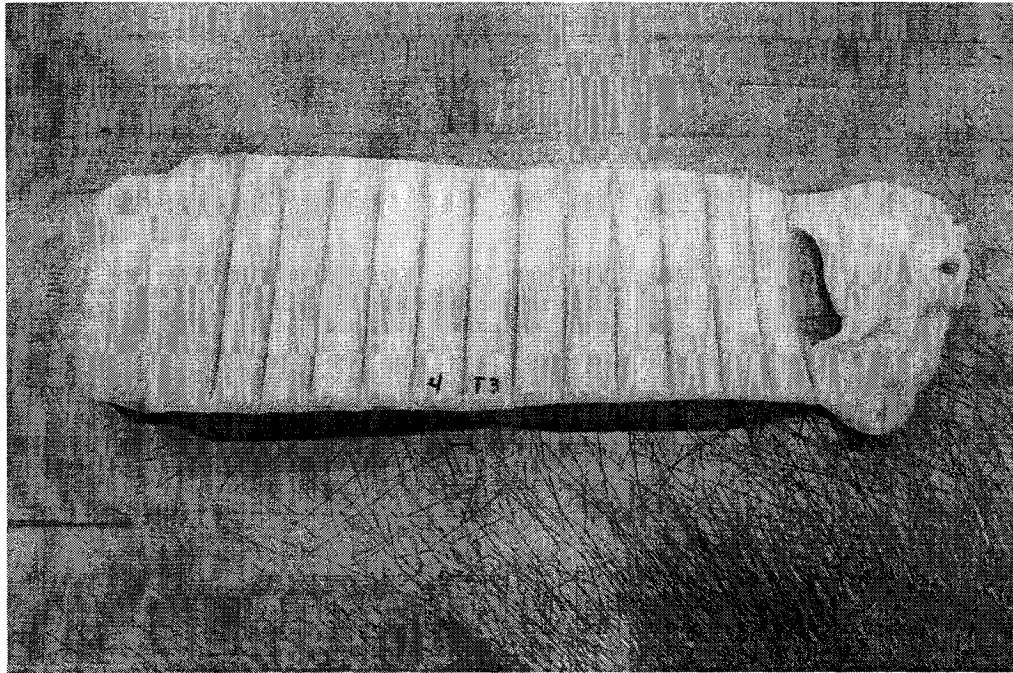


Figure 5-3 Pinched parison

5.4 Factors affecting parison length

The dimensions of the extruded parison are affected by the simultaneous phenomena of swell and sag. Swell is defined as the increase in the cross sectional area of the extruded parison.

Sag on the other hand is the time dependent stretching of the parison, and it is caused by the gravitational forces acting on the freely suspended parison. Swell and sag oppose each other. Parison swell is affected by a number of factors such as shear rate, melt temperature, die geometry, time, molecular weight of the resin, etc. A complete description of the factors affecting parison behavior can be found in chapter three.

5.5 Methodology

The simulation results are generally different from the experimental observations. The main causes of this discrepancy are:

- Material properties do not remain the same throughout the process.

- Actual operating conditions do not match the ones that were input into the simulation.
- Simplified simulation models.

If the simulation results are tuned to match the actual real world sensor output then the simulation can be used as a generalized “*soft sensor*”. A soft sensor is a system that allows measuring process variables that are not readily accessible. For example, the internal temperature of a sheet of plastic during heating can be predicted by using the surface temperature of the sheet and the heater temperature once a model of the system has been developed. The model can predict with good precision the temperature at any depth in the sheet, which is not measurable by normal techniques. One such technique was developed for the thermoforming process by Girard et al. (2003).

In our case, it is found that the thickness swell (the parameter which is obtained from the simulation) was causing the variations between the observed and simulation length of the parison. An equation of sigmoid type was fitted to the simulation results (both diameter and thickness swell) and subsequently tuned to match experimental observation. This tuning was done by adjusting one parameter of the equation, thereby moving the whole curve up and down on the y-axis, passing through the experimental swell point and thus giving a parison of required length

Intermittent extrusion blow molding features the flow rate variation during parison formation. This implies that the thickness and diameter swell, affected by the flow rate and die gap will be different along the parison.

This work is divided into two parts. The objective of part one is to estimate a flow rate, which will give a parison length of 550mm for an extrusion time of 9.5 seconds. In the second part, it is shown that the methodology is equally applicable to the case where both the extrusion time and flow rate are set by the operator while the die gap is the adjustable parameter on the machine to obtain a target length (e.g., 550mm). The flow chart (Fig 5.4) gives the complete description of the approach for the flow rate scenario.

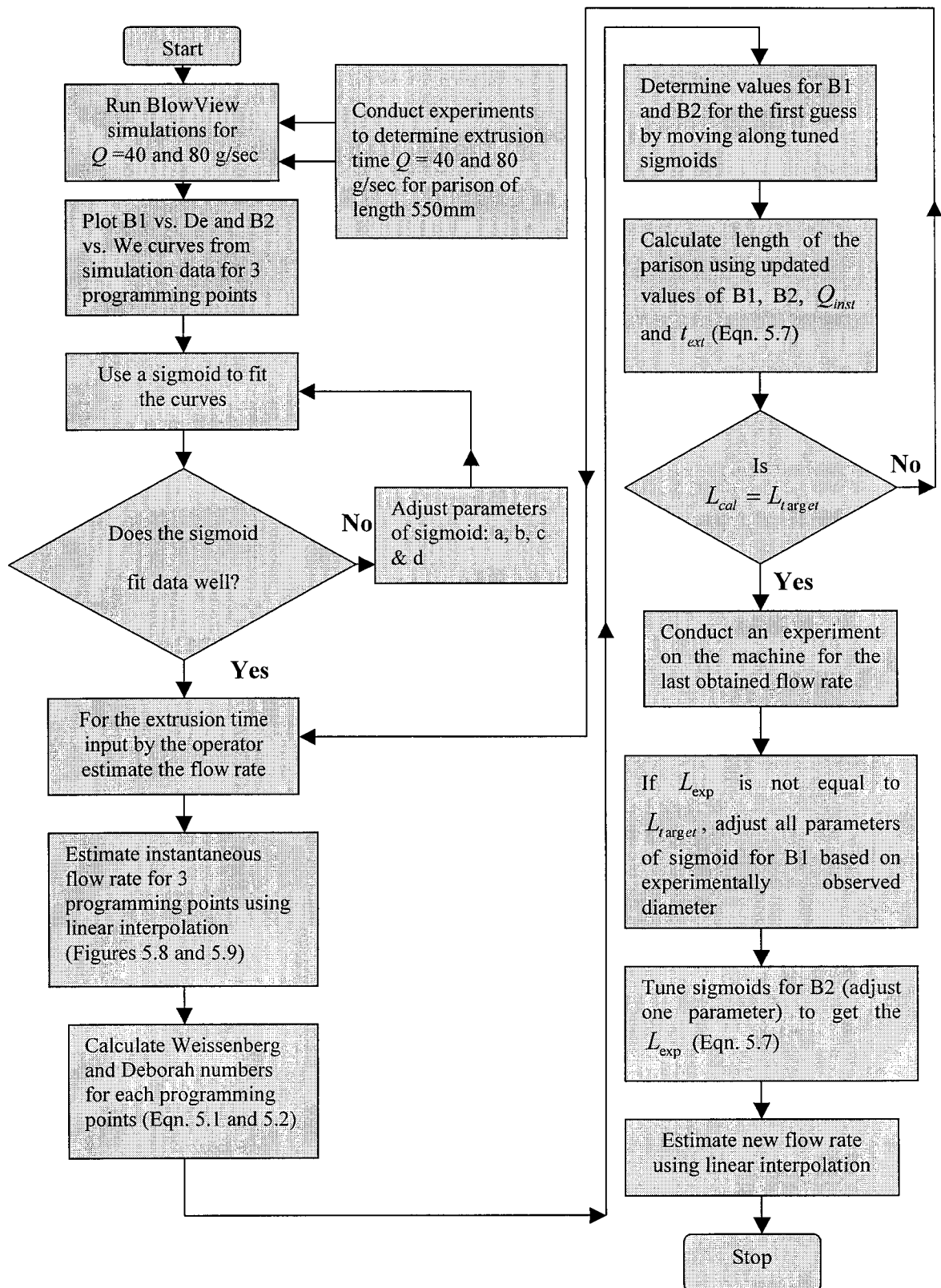


Figure 5-4 Methodology for parison length control

5.5.1 Flow rate scenario

5.5.1.1 Experimentation

Two experiments were conducted on the Placo intermittent extrusion blow molding machine to obtain the parison length evolution for a flow rate of 40g/sec and 80g/sec.

The input parameters for the experiments were:

- accumulated mass flow rate ($Q = 40$ and 80g/sec).
- die gap ($h = 2\text{mm}$).
- parison length ($L_{target} = 550\text{mm}$).

The two outputs from the experiment were:

- extrusion time ($t_{ext} = 7.8$ sec).
- flow rate evolution curve.

REMARK: The two start-up experiments can be replaced by simulations since the curve for parison length evolution versus extrusion time can be tuned through cycle-to-cycle adjustment of the swell curve as explained in the following steps. However, the flow rate evolution curve needs to be obtained experimentally at the upper and the lower bound of the achievable flow rate (or die gap) for a given machine. These curves are slightly dependent on the die gap, but this dependence can be interpolated as it is shown in this chapter.

First from the experiments, the total extrusion time to obtain a parison of length 550m for the corresponding flow rate (40 and 80 g/sec) was determined (14.3 and 7.8 s respectively). It should be mentioned that in intermittent extrusion, the flow rate set on the machine (via the screw speed) represents the accumulated flow rate, obtained by dividing the total parison weight by the total extrusion time. However, the real flow rate varies during the extrusion time. Since the parison swell is flow rate dependent, a second series of experiments were conducted to obtain this variation for each accumulated flow rate (40 and 80 g/sec). Table 5.2 shows the procedure for a flow rate of 40g/sec. Ten parisons were extruded for incremental times up to the total extrusion time of 14.3sec

(e.g. 0.1*14.3, 0.2*14.3, ..., 1.0*14.3). Dividing the weight of these parisons by their respective extrusion times gave the accumulated flow rate evolution up to the final extrusion time of 14.3 s (Table 5.2, column 4). Each experiment was repeated three times to check for the consistency. Average results were used. The last column in Table 5.2 represents, the percentage of flow rate evolution. For a continuous extrusion process, this value is 100% in all instances during the extrusion of the parison.

Table 5-2 Accumulated flow rate obtained on the machine

Parison no	Ext time measured (sec)	Weight (g)		Flow Rate (g/sec)	% Flow Rate $\left(\frac{Q_i}{Q_{10}}\right) \times 100$
			Average		
	Average		Average	Average	
1	1.43	28.50	32.87	22.98	57.28
		37.10			
		33.00			
2	2.86	68.00	71.67	25.06	62.45
		70.70			
		76.30			
3	4.29	134.50	133.40	31.10	77.50
		126.50			
		139.20			
4	5.72	189.80	188.27	32.91	82.03
		185.00			
		190.00			
5	7.15	256.50	257.50	36.01	89.76
		266.00			
		250.00			
6	8.58	325.20	327.73	38.20	95.20
		325.50			
		332.50			
7	10.01	382.00	387.67	38.73	96.52
		390.60			
		390.40			

8	11.44	458.20	457.60	40.00	99.69
		457.00			
9	12.87	519.00	523.00	40.64	100.00
		527.00			
10	14.3	574.00	578.65	40.47	100
		583.30			

5.5.1.2 Simulation results

This accumulated flow rate evolution information (Table 5.2) obtained from the experiments as described above was fed into the BlowView simulation software and the simulations were run for a flow rate of 40 and 80 g/sec.

The main objective for running the simulations was to obtain the values for the thickness and diameter swell, which are difficult to measure otherwise. Though many non-destructive techniques have been developed in the past, which outline different methods for measuring them (DiRaddo et.al, 1988; Langkamp and Michaeli, 1996), we relied on simulation results for our approach. The simulation results are presented in Table 5.3 and Table 5.4 respectively.

Table 5-3 Simulation results for die gap = 2mm and flow rate = 40g/sec

$h = 2\text{mm}; Q = 40\text{ g/sec}$								
Node no	Prog Point	Coordinates	h_p	We	De	D_{out}	B1	B2
1153	1	(-565.215, 44.241)	8.39	22.3213	0.4874	105.2622	1.5037	4.1950
12609	7	(-289.338, 30.467)	5.54	40.699	1.101	72.0148	1.0287	2.7702
19713	10	(-55.646, 32.408)	5.87	38.968	1.0495	76.5752	1.0939	2.9398

Table 5-4 Simulation results for die gap = 2mm and flow rate = 80g/sec

<i>h</i> = 2mm, <i>Q</i> = 80 g/sec								
Node no	Prog Point	Coordinates	<i>h_p</i>	<i>We</i>	<i>De</i>	<i>D_{out}</i>	B1	B2
1089	1	(-546.98, 45.78)	8.76	23.87	0.2912	109.09	1.5584	4.3825
14017	7	(-281.64, 32.64)	6.17	90.787	1.107	77.626	1.1089	3.0865
21697	10	(-63.67, 32.84)	6.26	86.49	1.055	78.202	1.1172	3.1305

where

h_p : parison thickness

We : Weissenberg number

De : Deborah number

D_{out} : parison outer diameter

B1: diameter swell

B2: thickness swell

All these parameters were obtained at the respective programming points (1,7 and 10).

In the simulation results (Table 5.3, Table 5.4), programming points were chosen along the length of the parison such that they represented the complete length of the parison. Fig 5.5 shows the extruded parison with the programming points.

Both Weissenberg and Deborah numbers are dimensionless numbers and are used to study viscoelastic flows. They have similar definitions, but they differ with each other in terms of the flow region considered by them. Weissenberg number considers the points at the die exit and represents the recoverable shear strain. Since the thickness swell is highly affected by the amount of this shear, the dependence of thickness swell on the flow rate and die geometry is represented via Weissenberg number. On the other hand, the

Deborah number considers the whole die region (Fig 5.6) and is defined as the ratio of the characteristic time of the resin to the characteristic time of the process (flow in the die). Diameter swell is highly dependent on the elongational deformation prevailing at the entrance to the die. This deformation history fades as the die becomes longer (and consequently the characteristic time of the flow increases). So, the diameter swell is related to the Deborah number in this work. Mathematically they are given by,

$$We = \frac{\lambda Q_{inst}}{Ah} \quad (5.1)$$

$$De = \frac{\lambda}{t} \quad (5.2)$$

where,

λ : relaxation time of the polymer (sec)

Q_{inst} : instantaneous flow rate at the corresponding programming points (mm^3 / sec)

A : cross section area (mm^2)

h : die gap (mm)

t : flow time in die (sec)

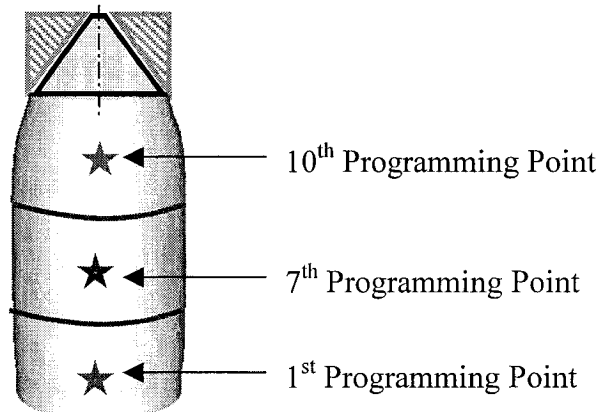


Figure 5-5 Extruded parison with programming points

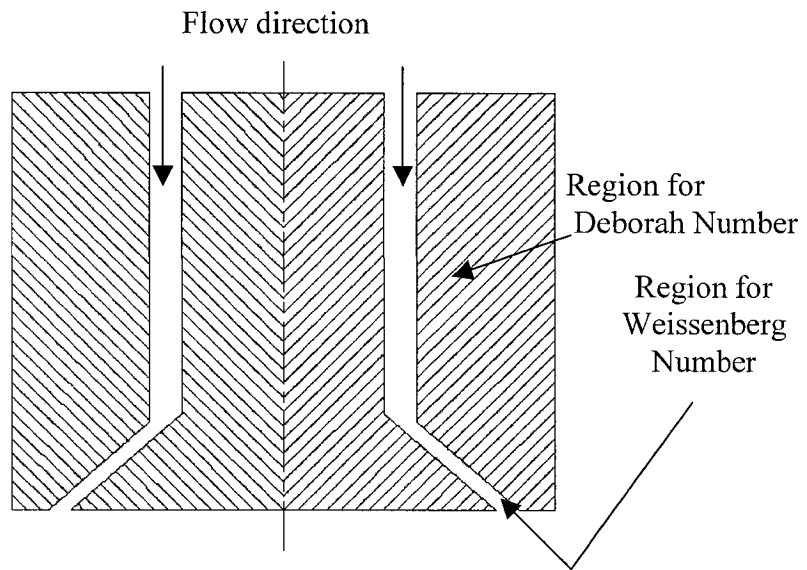


Figure 5-6 Diverging die

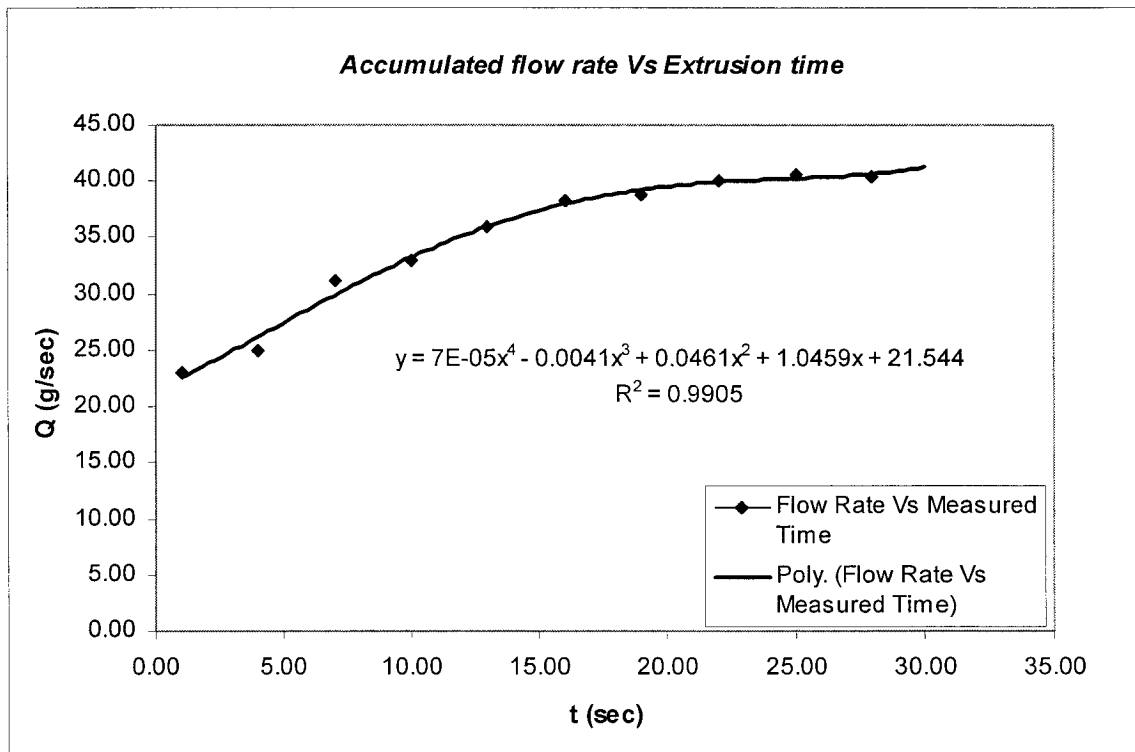


Figure 5-7 Accumulated flow rate at different extrusion times for $Q = 40\text{g/sec}$

The flow rate in the We number definition is the instantaneous (true) flow rate. So, the accumulated flow rate data were used to calculate the true flow rate for each instance of the extrusion period. As seen in Fig 5.7, a fourth order polynomial is fitted to the

accumulated flow rate data points (because order 3 was not accurate enough). The accumulated flow rate interval is then divided into smaller equal intervals and the instantaneous flow rate is obtained using formula:

$$Q_{inst} = \frac{W_{i+1} - W_i}{t_{i+1} - t_i} \quad (5.3)$$

where,

$W_{i+1} - W_i$ = weight difference between two successive parisons (Table 5.2) and

$t_{i+1} - t_i$ = corresponding extrusion time difference.

Figs 5.8 and 5.9 shows the instantaneous flow rate evolution curves for the considered flow rates, where the solid line is a polynomial curve fitted to the data.

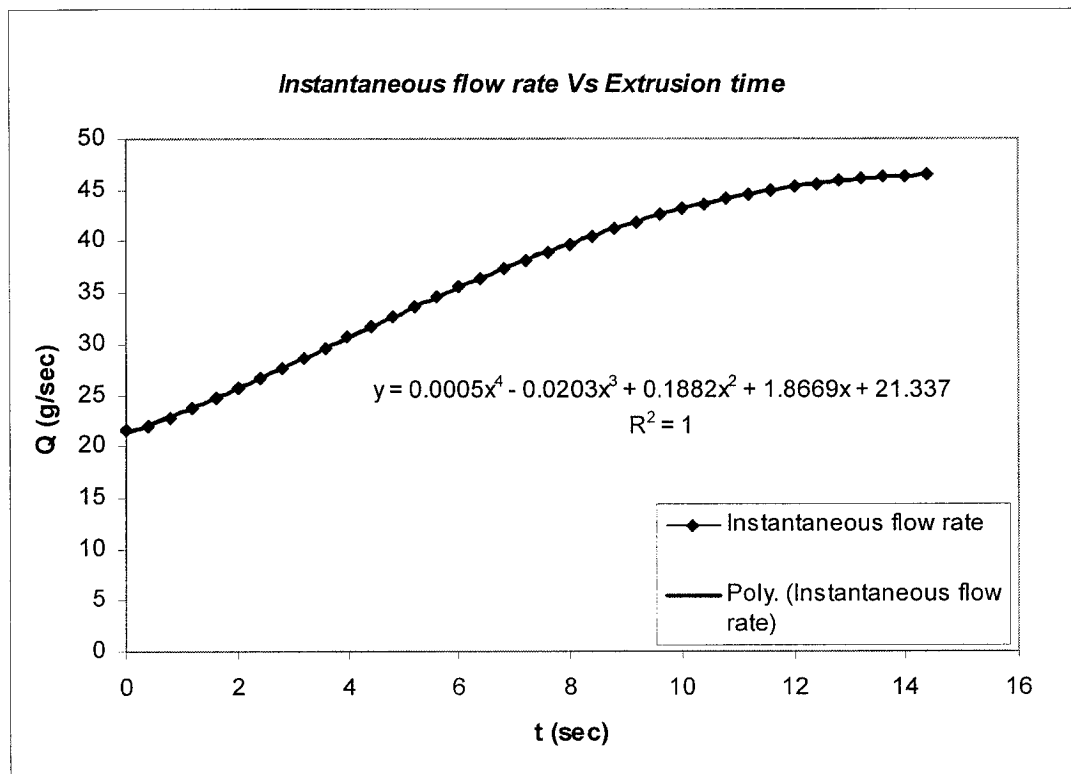


Figure 5-8 Instantaneous flow rate curve ($Q = 40\text{g/sec}$)

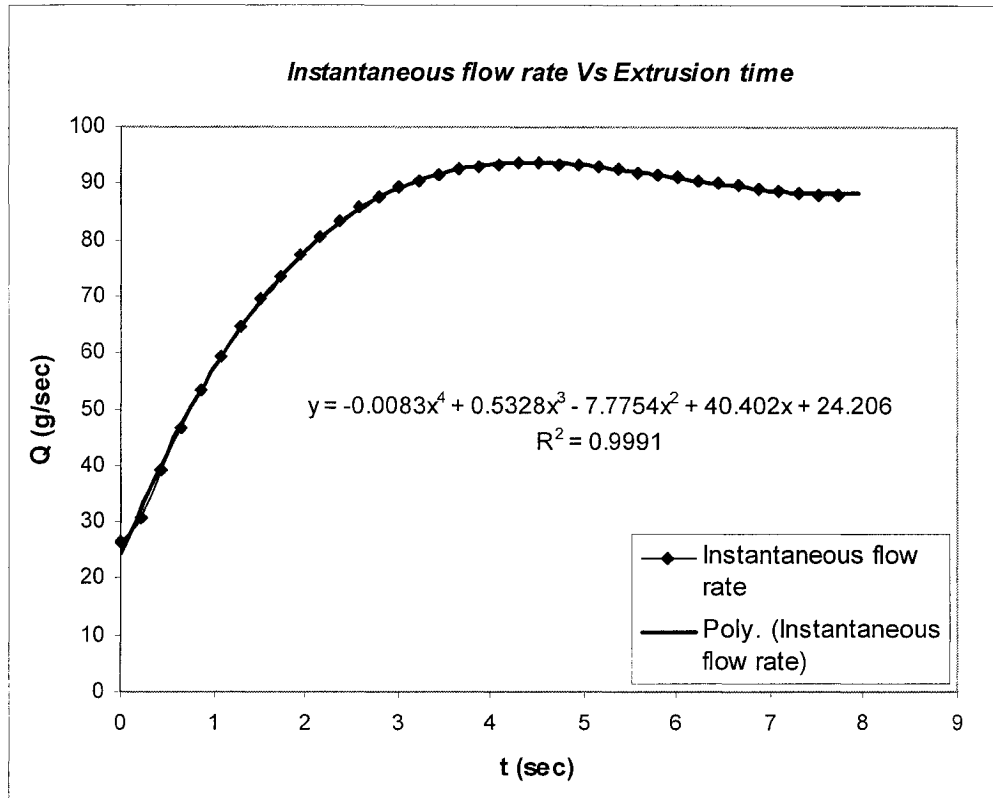


Figure 5-9 Instantaneous flow rate curve ($Q = 80\text{g/sec}$)

5.5.1.3 Weissenberg and Deborah number calculation

The instantaneous flow rate evolution obtained earlier was used to estimate the Weissenberg and Deborah numbers at three programming points that represent three different points on the parison (Table 5.5).

Table 5-5 Weissenberg number calculations for $Q = 40$ and 80 g/sec

$Q =$	Prog Pt	time	$Q_{inst,i}$ (g/sec)	$Q_{inst,i}$ (mm ³ /sec)	λ	h	Area	We
40g/s	1	1.433	24.3411	31985.685	0.6317	2	427.256	23.6454
	7	10.033	43.5771	57263.046		2	427.256	42.3317
	10	14.333	48.0865	63188.641		2	427.256	46.7122

$Q =$	Prog Pt	time	$Q_{inst,i}$ (g/sec)	$Q_{inst,j}$ (mm ³ /sec)	λ	h	Area	We
80g/s	1	0.78	51.2387	67330.848	0.6317	2	427.2566	49.7744
	7	5.46	92.3519	121355.981		2	427.2566	89.7125
	10	7.8	88.4050	116169.609		2	427.2566	85.8785

For the Deborah number calculation, the flow time in the die was obtained from the *parmesh.log* file from the simulation runs. It can also be calculated by the equation given in the previous chapter (Eqn. 4.7)

For a Hookean elastic solid, the relaxation time is infinite ($\lambda = \infty$), whereas for a Newtonian viscous liquid it is zero ($\lambda = 0$). For HDPE DMDF-6200, the relaxation time equation is given by,

$$\lambda = a + bT \quad (5.4)$$

where a, is the intercept ($a = 3.2567$) and b is the slope of the line ($b = -0.0125$). These values were obtained from the IMI material's database.

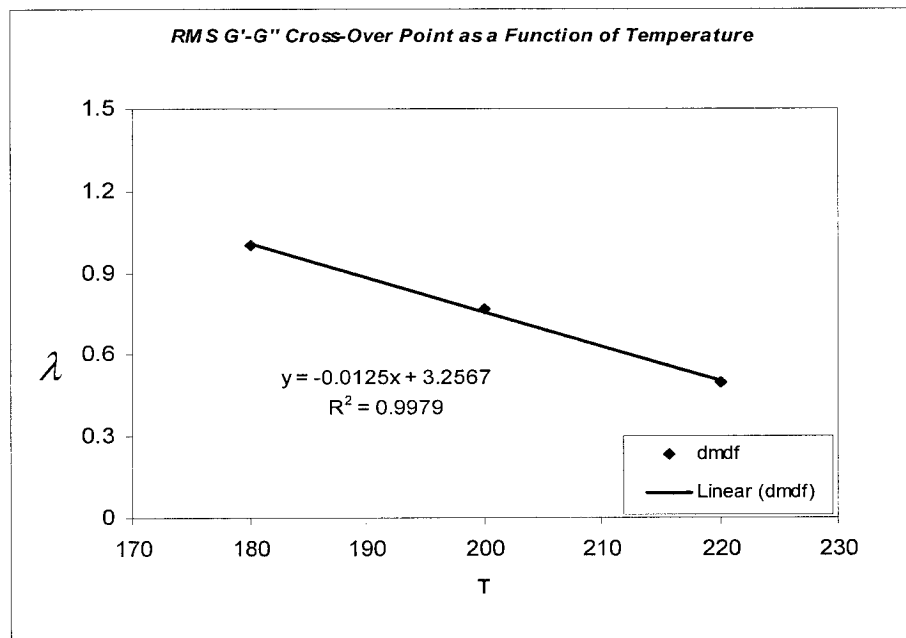


Figure 5-10 Relaxation time as a function of temperature for HDPE DMDF-6200
(Source: IMI material database)

5.5.1.4 Sigmoid fitting and parison length calculation

The graph for diameter swell (B1) versus Weissenberg number and thickness swell (B2) versus Deborah number was plotted using the data obtained from the simulation runs (Figs 5.11 and 5.12).

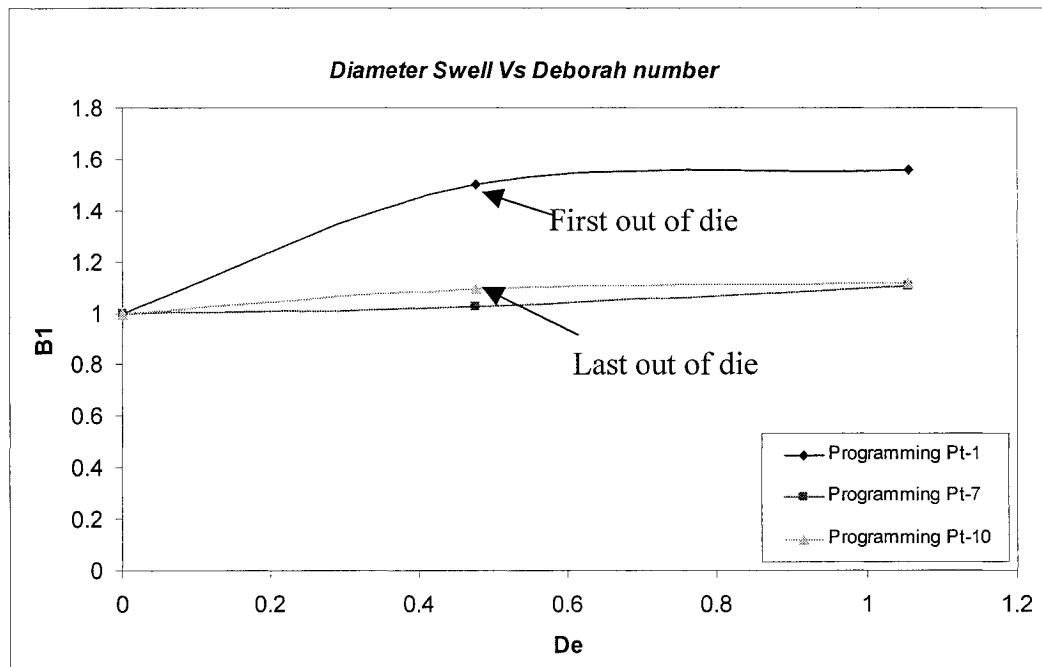


Figure 5-11 Diameter swell (B1) versus Deborah number (De)

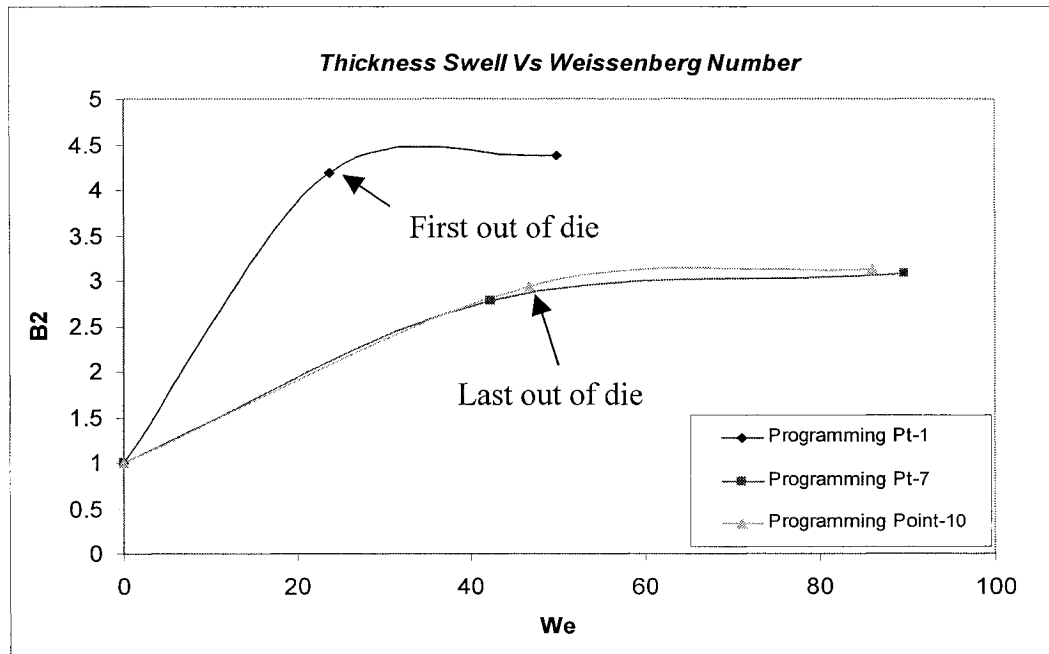


Figure 5-12 Thickness swell (B2) versus Weissenberg number (We)

Based on experimental observations in the literature, the dependence of thickness and diameter swell on Weissenberg and Deborah numbers has a sigmoid shape (leveling off to constant value at high values of We and De numbers). The BlowView software predicts this sigmoid shape for the thickness swell and to some extent for the diameter swell. So, the swell model we were aiming to develop had to conserve the shape of the sigmoid for the swell curves. Different data fitting software were tried to fit various equations to the data. Though hundreds of equations fit the data well, no equation was found, which could shift the whole curve, up or down by adjusting just one variable of the equation (to conserve the sigmoid shape specially for the thickness swell). After trial and error, an equation of Weibull-Sigmoid type Eq.5.5 was found to meet the requirement.

$$y = a - b * (\exp(-cx^d)) \quad (5.5)$$

Figs 5.13 and 5.14 show the sigmoid curves fitted to the simulation data.

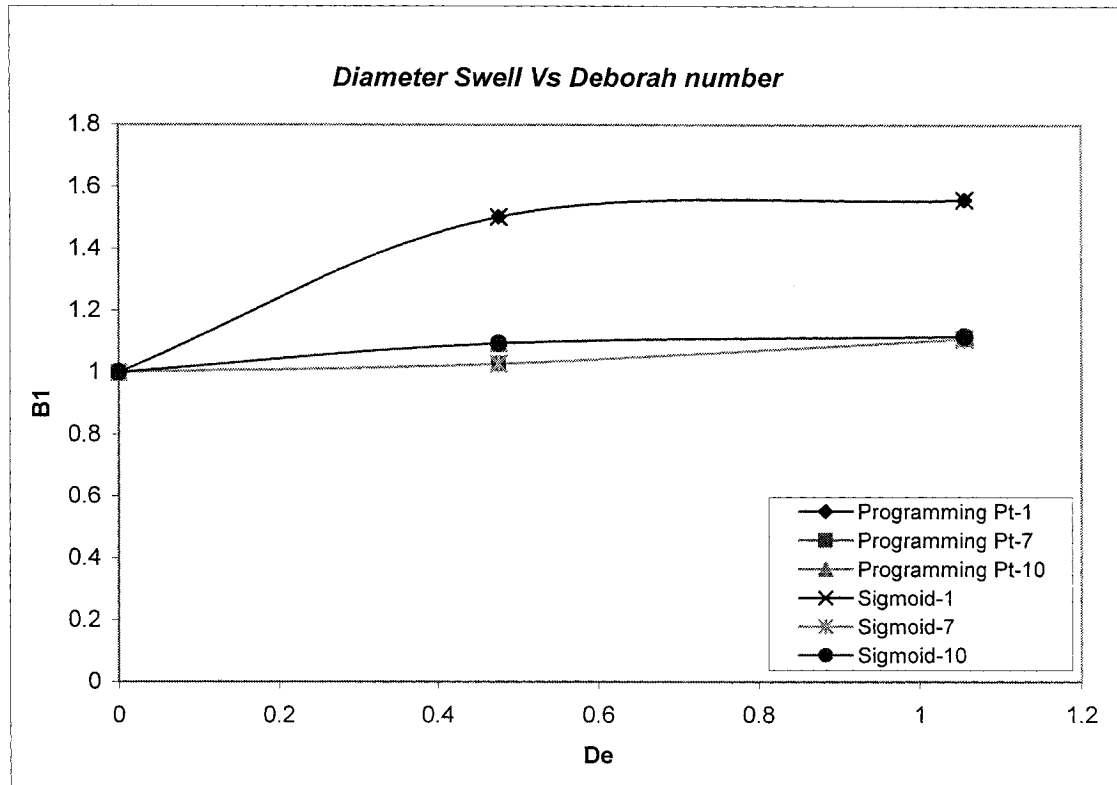


Figure 5-13 Fitted Sigmoids (B1 versus De)

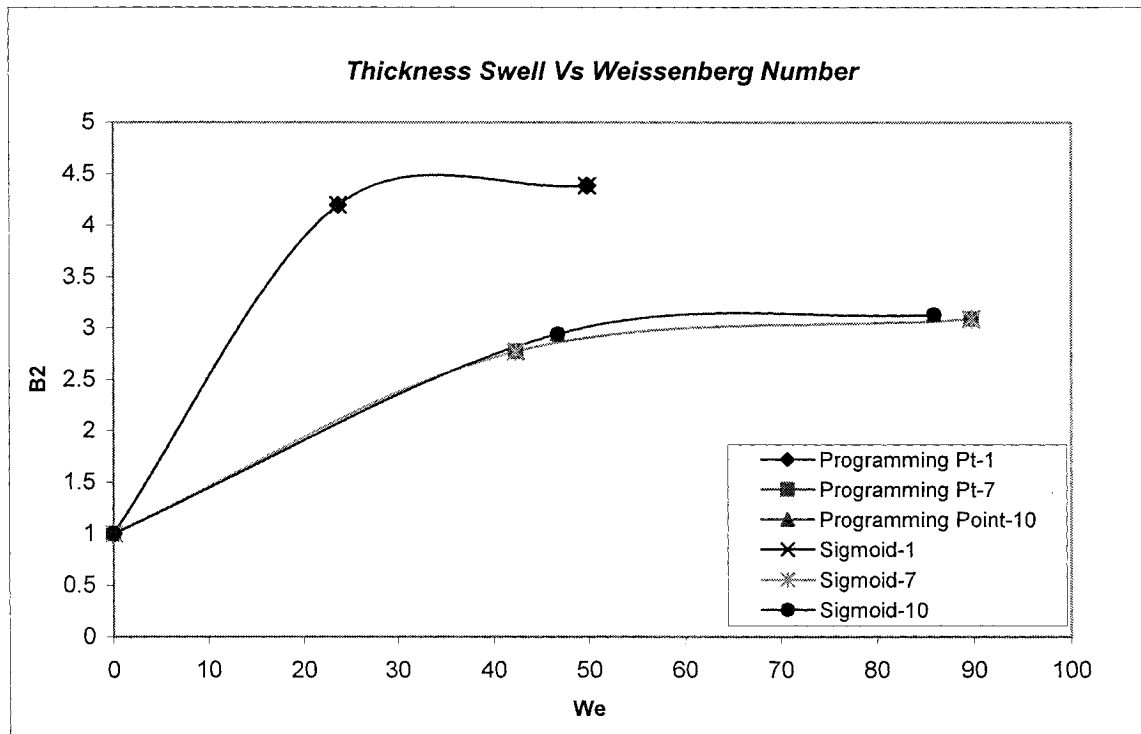


Figure 5-14 Fitted Sigmoids (B2 versus We)

Data fitting was obtained by tuning the variables a, b, c and d of the equation representing the curve based on the least squares method. The following values of variables were obtained for the two curves:

Table 5-6 Values of variables of sigmoids, which gave best fit for the data

Variables	Progpt-1	Progpt-7	Progpt-10
a	0.7279	0.7148	0.7001
b	-0.2720	-0.2851	-0.2998
c	-1.1113	-0.2980	-0.3255
d	0.0789	1.5218	0.2395

The objective of the analysis was to obtain a flow rate which when set on the machine would give a parison of length 550mm (L_{target}) for an extrusion time of 9.5 seconds.

Earlier experiments conducted on the Placo machine gave an extrusion time of 7.8 and 14.33 seconds for a flow rate of 80 and 40 g/sec to obtain a parison of length 550 mm. Using linear interpolation we obtained a flow rate of 69.58 g/sec a first guess for a given extrusion time to give a parison of length 550mm.

For an accumulated flow rate of $Q = 69.58$ g/sec, using linear interpolation (based on Figs 5.8 and 5.9), the value of instantaneous flow rates and Deborah number at each of the programming points was obtained. Using flow rates at the respective programming points, the values of Weissenberg numbers were calculated for 1st, 7th and 10th programming points along the length of the extruded parison. Now, graphs were plotted for diameter swell versus Deborah number and thickness swell versus Weissenberg number, and sigmoids were fitted to them. Diameter and thickness swells for the new flow rate ($Q = 69.58$ g/sec) were obtained after substituting the Weissenberg and Deborah number values to the fitted sigmoids. Parison length was then calculated for the updated $Q_{inst,i}$, B1, B2, We , De , $t_{ext,i}$. Table 5.7 shows the values obtained for the estimated flow rate.

Table 5-7 Parison length calculation ($Q = 69.58$ g/sec, Iteration-1)

Prog pt	h	Area	λ	$Q_{inst,i}$ (g/sec)	$Q_{inst,i}$ (mm ³ /s)	$t_{ext,i}$
1	2	427.25	0.6317	44.23	58129.17	0.95
7	2	427.25	0.6317	79.65	104670.17	5.7
10	2	427.25	0.6317	77.90	102376.67	2.85

Prog Pt	B1	We	B2	$D_{out,i}$	$h_{p,i}$	$L_{p,i}$	Length Required
1	1.54727	42.972	4.3488	108.309	8.69	20.2	550
7	1.0831	77.377	3.0281	75.819	6.05	449.4	
10	1.1122	75.682	3.0936	77.854	6.18	209.4	
						L_{Total}	679.2

Total length of the parison is obtained by summing the length of the individual sections, as shown below,

$$L_{Total} = L_{p,1} + L_{p,2} + L_{p,3} \quad (5.6)$$

where,

$$L_{p,i} = \frac{(4 * Q_{inst,i} * t_{ext,i})}{\pi * (D_{out,i}^2 - (D_{out,i} - 2h_{p,i})^2)} \quad (5.7)$$

where,

$$D_{out} = D_{die} * B1 \text{ and } h_p = h * B2 \text{ (} D_{die} \text{ and } h \text{ being the die outer diameter and the die gap).}$$

Substituting the values of the parameters in the equations (5.6 and 5.7) and summing the length of the parison for each section, we obtained,

$$L_{Total} = 679.2 \text{ mm} \quad (5.8)$$

The length of the parison was more than the requirement. This suggested that the estimated flow rate was more than the requirement. Hence, a new guess was required. The new guess was estimated using linear interpolation as shown.

$$L_{parison,Guess\#1} = 679.2 \text{ mm.}$$

$$L_{parison,reqd} = 550 \text{ mm.}$$

$$Q_{guess1} = 69.58 \text{ g/sec.}$$

$$Q_{guess2} = ?.$$

$$\frac{(L_{parison,guess1} - L_{parison,reqd})}{L_{parison,guess1}} = \frac{(Q_{guess1} - Q_{guess2})}{Q_{guess1}} \quad (5.9)$$

Substituting values in the above equation, we obtained,

$$\therefore Q_{guess2} = 56.34 \text{ g/sec.} \quad (5.10)$$

As before, a similar procedure was used to obtain updated flow rates and Weissenberg numbers at the different programming points for $Q = 56.347 \text{ g/sec}$. Again, new diameter swell and thickness swell values were obtained by moving along the fitted sigmoids and a new length of the parison was estimated. It was found that for $Q = 56.347 \text{ g/sec}$, a parison of length 573.740 mm was obtained (Table 5.8).

Table 5-8 Parison length calculation ($Q = 56.347 \text{ g/sec}$, Iteration-2)

Prog pt	h	Area	λ	$Q_{inst,i}$ (g/sec)	$Q_{inst,i}$ (mm ³ /s)	$t_{ext,i}$
1	2	427.256	0.6317	35.333	46430.61	0.95
7	2	427.256	0.6317	63.510	83456.66	5.7
10	2	427.256	0.6317	64.564	84840.99	2.85

Prog Pt	B1	We	B2	$D_{out,i}$	$h_{p,i}$	$L_{p,i}$	Length Req
1	1.5306	34.3239	4.2941	107.1410	8.5882	16.5884	550
7	1.0555	61.6954	2.9344	73.8876	5.8688	379.3230	
10	1.1050	62.7188	3.0361	77.3500	6.0722	177.8294	
						L_{Total}	573.7

The above iterations were repeated until a parison of length close to the requirement was obtained, but calculations were limited to a maximum of three iterations. Table 5.9 summarizes the results obtained for the third iteration. As can be seen, a parison of length 554.3 mm was obtained.

Table 5-9 Parison length calculation ($Q = 54.015$ g/sec, Iteration-3)

Prog pt	h	Area	λ	$Q_{inst,i}$ (g/sec)	$Q_{inst,i}$ (mm ³ /s)	$t_{ext,i}$
1	2	427.256	0.6317	33.76	44370.34	0.95
7	2	427.256	0.6317	60.66	79720.686	5.7
10	2	427.256	0.6317	62.21	81752.73	2.85

Prog Pt	B1	We	B2	$D_{out,i}$	$h_{p,i}$	$L_{p,i}$	Length Req
1	1.5273	32.8008	4.2826	106.9086	8.5652	15.99	550
7	1.0512	58.9336	2.9149	73.5869	5.8298	366.17	
10	1.1036	60.4358	3.0243	77.2517	6.0487	172.20	
						L_{Total}	554.304

5.5.1.5 Simulation (sigmoid) tuning

For the final flow rate ($Q = 54.015$ g/sec), obtained from the 3rd iteration, an experiment was conducted on the Placo machine as to get the experimental diameter and length of the parison for subsequent tuning of the swell curves. Pinch off mold data were used for

this purpose to demonstrate the potential of the parison length control approach¹. Table 5.10 lists the pinch-off mold data. From these data, the diameter swell values were determined for the flow rate of $Q = 54.015$ g/sec. It was found that the extruded parison had a length of 510 mm (instead of approximated length of 554.304 from the 3rd iteration) and a higher diameter than the one represented by the diameter swell curve. This implies that the thickness swell curve is overestimating the true parison swell while the diameter swell is underestimated. The next step was to tune the diameter swell curve based on the experimental pinch-off values (or sensor values in an online system) in the simulation. Consequently, the thickness swell curve is the only parameter left to be tuned, by the iterations (Eq.5.7) aiming to get the observed parison length (510 mm in our case for a flow rate of 54.015).

Table 5-10 Diameter swell measurements from the pinch-off mold

$Q = 54.015$ g/sec			
Pinch-off mold data			
Pillow #	B1	Pillow #	B1
1	1.3971	10	1.5948
2	1.4245	11	1.6124
3	1.4427	12	1.6286
4	1.4663	13	1.6353
5	1.4871	14	1.6269
6	1.5109	15	1.5861
7	1.5325	16	1.5166
8	1.5539	17	1.39731
9	1.5762		

As it is stated earlier, both diameter and thickness swell curves have to follow a sigmoid shape. The simulation does not provide this sigmoid shape for the diameter swell. So, we are allowed to tune all 4 parameters of the sigmoid to increase the B1 curve to match the experimental observation for the parison diameter (Fig 5.15). In the case of the thickness swell, the sigmoid shape coming from the simulation had to be shifted downward to

¹ We used pinch-off data for diameter swell, but in real time it will be measured online by means of laser sensors mounted on the machine. For thickness swell we have to depend on the simulation data, as no reliable non-destructive technique for thickness measurement is available yet.

correct the overestimation of the thickness swell discussed earlier. It was found that the thickness swell had to be reduced by 23.80 % in order to get the experimental length observed on the machine (510 mm) using the Eqn.5.7. This high adjustment is in part because of the simultaneous correction in the B1 curve (boosting diameter swell curve leading to length reduction). The experimental tuning of the thickness swell curve gave us one real point (based on actual experimental length) on the sigmoid plot (B2 vs. We). Table 5.11 gives modified values for diameter and thickness swell for an accumulated flow rate of 54.015 g/sec based on the new swell curves. It can be seen that the calculated length (509.9) matches the experimental observation. Tables 5.12 and 5.13 summarize the new parameters for B1 and B2 sigmoids (for the three programming points on the parison). Figs 5.15 and 5.16 show the tuned sigmoids. The new experimental points are also shown.

Table 5-11 Revised B1 and B2 and parison length calculation

Revised B1 (Pinch-off data)	We	B2	D_{out}	$h_{p,i}$	$L_{p,i}$
1.51665	32.8008	3.2633	106.1658	6.5266	20.63
1.5325	58.9336	2.2211	107.2796	4.4423	316.61
1.39718	60.4358	2.3045	97.8030	4.6090	172.66
				L_{Total}	509.91

B2	B2
From simulation	Experimental tuning
4.2825	3.2633
2.9149	2.2211
3.0243	2.3045

Table 5-12 Tuned sigmoid results for diameter swell (B1)

PROG PT-1		
ppt-1 <i>De</i> (old)	ppt-1 <i>De</i> (new)	Tuned B1 values
0	0	0.9999
0.4755	0.4755	1.4932
1.0553	0.6786	1.5166
	1.0553	1.5469

PROG PT-7		
ppt-7 <i>De</i> (old)	ppt-7 <i>De</i> (new)	Tuned B1 values
0	0	0.9999
0.4755	0.4755	1.2761
1.0553	0.6786	1.5325
	1.0553	2.4120

PROG PT-10		
ppt-10 <i>De</i> (old)	ppt-10 <i>De</i> (new)	Tuned B1 values
0	0	1.000
0.4755	0.4755	1.3615
1.0553	0.6786	1.3971
	1.0553	1.4475

Table 5-13 Tuned sigmoid results for thickness swell (B2)

PROG PT-1		
ppt-1 <i>We</i> (old)	ppt-1 <i>We</i> (new)	Tuned B2 values
0	0	0.9999
23.6454	23.6454	3.1444
49.7744	32.8008	3.2633
	49.7744	3.4157

PROG PT-7		
ppt-7 <i>We</i> (old)	ppt-7 <i>We</i> (new)	Tuned B2 values
0	0	1.0000
42.3317	42.3317	2.0882
89.7125	58.9336	2.2211
	89.7125	2.4006

PROG PT-10		
ppt-10 <i>We</i> (old)	ppt-10 <i>We</i> (new)	Tuned B2 values
0	0	1.000
46.7122	46.7122	2.2144
85.8785	60.4358	2.3045
	85.8785	2.4312

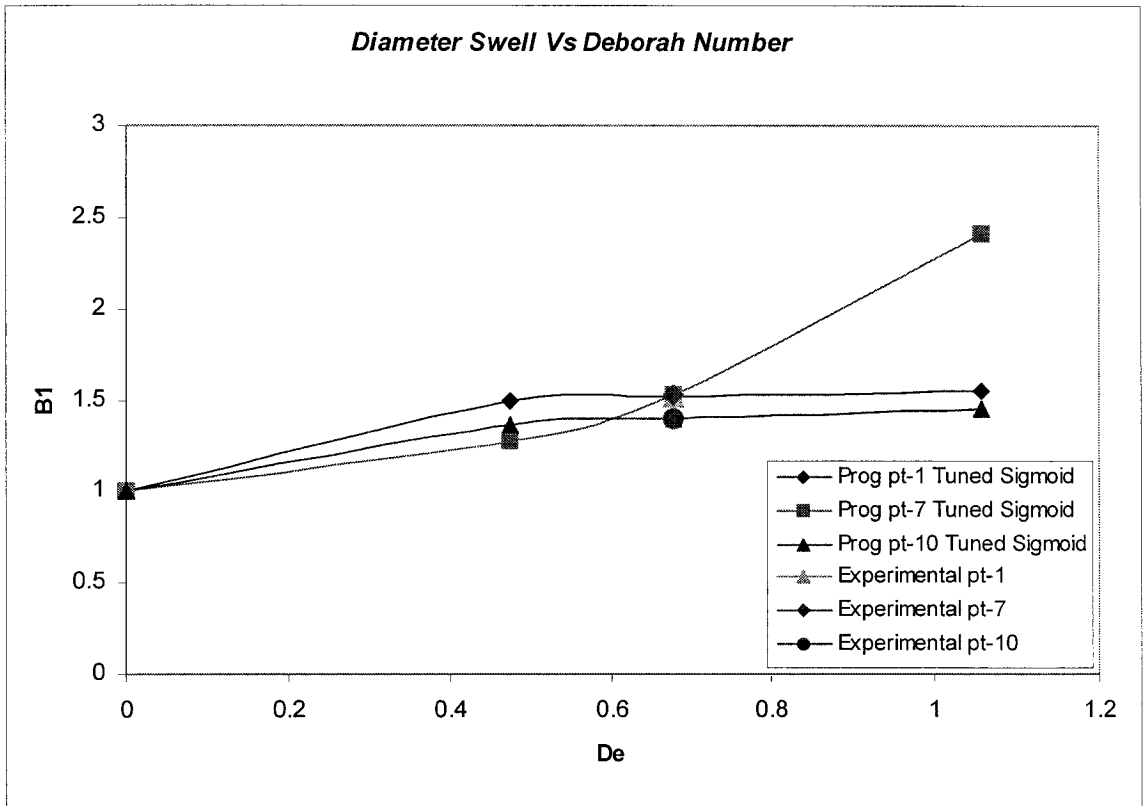


Figure 5-15 Tuned sigmoids for diameter swell (See the end of this chapter regarding the shape of these curves.)

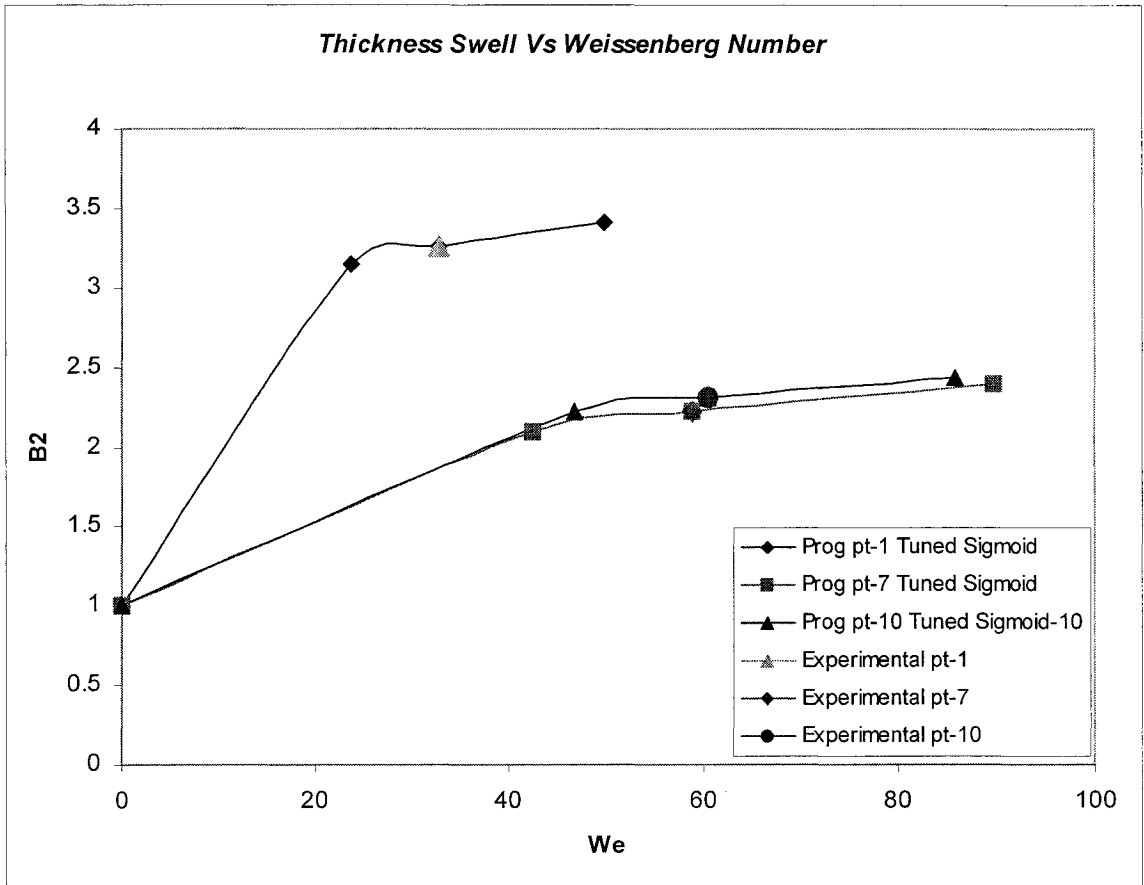


Figure 5-16 Tuned sigmoids for thickness swell

Now that the swell curves are tuned, the final controller output (recommended flow rate) will come from linear interpolation of the flow rate vs. length as outlined below.

$$L_{p,observed} = 510 \text{ mm.} \tag{5.11}$$

$$L_{p,required} = 550 \text{ mm.}$$

$$Q_{observed} = 54.015 \text{ g/sec.}$$

$$Q_{required} = ?$$

Hence, the required flow rate which will give a parison of length 550 mm can be obtained from linear interpolation of tuned sigmoids;

$$\frac{L_{p,observed} - L_{p,required}}{L_{p,observed}} = \frac{Q_{observed} - Q_{required}}{Q_{observed}} \quad (5.12)$$

Substituting values in Eq.5.12, we have:

$$Q_{required} = 58.262 \text{ g/sec.} \quad (5.13)$$

An experiment conducted on the Placo machine showed that a flow rate of 60 g/sec was required to obtain a parison of length 550mm for an extrusion time of 9.5 seconds. Hence good accuracy was obtained between predicted and observed flow rate measurements.

5.5.2 Die gap scenario

It can be shown that this methodology is also applicable to the cases where both the extrusion time and flow rate are set by the operator while the die gap is the adjustable parameter on the machine to obtain a target length (e.g., 550mm). In this scenario, the simulations are run at two extreme die gaps (instead of two flow rates). The steps to follow remain the same. For the die gap case, it has been determined experimentally that the diameter swell varies with the aspect ratio of the die (h/L). The B1 curve is plotted versus h/L (die aspect ratio) instead of Deborah Number. The iterations will lead to a die gap that provides the desired length for a preset flow rate and extrusion time. This scenario can be extended to the control of blow molding operations for complex parts where parison programming (die gap adjustment during extrusion) is used.

5.5.2.1 Experimentation

As for the flow rate case, two experiments were conducted to obtain the parison evolution where the flow rate was changed. The experiments for the die gap case were conducted at a constant flow rate of 80g/sec with the die gap of 2 and 6mm.

Input parameters:

- die gap ($h = 2$ and 6mm)
- flow rate ($Q = 80\text{g/sec}$)
- parison length ($L_{\text{target}} = 550\text{mm}$)

Output parameters:

- extrusion time
- flow rate evolution curve

The total extrusion time to obtain a parison of length 550mm for the corresponding die gaps (2 and 6mm) for an accumulated flow rate of 80 g/sec was determined (7.8 and 11.7 sec). To obtain the instantaneous flow rate (which is different from the accumulated flow rate), the total extrusion time of the parison was divided into 10 intervals (for e.g. $.1*7.8$, $.2*7.8$, up till $1*7.8$). For each time interval, a parison was extruded and weighed. Dividing the weight of the parison with the corresponding extrusion time gave the instantaneous flow rate of the parison extruded. Dividing this flow rate with the final flow rate, gave the flow rate for that section of parison in percentage.

5.5.2.2 Simulation Results

The information obtained from the experiments was fed into BlowView simulation software (NRC-IMI) and the simulations were run.

Input parameters:

- die geometry
- parison evolution
- flow rate ($Q = 80\text{g/sec}$)
- die gap ($h = 2$ and 6 mm)

A total of two simulations were run for two different die gaps. Each simulation took approximately six hours to run. The end result of a simulation was a 3-dimensional meshed image of the parison. The parison was divided into ten sections identified by ten

programming points ranging from one to ten from bottom to the top of the parison. Three points (ppt-1, 7 and 10) were chosen along the length of the parison such that they represent the complete parison. The following parameters were obtained from the simulation for the selected programming points.

Output parameters:

- parison thickness (h_p)
- parison outer diameter (D_{out})
- Weissenberg number (We)
- Deborah number (De)

These parameters are listed in Table 5.14 for the flow rate of 80g/sec and die gap of 2 and 6 mm respectively.

Diameter swell (B1) and thickness swell (B2) were calculated by dividing outer diameter and thickness of the parison by outer die diameter and the die gap respectively.

$$\text{Diameter swell (B1)} = \frac{D_{out}}{D_{die}} ; \text{Thickness swell (B2)} = \frac{h_p}{h} \quad (5.14)$$

where

D_{out} : outer diameter of the parison (mm)

D_{die} : outer diameter of the die (mm)

h_p : parison thickness (mm)

h : die gap (mm)

Table 5-14 Simulation data for $Q = 80$ g/sec, $h = 2$ and 6 mm

$h = 2$ mm, $Q = 80$ g/sec								
Node no	Prog Point	Coordinates	h_p	We	De	D_{out}	B1	B2
1089	1	(-546.98, 45.78)	8.765	23.87	0.2912	109.09	1.5584	4.3825
14017	6	(-281.64, 32.64)	6.173	90.787	1.107	77.626	1.1089	3.0865
21697	10	(-63.67, 32.84)	6.261	86.49	1.055	78.202	1.1172	3.1305

$h = 6 \text{ mm}, Q = 80 \text{ g/sec}$								
Node no	Prog Point	Coordinates	h_p	We	De	D_{out}	B1	B2
705	1	(-524.877, 45.827)	11.4279	3.0514	0.2738	114.5098	1.6359	1.9047
6465	6	(-272.91, 36.984)	9.6454	10.3239	0.9263	93.2588	1.3323	1.6076
10625	10	(-56.995, 37.499)	9.898	11.9819	1.0751	94.794	1.3542	1.6497

5.5.2.3 Weissenberg number calculation

The simulation results provided Weissenberg number values (Table 5.14) at the respective programming points, but we relied on experimental measurements for the same. As in flow rate case, the Weissenberg number is calculated using following formula,

$$We = \frac{\lambda Q_{inst}}{Ah} \quad (5.15)$$

Here, Q_{inst} is the instantaneous flow rate, which is estimated using a procedure outlined in the flow rate scenario (Section 5.5.1.2). In the flow rate case, the die gap and die area were constant because the flow rate was the only variable parameter. In the die gap case, the die gap is variable with values of 2 and 6 mm respectively. The results obtained are shown in Table 5.15.

Table 5-15 Weissenberg number calculations for $h = 2$ and 6 mm

$h =$	Prog Pt	time	Inst Q (g/sec)	Inst Q (mm ³ /sec)	λ	h	Area	Inst We
2mm	1	0.78	51.238	67330.848	0.6317	2	427.256	49.7744
	6	5.46	92.351	121355.981		2	427.256	89.7126
	10	7.8	88.405	116169.609		2	427.256	85.8785

$h =$	Prog Pt	time	Inst Q (g/sec)	Inst Q (mm ³ /sec)	λ	h	Area	Inst- We
6mm	1	1.17	72.337	95056.430	0.6317	6	1206.371	8.2958
	6	7.02	89.173	117178.695		6	1206.371	10.2265
	10	11.7	100.680	132299.903		6	1206.371	11.5462

5.5.2.4 Data plotting and sigmoid fitting

The graphs were plotted for diameter swell (B1) versus aspect ratio (h/L) and thickness swell (B2) versus Weissenberg number (We). As outlined before, the dependence of thickness and diameter swell on Weissenberg and h/L ratio has a sigmoid shape. The swell model for which we were aiming had to conserve this shape of sigmoid for the swell curves.

A sigmoid equation of four variables was sought and made to fit the simulation data, by adjusting its variables. The equation was chosen such that adjusting one parameter of the curve would shift the whole curve up or down without changing the shape of the curve. Figs 5.17 and 5.18 show the sigmoids, which fit the simulation data.

The sigmoid equation is given by:

$$y = a - b * (\exp(-cx^d)) \quad (5.16)$$

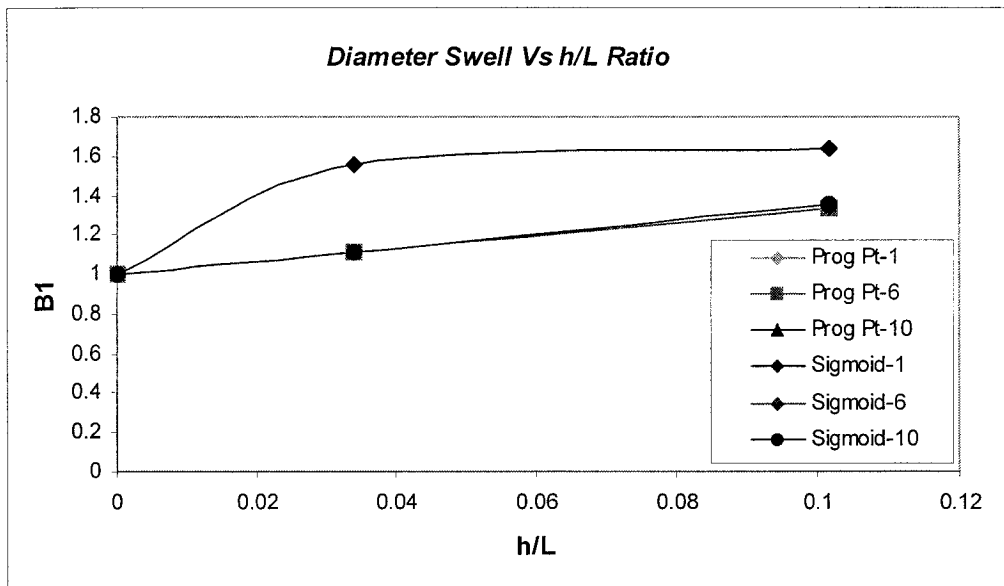


Figure 5-17 Diameter swell (B1) versus aspect ratio at different programming points

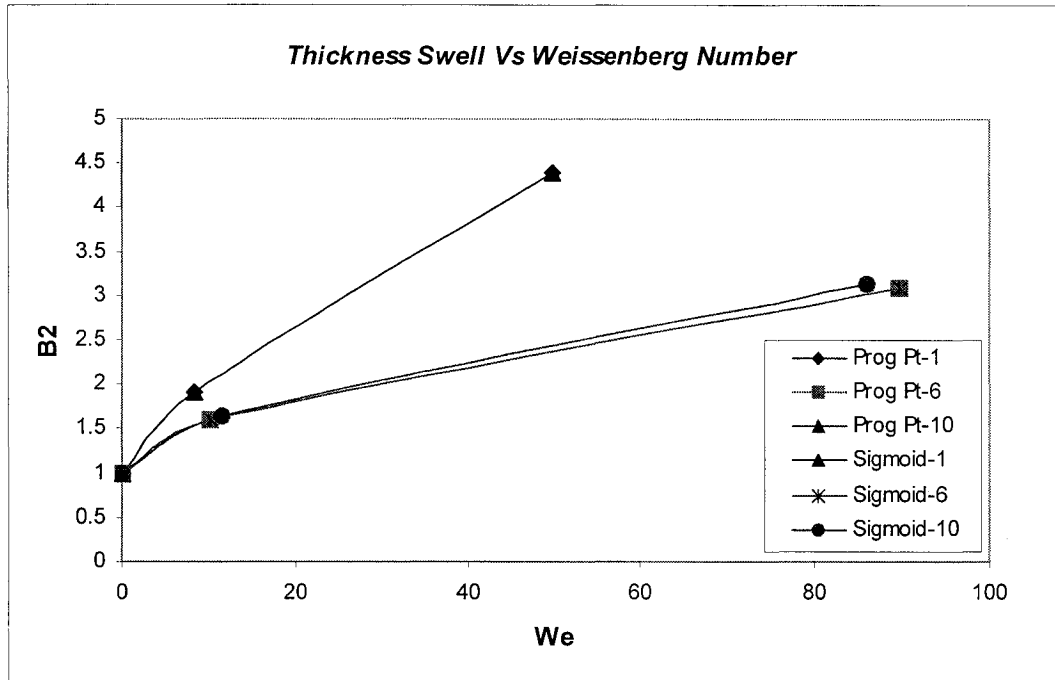


Figure 5-18 Thickness swell (B2) versus Weissenberg numbers at different programming points

5.5.2.5 Operator input estimation

Now different guesses for the die gap, which when set on the machine, will give a parison of length 550 mm (target length) for a flow rate of 80 g/sec and extrusion time of 10.3 seconds are estimated by moving along the fitted sigmoids.

Initial guess for the die gap was based on the following formula;

$$\frac{h_2 - h_1}{h_{Guess} - h_1} = \frac{t_{ext2} - t_{ext1}}{t_{ext,guess1} - t_{ext2}} \quad (5.17)$$

$$h_1 = 2 \text{ mm.}$$

$$h_2 = 6 \text{ mm.}$$

$$t_{ext1} = 7.8 \text{ sec.}$$

$$t_{ext2} = 11.7 \text{ sec.}$$

$$t_{ext,guess1} = 10.3 \text{ sec.}$$

$$h_{Guess1} = ?.$$

Using the above formula for the first iteration, we obtained a die gap of 4.564 mm. For the die gap obtained, the new values for the instantaneous flow rate at the respective programming points was determined. Using updated values for die gap, instantaneous flow rates and area, new Weissenberg numbers at different programming points were estimated. Diameter and thickness swell values at the different points along the parison were then determined by using Gregory-Newton linear interpolation technique. Substituting revised values of parison thickness, instantaneous flow rate and parison outer diameter gave us new parison length. Table 5.16 outlines, the results for the first iteration.

Table 5-16 Calculation results for the first iteration

Prog pt	h	Area	λ	$Q_{inst,i}$ (g/sec)	$Q_{inst,i}$ (mm ³ /s)	$t_{ext,i}$
1	4.5641	938.256	0.6317	64.7633	85102.909	1.03
6	4.5641	938.256	0.6317	90.3142	118678.266	5.15
10	4.5641	938.256	0.6317	96.2734	126509.122	4.12

Prog Pt	h/L	B1	We	B2	D_{out}	h	$L_{p,i}$	$L_{required}$	
1	0.0774	1.6175	12.5539	2.3521	113.2261	10.73	25.35	550	
6	0.0774	1.2495	17.5067	2.2659	87.4628	10.34	243.92		
10	0.0774	1.2719	18.6619	2.2491	89.0348	10.26	205.18		
							L_{Total}	474.46	

The total length of the parison (474.46 mm) was less than the requirement (550 mm). This suggested that the die gap had to be decreased in order to increase the length of the parison since the amount of the plastic and shot time were fixed. A new die gap was determined using linear interpolation for the die gap based on the new length of the parison. The objective was to get a parison of length close to the requirement, but since this did not happen, we limited the number of iterations to three. Table 5.17 gives the summary of results obtained for three iterations.

Table 5-17 Summary of parison length obtained for different iterations

Summary of results		
	(h)	$L_{parison}$
1	4.56410256	474.46
2	3.83753615	484.41
3	3.31797708	500.42

To check the accuracy of the model, a test based on the final die gap (3.317 mm) was run on the machine. The extruded parison was pinched to determine the diameter swell at the respective programming points from the pinch-off technique (Table 5.18). We obtained a parison of length 645.45 mm (instead of the approximated length of 500.42 mm from the 3rd iteration as expected). This suggested that the simulation was overestimating thickness swell and thickness swell (B2) versus Weissenberg number (We) curves. So, these need to be tuned to match experimental observations.

Now, the diameter swell values were replaced by the experimental diameter swell⁶ measurements for the last die gap ($h = 3.317$ mm).

Table 5-18 Diameter swell measurements from pinch-off mold

$h = 3.317$ mm			
Pinch-off mold data			
Pillow #	B1	Pillow #	B1
1	1.4320	10	1.6564
2	1.4614	11	1.67993
3	1.4837	12	1.6994
4	1.5066	13	1.7119
5	1.5303	14	1.7109
6	1.5557	15	1.6839
7	1.5802	16	1.6176
8	1.6062	17	1.4865
9	1.6322119		

⁶ We used pinch-off data for diameter swell, but in real time it will be measured online by means of laser sensors mounted on the machine. For thickness swell we have to depend on the simulation data as no reliable non-destructive technique for thickness measurement is available yet.

5.5.2.6 Simulation tuning

As with the flow rate case, on replacing the simulation diameter swell values with parison pinch-off measurements for the respective programming points and substituting them in the length calculation, the length of the parison was reduced. This indicated that the simulation was overestimating thickness swell (not diameter swell as these values come from the experiment). Therefore, thickness swell sigmoids had to be tuned to the experimental data to give a parison of the required length ($L_{parison} = 645.45$ mm). To achieve this, the thickness swell had to be reduced by 40.5% to obtain the observed length (Table 5.19)

Table 5-19 Revised B1 and B2 and parison length calculation

Prog Pt	(B2)	(B2)	Tuning Factor
	Simulation	Experimental tuning	
1	3.0892	1.8380	40.50%
6	2.9828	1.7748	
10	2.9670	1.7653	

Revised B1	We	B2	D_{out}	h	L_p
1.6176	20.9448	1.8381	113.233	6.0987	38.369
1.5802	32.8634	1.7748	110.615	5.8888	318.922
1.4321	33.2756	1.7654	100.246	5.8575	288.162
				L_{Total}	645.45

The sigmoids were tuned by adjusting one parameter to match the updated values of diameter and thickness swells (Figs 5.19 and 5.20). This tuning was done by using a least square approach for the initial and the new experimental point. The values at other programming points were calculated after inputting the h/L ratio and Weissenberg numbers into the tuned sigmoids. Tables 5.20 and 5.21 list the tuned parameters.

Table 5-20 Tuned sigmoid results for diameter swell (B1)

PROG PT-1		
ppt-1 h/L (old)	ppt-1 h/L (new)	Tuned B1 values
0	0	1.0000
0.0339	0.0339	1.5838
0.1017	0.0562	1.6176
	0.1017	1.6546

PROG PT-6		
ppt-6 h/L (old)	ppt-6 h/L (new)	Tuned B1 values
0	0	0.9999
0.0339	0.0339	1.3248
0.1017	0.0562	1.5802
	0.1017	2.2386

PROG PT-10		
ppt-10 h/L (old)	ppt-10 h/L (new)	Tuned B1 values
0	0	0.9999
0.0339	0.0339	1.3041
0.1017	0.0562	1.4320
	0.1017	1.6310

Table 5-21 Tuned sigmoid results for thickness swell (B2)

PROG PT-1		
ppt-1 <i>We</i> (old)	ppt-1 <i>We</i> (new)	Tuned B2 values
0	0	0.9998
8.2958	8.2958	1.3095
49.7744	20.9448	1.8381
	49.7744	2.8786

PROG PT-6		
ppt-6 <i>We</i> (old)	ppt-6 <i>We</i> (new)	Tuned B2 values
0	0	1.0000
10.2265	10.2265	1.1081
89.7126	32.8634	1.7748
	89.7126	2.9818

PROG PT-10		
ppt-10 <i>We</i> (old)	ppt-10 <i>We</i> (new)	Tuned B2 values
0	0	1.0000
11.5462	11.5462	1.1302
85.8785	33.2756	1.7654
	85.8785	2.9662

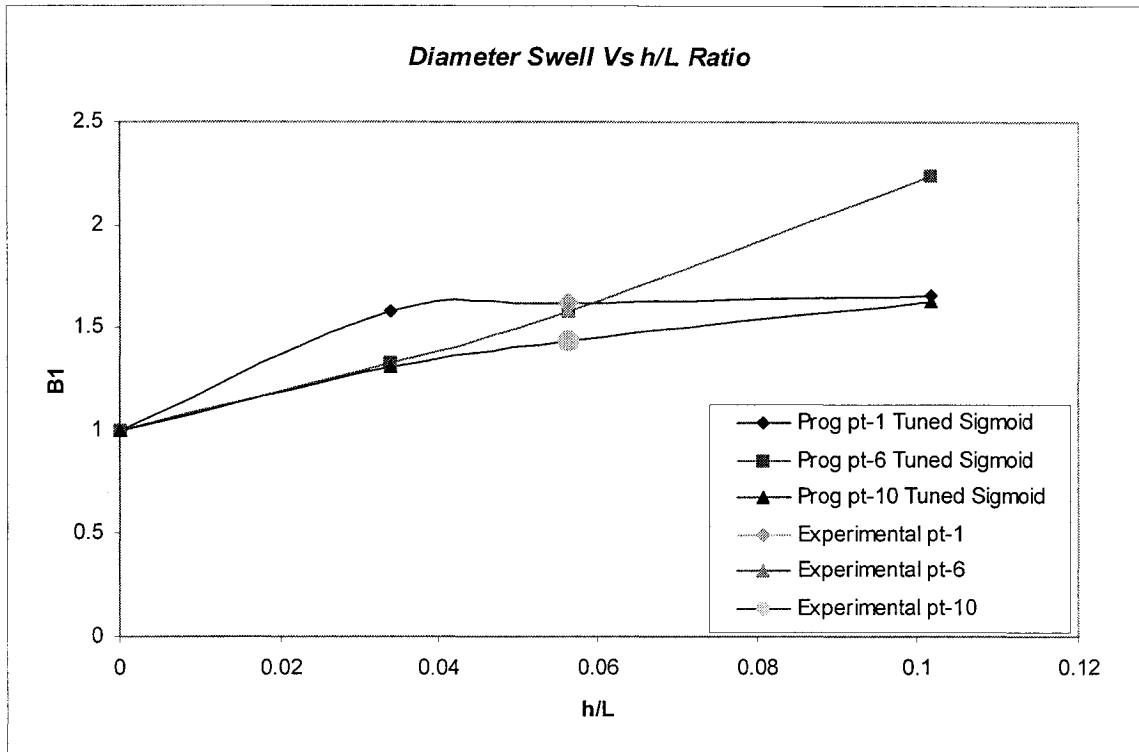


Figure 5-19 Sigmoid tuned to parison pinch-off results

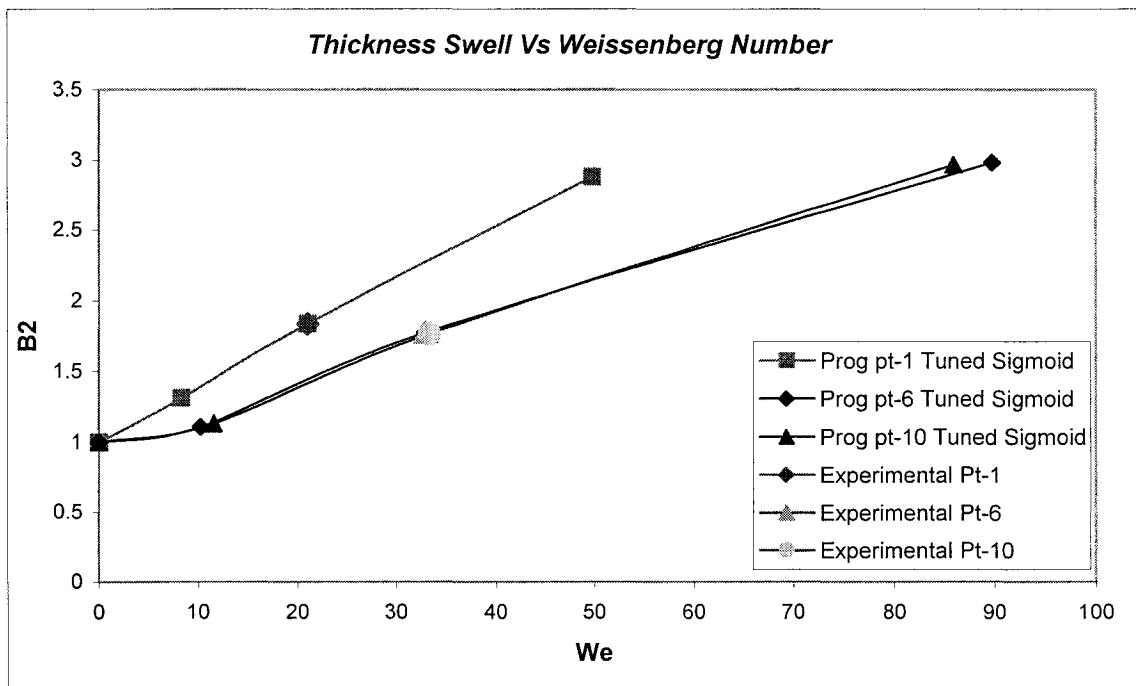


Figure 5-20 Sigmoid tuned to experimental observations

Now since the sigmoids were tuned to the experimental measurements, linear interpolation based on the length of the parison was used to determine the final die gap, which when set on the machine will give a parison of length 550mm (L_{target}). The final die gap was found to be 3.81 mm. After conducting an experiment on the Placo machine, we determined that a die gap of 4mm was to be set on the machine to obtain a parison of length 550mm for a flow rate of 80g/sec. Hence, the sigmoid interpretations were very close to the actual requirement.

5.6 Further details on the shape of the sigmoid fitting curves

From Fig 5.15, we observe that the sigmoid for programming point 7 overshoots after the experimental point to give a diameter swell (B1) of approximately 3. In general, for any resin this value does not exceed 2.5 regardless of De number. Therefore, we find that the sigmoid shape is dependent on the choice of initial tuning parameters (a, b, c and d). The user has to choose the initial guess such that the final curve has a shape corresponding to the curves for programming points 1 and 10 and not 7. We chose the solver program available in the MS-Excel to shift sigmoids to match experimental observations. The solver also has a built in constraint function with the help of which a user can restrict the values of different parameters of the sigmoid to a certain limit.

For this purpose we found another equation (Eq. 5.21), which was fitting very well to the simulation data and was fulfilling the requirement of sigmoid tuning by a changing single parameter. This equation has three variables and is of the type,

$$Y = a - b * \exp(-c^d) \quad (5.18)$$

Using a similar procedure as outlined for the flow rate and die gap scenario, we obtained a flow rate of 57.848 g/sec and die gap of 4.29 mm to obtain a parison of length 550mm (target length in our case). The final curves for the flow rate case obtained using this equation are shown in Figs 5.21 and 5.22. As can be seen, all the curves for the diameter

swell case have a maximum diameter swell of less than 2mm. However, this equation has a limitation in terms of achievable maximum diameter swell.

We would recommend using the equation with four variables instead of the one with three variables because of the greater flexibility offered by the equation with four variables. Cares must be taken by choosing the best initial guesses to conserve the sigmoid shape that levels off to a constant value at high De numbers.

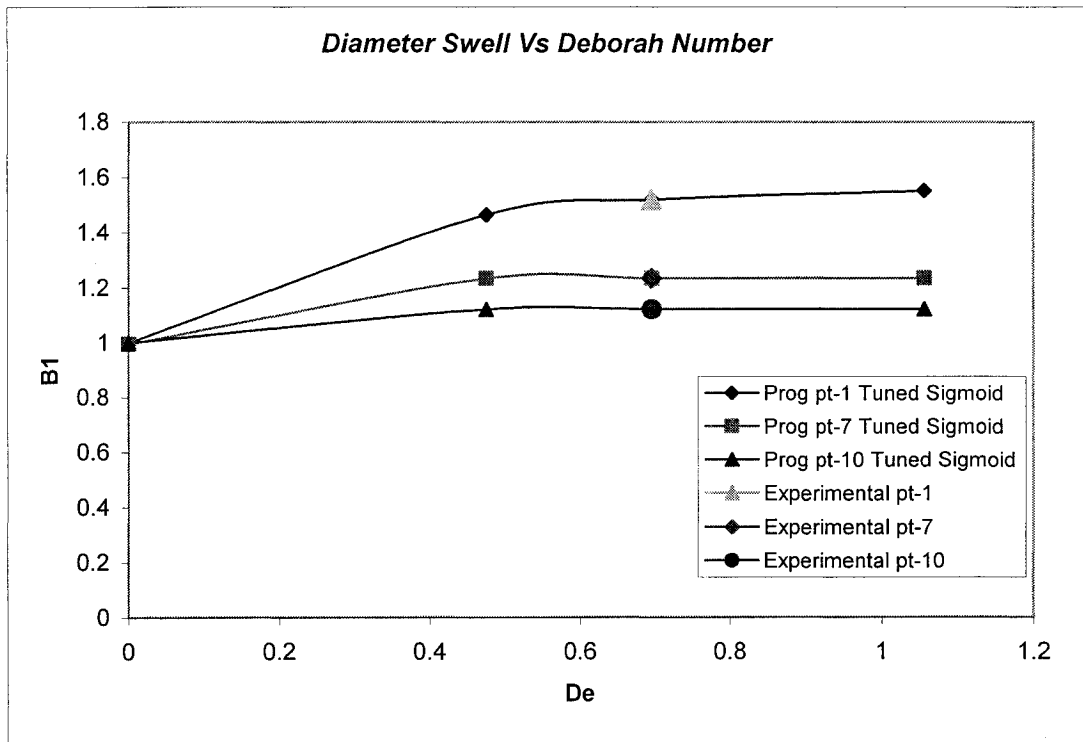


Figure 5-21 Diameter swell versus Deborah number for the flow rate case (Eq.5.18)

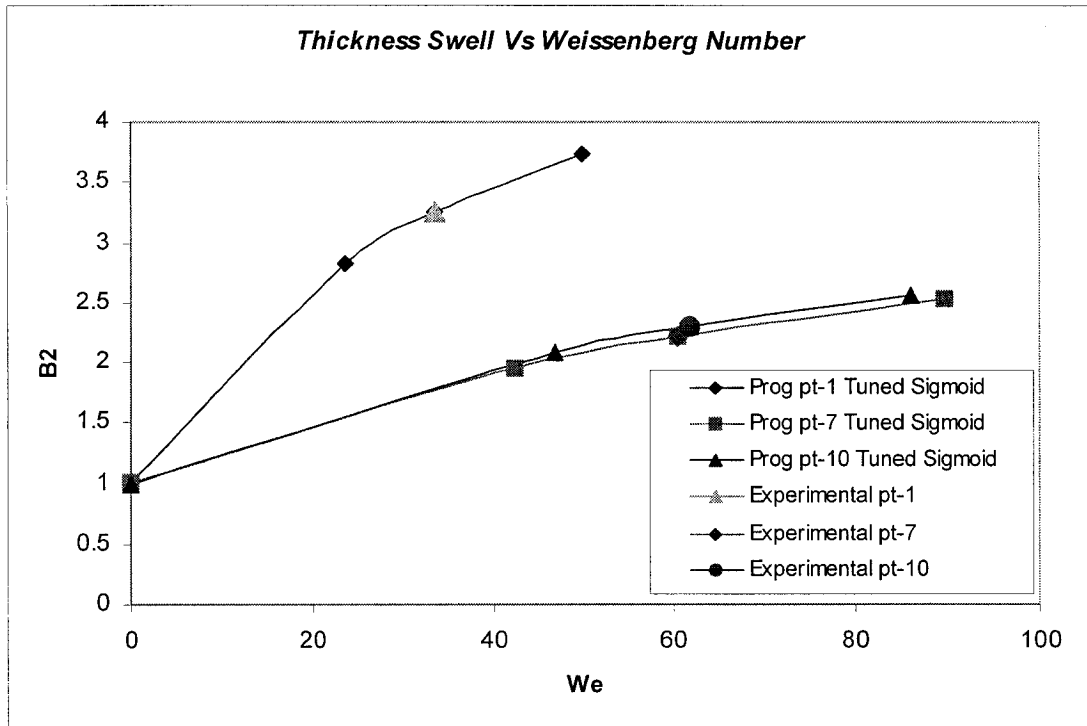


Figure 5-22 Diameter and thickness swell for the flow rate case (Eq.5.18)

5.7 Summary

The technique for cycle-to-cycle control of parison length in intermittent extrusion blow molding was presented and tested. The approach was tested for both the flow rate and die gap scenario. Good agreement between the calculated and set flow rate and die gaps was obtained.

For both cases, the variation of diameter swell and thickness swell with Deborah and Weissenberg numbers; and h/L ratio and Weissenberg number are identified. Flow rate (or die gap) to be set on the machine for the target length was determined after inputting various parameters into the model. This flow rate (or die gap) was then set on the machine and an experiment was conducted. The diameter and thickness swell curves were then tuned to match the experimental observed length. Once the curves were tuned, the modified parameters were re-inputted into the model which now gave a flow rate (or die gap) for the target parison length, which was close to the required one.

The main contribution of this M.Eng. thesis, is the development and testing of a new technique which will allow the cycle-to-cycle control of parison length in intermittent extrusion blow molding.

A basic introduction to the extrusion blow molding, the process, its applications and the phenomena of swell and sag were briefly presented in chapter 1.

A detailed description of different types of blow molding with more emphasis on extrusion blow molding and its types, their advantages and disadvantages were presented in chapter 2. It was learnt that though there are numerous techniques available for manufacturing small bottles, for some large industrial parts intermittent extrusion blow molding is used, as the parison is heavy and it will sag if continuous extrusion is used.

The motivation for this work and a literature review were presented in Chapter 3. The literature review showed that over the years extensive research has been done to determine the various factors affecting the parison dimensions. It also outlined the various offline and online techniques for estimating parison dimensions for the blow molding process. The offline techniques such as the one developed by Sheptak and Beyer (1965) were good at determining the final parison dimensions, but could not be used in a real industry as it would otherwise result in loss of production and money. The online techniques discussed in the chapter required extensive experimental setup and initial investment and were moreover tested for a continuous extrusion blow molding process only. Our objective was to develop a methodology, which would be accurate, quick yet inexpensive to the end user.

Chapter 4 presented a new method for estimating average relaxation time of a polymer resin (HDPE in our case). Relaxation time is an important phenomenon. It regulates the amount of swell that a polymer melt will undergo upon exiting the die head. The method described was based on the combination of Carreau and Maxwell model's. To obtain the flow kinematics required by Maxwell model, the changes in the Carreau model viscosity caused by temperature and shear rate in the die were obtained by conducting an

experiment on the machine. The resulting viscosity and shear rate values were then inputted into the Maxwell model to determine the amount of shear history that the material experienced during its flow in the die as a result of viscoelastic deformations. This shear history is responsible for the stress relaxation outside the die leading to time-dependent parison swell. The combination of inside and outside stresses were used to get an estimation of the average relaxation time.

In Chapter 5 we presented a soft sensor system for cycle-to-cycle control of parison length in intermittent extrusion blow molding. In a blow molding process the length of the extruding parison can be altered by changing either the flow rate or the die gap. The proposed methodology was applied and tested for both scenarios. Good accuracy was obtained between the recommended values and true flow rate and die gaps obtained on the Placo machine.

The objectives of this thesis were:

- 1) to develop a technique for online estimation of average relaxation time,
- 2) to identify the changes in the rheological properties of the melt from temperature increase in the die, and
- 3) to develop a model to predict the total length of the parison at any given time taking in to consideration the combined effect of swell and sag.

These objectives have been achieved and a new technique for cycle-to-cycle control of parison length in intermittent extrusion blow molding has been developed.

6.1 Recommendations for Extensions of this Work

Both the approaches (average relaxation time and parison length estimation) described in this thesis are generic, i.e., they are equally applicable to different resins and die geometries. However, since the methodology and the test described involved only one resin (HDPE-DMDF 6200) and die geometry, it is recommended to test the approach by using different blow molding resins and die geometries. This approach also has the

potential of being extended to optimize the cycle time for a desired parison length using moving mandrels (programming points).

The accuracy of the parison length estimation approach can be further improved by conducting two experiments on a machine rather than conducting just one as outlined in the approach in this thesis. As the number of experiments is increased, the dependency of the tuned swell curves (sigmoids) on the simulation results is reduced. If the number of experiments are increased the swell curves can then be tuned by adjusting all four parameters rather than adjusting just one thus allowing the sigmoid to change its shape.

The approach for estimating average relaxation time could be extended to multiple relaxation times by using a generalized Maxwell model.

References

- Agassant, J.F., Avenas, P., Sergent, J.Ph., Carreau, P.J., 1991, *Polymer processing: principles & modeling*, Hanser Gardner Publications, New York.
- Ajroldi, G., 1978, "Determination of rheological parameters from parison extrusion experiments", *Polymer Engineering and Science*, Vol.18, No.10, pp.742-749.
- Basu, S., and Fernandez, F., 1983, "Theoretical and experimental study of non-isothermal deformation of a blow molding parison", *Advances in Polymer Technology*, Vol.3, No.2, pp.143-155.
- Berins, M.L., 1991, *Plastics engineering handbook of the society of the plastics industry, Inc*, Van Nostrand Reinhold, Boston, 5th Edition.
- Byron Bird, R., Armstrong, R.C., and Hassager, O., 1987, *Dynamics of polymeric liquids*, John Wiley & Sons, Inc, New York, 2nd Edition.
- Crawford, R.J., 1998, *Plastics engineering*, Butterworth-Heinemann, Oxford, 3rd Edition.
- Crocker Limited, The Blow Molding Process: Step1, Crocker limited, Michigan, 2004, URL: http://www.crockerltd.com/mainsite/public/html/step_1.html.
- Dealy, J.M., and Orbey, N., 1985, "A model for parison behavior in the extrusion blow molding process", *AIChE Journal*, Vol.31, No.5, pp.807-811.
- Dealy, J.M., and Wissbrun, K.F., 1990, *Melt rheology and its role in plastics processing: theory and applications*, Van Nostrand Reinhold, New York.
- DiRaddo, R.W., Patterson, W.I., and Kamal, M.R., 1988, "On-line measurement and estimation of parison dimensions in extrusion blow molding", *Advances in Polymer Technology*, Vol.8, No.3, pp.265-274.
- DiRaddo, R.W., and Garcia-Rejon, A., 1992, "Noncontact measurement of parison thickness profiles affected by swell and sag in continuous extrusion blow molding", *Polymer Engineering and Science*, Vol.32, No.19, pp.1401-1410.
- DiRaddo, R.W., and Garcia-Rejon, A., 1993, "On-line prediction of final part dimensions in blow molding: A neural network computing approach", *Polymer Engineering and Science*, Vol.33, No.11, pp.653-664.
- Eggen, S., and Sommerfeldt, A., 1996, "On-line measurement of parison geometry during blow molding: Parison swelling for three high density polyethylenes with different

molecular weights and molecular weight distributions”, *Polymer Engineering and Science*, Vol.36, No.3, pp.336-346.

Garcia-Rejon, A., DiRaddo, R.W., and Ryan, M.E., 1995a, ”Effect of die geometry and flow characteristics on viscoelastic annular swell”, *Journal of Non-Newtonian Fluid Mechanics*, Vol.60, pp.107-128.

Garcia-Rejon, A., 1995b, *Advances in blow moulding optimization*, Rapra Technology Ltd, Shawsbury.

Girard, P., Hou, B.Q., Thomson, V., Yousefi, A.M., and DiRaddo, R.W., 2003, “On-line hybrid model based tuning of simulation provides soft sensors for the estimation of sheet temperature distributions in thermoforming”, *S.P.E Antec Technical Papers*, Vol. A, pp.776-779.

Huang, H.X., and Liao, C.M., 2002, ”Prediction of parison swell in plastics extrusion blow molding using a neural network method”, *Polymer Testing*, Vol.21, pp.745-749.

Huneault, M.A., Lafleur, P.G., and Carreau P.J., 1990, “Extrudate swell and drawdown effects on extruded profile dimensions and shape”, *Polymer Engineering and Science*, Vol.30, No.23, pp.1544-1550.

Kalyon, D., Victor, T., and Kamal, M.R., 1979, “The dynamics of parison development in blow molding”, *S.P.E. Antec Technical Papers*, pp.992-995.

Kalyon, D., Tan, V., and Kamal, M.R., 1980, “The dynamics of parison development in blow molding”, *Polymer Engineering and Science*, Vol.20, No.12, pp.773-777.

Kamal, M.R., Tan, V and Kalyon, D., 1981, “Measurement and calculation of parison dimensions and bottle thickness distribution during blow molding”, *Polymer Engineering and Science*, Vol.33, No.21, pp.331-338.

Koopmans, R.J., 1992a, ”Extrudate swell of high density polyethylene. Part I: Aspects of molecular structure and rheological characterization methods”, *Polymer Engineering and Science*, Vol.32, No.23, pp.1741-1749.

Koopmans, R.J., 1992b, ”Extrudate swell of high density polyethylene. Part II: Time dependency and effects of cooling and sagging”, *Polymer Engineering and Science*, Vol.32, No.23, pp.1750-1754.

Koopmans, R.J., 1992c, ”Extrudate swell of high density polyethylene. Part III: Extrusion blow molding die geometry effects”, *Polymer Engineering and Science*, Vol.32, No.23, pp.1755-1764.

Langkamp, U., and Michaeli, W., 1996, ”On-line monitoring of parison geometry to prevent sag and swell”, *Plastics Engineering*, pp.29-31.

- Laroche, D., 1997, "Modelling the effect of operating conditions on the blow moulding of a gas tank", *S.P.E. Antec Technical Papers*, Vol.1, pp.43-49.
- Laroche, D., Kabanemi, K.K., Pecora, L., and DiRaddo, R.W., 1999, "Integrated numerical modeling of the blow molding process", *Polymer Engineering and Science*, Vol.39, No.7, pp.1223-1233.
- Lee, N.C., 1990, *Plastic blow molding handbook*, Van Nostrand Reinhold, New York.
- Midgley, A., and Peszel, E.A., 2002, "Parison verification for extrusion blow molding simulation software", *S.P.E. Antec Technical Papers*, Vol.1, pp.3450-3455.
- Millar, B.G., Laughlin, P., McNally, G., and Murphy, R., 2003, "The effect of melt temperature and extrusion rate on the die swell of Metallocene and conventional polyethylenes", *S.P.E. Antec Technical Papers*, Vol.1, pp.2000-2004.
- Modern plastics world encyclopedia, 2002, Hightstown, NJ: Modern Plastics.
- Orbey, N., and Dealy, J.M., 1984, "Isothermal swell of extrudate from annular dies; Effects of die geometry, flow rate, and resin characteristics", *Polymer Engineering and Science*, Vol.24, No.7, pp.511-518.
- Rosato, D.V., and Rosato, D.V., 1989, *Blow molding handbook*, Hanser Gardner Publications, New York.
- Sentelices, P., 1994, "Die swell of viscoelastic polymers", *S.P.E. Antec Technical Papers*, pp.1885-1887.
- Sheptak, N., and Beyer, C.E., 1965, "Know your parison", *S.P.E. Journal*, Vol.21, pp.190-196.
- Swan, P.L., Dealy, J.M., Garcia-Rejon, A., and Derdouri, A., 1991, "A new measurement method and effect of molecular weight distribution for a high density polyethylene", *Polymer Engineering and Science*, Vol.31, No.10, pp.705-710.
- Swan, P.L., Kamal, M.R., Garcia-Rejon, A., and Cielo, P., 1996, "Optical on-line measurement of the thickness distribution of blow molding parisons", *Polymer Engineering and Science*, Vol.36, No.36, pp.985-992.
- Tanoue, S. (Kyushu Univ.), Kajiwara, T., Funatsu, K., Terada, K., and Yamabe, M., 1996, "Numerical simulation of blow molding – Prediction of parison diameter and thickness distributions in the parison formation process", *Polymer Engineering and Science*, Vol.36, No.15, pp.2008-2017.
- Wong, A.C.Y., and Liang, J.Z., 1997, "Relationship between die swell ratio and melt flow index", *Journal of Chemical Engineering Science*, Vol.52, No.18, pp.3219-3221.

Wong, A.C.Y., 1998, "Factors affecting extrudate swell and melt flow rate", *Journal of Material Processing Technology*, Vol.79, pp.163-169.

Yang, B., and Lee, L.J., 1987, " Effect of die temperature on the flow of polymer melts Part II: Extrudate swell", *Polymer Engineering and Science*, Vol.27, No.14, pp.1088-1094.

Yousefi, A.M., Collins, P., and DiRaddo, R.W., 2002, "A comprehensive study of die geometry and operating conditions effects on parison dimensions", *S.P.E. Antec Technical Papers*.